ABSTRACT

Title of Dissertation:	DESIGN OF ENZYME CASCADE AND CRISPR-CAS9 NETWORKS FOR ENABLING BIOELECTRONIC COMMUNICATION
	Narendranath Bhokisham,
	Doctor of Philosophy, 2017
Dissertation directed by:	Professor William E. Bentley,
	Fischell Department of Bioengineering

There is an increasing emphasis on building closed loop systems in human health where real time monitoring and analysis is connected to feedback and treatment. Building such systems requires bridging the information loop across the different signal modalities of biology and electronics. In this work, I have created two

different networks at biology-electronic interface to enable the communication from biology to electronics and vice versa.

The first network is a multi-step enzyme cascade assembled on a microchip to enable conversion of biologic information into electro-chemical information. I first devised a modular construction approach using microbial transglutaminase (mTG) based conjugation chemistry where multiple enzyme components are assembled on an abiotic surface in a ‘plug and play’ fashion. Integration of bio-components with electronics requires a scaffold material for functionalization of the bio-electronic interface. To address this challenge, I engineered a self-assembling Tobacco Mosaic Virus-Virus Like Particle into a 3D scaffold displaying desired functional groups at the interface. Using the 3D scaffolds and mTG mediated conjugation chemistry, I assembled a synthetic 3-enzyme cascade on a microchip for conversion of methyl cycle intermediates into homocysteine, an electrochemically readable molecule. The modular construction approach and the scaffold materials that I developed can enable facile assembly of multi-subunit bio-components and diversify the range of metabolites that can be detected on a microchip for use in biosensing applications.

Next, I focused on mediating communication from electronics to specific genes in the genome of biological systems. An electrogenetic promoter that is responsive to the electrical stimuli was reported in *E. coli.* In this work, I integrated the precise gene targeting capabilities of the CRISPR-Cas9 system with the electrogenetic promoter to target specific host transcriptional processes. I displayed temporal silencing of several host defense mechanisms against the electrical signals resulting in an overall enhancement for electrogenicity in *E. coli*. A more

sophisticated control of host transcriptional processes by the CRISPR-Cas9 system is a valuable addition to the existing electrogenetic toolbox, one that could enhance the interoperability of electrogenetic systems and mediate bio-electronic communication between strains and species.

DESIGN OF ENZYME CASCADE AND CRISPR-CAS9 NETWORKS FOR ENABLING BIOELECTRONIC COMMUNICATION

by

Narendranath Bhokisham

Dissertation submitted to the Faculty of the Graduate School of the
University of Maryland, College Park, in partial fulfillment
of the requirements for the degree of
Doctor of Philosophy
2017

Advisory Committee:
Professor Dr. William E. Bentley, Chair
Professor Dr. James N. Culver, Dean's Representative
Professor Dr. Gregory F. Payne
Professor Dr. Edward Eisenstein
Assistant Professor Dr. Daniel J. Dwyer

Dedication

I dedicate my PhD Dissertation to my parents Dr. M. Subhashini and B. K. Pandarinath.

Acknowledgements

Firstly, I would like to thank my advisor Prof. Bentley for giving me the freedom to explore as many things as possible and the space to fail, learn and fail again. I would like to express my gratitude to Dr. Gregory F. Payne and Dr. James N. Culver for all their valuable suggestions and mentoring at several instances right through my time in graduate school.

I would like to thank all the past and present research assistant professors, post docs, graduate students, and undergraduates of the Bentley lab. Specifically, I would like to thank Dr. David N. Quan and Dr. Chen-Yu Tsao for all the coffee table conversations covering everything from science to stock broking. I would like to thank Adam Brown from the Culver lab for all the help with the TMVs, Dr. Liu and Dr. Kim from the Payne lab for their valuable insights on biofabrication and electrochemical experiments. All the late-night conversations with Prof. Shyam Dube were thought provoking and inspiring.

Finally, I would like to express my gratitude to all my family and friends in India and US for all their motivation and cheer.

Table of Contents

List of Tables

List of Figures

List of Illustrations

Chapter 1 Introduction

1.1 Digital systems in medicine

In the era of artificial intelligence and self-driving cars, it is not too farfetched to expect autonomous health monitoring and control systems to play a crucial role in human health. A GPS enabled smartphone in addition to a heart rate sensor can accurately track various fitness parameters. Several wearable and implantable bio-sensors monitor vital parameters like heart rate, cardiac rhythms, sleep patterns, glucose levels independently or in tandem with a smartphone.[1, 2]. Through extensive information gateways in place, information gathered by the sensors can relayed and analyzed in real time and a suitable feedback can be provided. With smartphone being at the center of this new diagnostic ecosystem (termed as ‘mHealth’), newer models of patient centric health care need to be put in place.[3, 4] This not only includes sensors for real time monitoring and analysis but also newer ways of delivering effective feedback including ‘smart’ drug delivery devices that autonomously communicate to sensors in real time.

1.2 Closed-loop systems: therapeutic systems ensconced with feedback

Intelligent therapeutic delivery systems that adapt to body conditions and modulate treatments are referred as to Closed-loop systems. Serval such systems are in

use and development and it is not a coincidence that many of these systems have first sprung in the field of neuromodulation where application of electric signals for neural stimulation and therapy is well established. Epilepsy, Parkinson's and motor pain are some of the conditions for which closed-loop systems have been developed till date.[5] Developing closed-loop systems for non-neuromuscular conditions can be a challenge because of the lack of sensing and drug delivery techniques that are integrated with

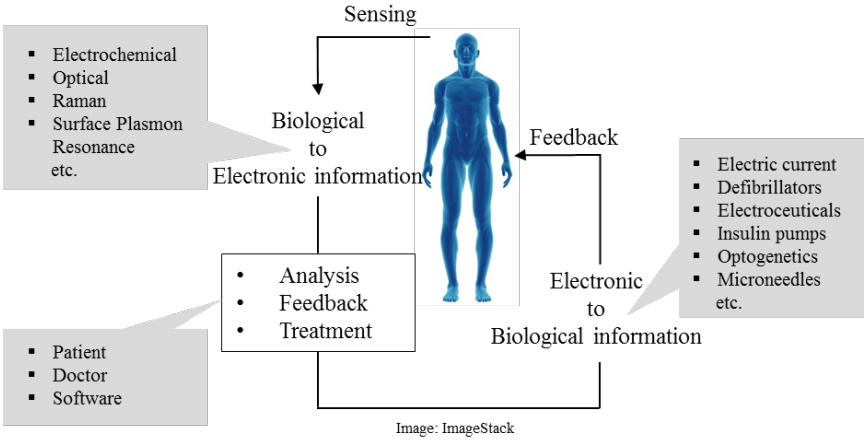

Scheme 1-1 Elements of a closed loop system.

Closed loop systems integrate sensing, analysis, and feedback. Sensing and feedback can be performed by a variety of techniques and analysis can be done at various levels by the doctor, patient or a software.

and controlled by electrical systems. In 2016, FDA approved a closed-loop insulin pump that automatically senses glucose levels and delivers insulin.[6, 7] Several other technologies aiming to address the close-loop challenge in diabetes have appeared including the use of a microneedle patch filled with glucoresponsive-insulin[8]; an optogenetic circuit in mice that responds to a smartphone signal with insulin production etc.[9] While all of this works in relation to diabetes are significant and innovative, it

is not to be missed that most of the sensing is capitalized on the rich literature available for glucose sensing.

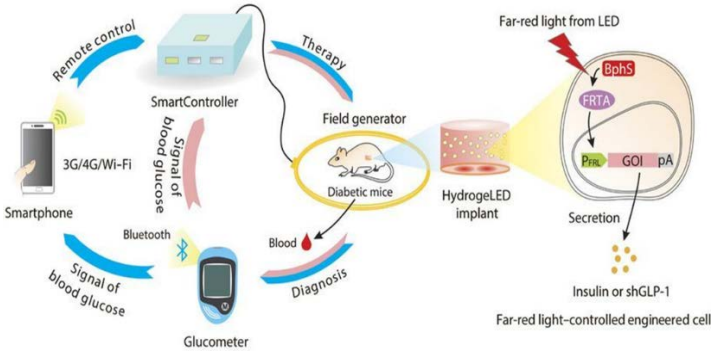

Scheme 1-2 Optogenetics based closed-loop system for diabetes.

Scheme of the optogenetics based closed-loop system demonstrated by Shao et.al, in Science Translational Medicine [9]. A genetically engineered mouse that responds to far-red light source with production of insulin is created. Glucose levels in mice are sensed with glucose sensors and relayed to smartphones which in turn controls a far-red light source. Duration and intensity of far-red light controls the amount of insulin secreted in mice.

Therefore, to create closed-loop systems for other important conditions **(Scheme 1-1)**, there is a need to create new sensors to mediate communication across the signal modalities. On the other end of the information loop, new methodologies need to be developed to mediate reverse signal transduction from electrical systems to biological systems to deliver or actuate therapeutics with electrical signals like the vagus nerve stimulation for epileptic seizures, deep brain stimulation for movement disorders, wirelessly controlled human parathyroid hormone release using microchips[10] etc.

1.3 Sensing: One half of the closed loop

1.3.1 New age digital sensors

New age digital sensors are being developed that not only monitors various physiological parameters but also relays information in real time. Some of the sensors already approved by FDA include 1: Blood pressure through applanation tonometry across the radial artery in the hand through watch like sensors[11]; 2: A fully implantable 'CardioMEMS device' for pulmonary artery pressure monitoring system[12, 13]; 3: Smart drug digital sensor for reporting treatment compliance.[14] All the above mentioned sensors are completely integrated with smartphones or other digital systems so that the information is obtained, analyzed and relayed to the caregiver or back to the user enabling instantaneous feedback.

1.3.2 'Traditional' sensors- Point of Care (POC) diagnostic devices

Predating the 'digital' sensors, there is a generation of sensors developed for POC invitro diagnostic applications. In fact, the earliest POC sensor was the urinalysis dipstick embedded with a pH dye for urinary protein measurements (1957) and the first glucose sensor was elaborated in 1962.[15] Since then there have been many sensors developed and the most common ones in use today include tests for pregnancy, glucose levels, cholesterol, cancer, HIV, drugs of abuse, microbes like *E. coli* and *H. pylori* etc.[1] Some of the targets for sensing includes metabolites such as glucose, cholesterol, triglycerides, creatinine, lactate, ammonia, urea etc.[16] i-STAT system

for blood chemistry uses electro-chemical methods for detection of various blood components.[17] Proteins including enzymes and antibodies are the most common of all target molecules in POC applications with the most famous tests include pregnancy sticks through detection of human chorionic gonadotrophin (hCG) and Ora Quick ADVANCE Rapid Antibody test for HIV. Nucleic acid diagnostics, also referred to as 'molecular diagnostics' uses nucleic acid sequence recognition as the mode for detection; whole cell both human[18, 19] and microbial[20] are also used as targets; small molecule drugs for abuse or contaminants in foods are also determinants of POC assays.[21] Mode of detection in POC assays include electro-chemical detection (as in the case of glucose sensor that is mass produced in the order of billions/year) and optical methods (used in lateral flow assays for pregnancy and fluorescent assays, produced in millions per year). Under electro-chemical detection techniques, there are amperometry, potentiometry, impedance measurements.[22, 23] Under optical methods, fluorescence[24], fluorescence resonance energy transfer (FRET) [25], luminescence[26], absorbance, surface plasmon resonance, light scattering techniques including rayleigh, mie, geometric, raman etc.[1] More sophisticated methods like magnetic particle detection using spin-valve methods are also used for single molecule detection.

1.3.3 Fabricating enzyme for bio-device communication

A typical biosensor is a device that combines a bio-logical component with an electronic component and transduces the sensing signal from bio component into an

electric signal compatible with electronic circuits. An enzyme is the most preferred choice for bio-component assembly onto the electrode due to its molecular recognition capability and enzyme electrodes are one of the most versatile and well-studied of all biosensor types. Most of the current generation of enzyme electrodes have single enzyme (mostly oxido-reductases) immobilized on the electrode surface. While these enzymes have high direct electron transfer coefficients (DET) and better sensitivities, they reduce the range of analytes that can be detected.

If methods of assembling multiple enzymes are ironed out, multi-enzyme cascade capable of detecting a wide range of analytes and converting into electroactive species could be assembled on electrode surface. Some existing methods and materials available for enzyme assembly onto sensors are detailed below.

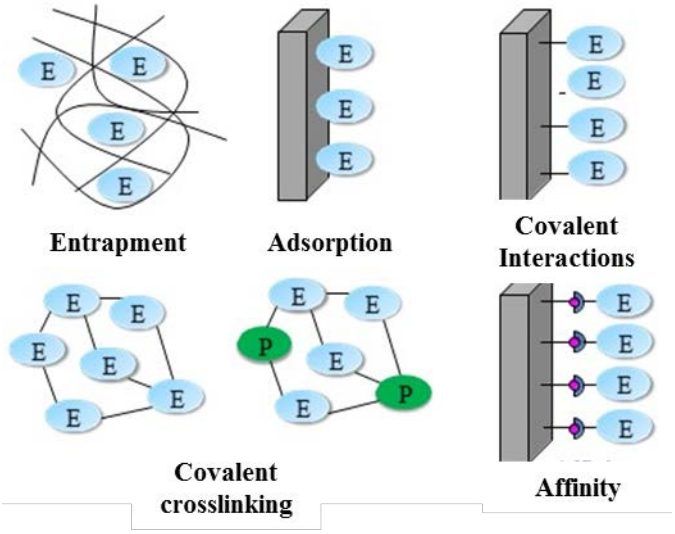

Scheme 1-3 Different methods of enzyme assembly

Scheme indicating different strategies used for enzyme immobilization. (Image adopted from Sassolas et. al.[27])

1.3.3.1 Entrapment

Entrapment is the most benign method for enzyme assembly. However, enzymes leach out due to the porosity of the matrix. Some of the materials used for entrapment and the enzymes immobilized are listed below. Electro-polymerization with naturally soluble electro conductive monomers like polypyrrole (PPy) are used for entrapment of enzymes. Glucose oxidase (GOD)[28], nitrate reductase[29], horse radish peroxidase based levetiracetam sensor[30] are some of the examples of enzymes immobilized. Polyaniline is another molecule used to immobilize enzymes like xanthine oxidase[31], tyrosinase.[32] Most of the sensors had long shelf life and produced repeatable results. Amphiphilic network comprising hydrophilic poly(2-hydroxyl acrylate) (PHEA) and a hydrophobic phase of polydimethylsiloxane (PDMS) was used to trap horse radish peroxidase (HRP) to detect butylhydroxyperoxides.[33] Photo polymerization of poly(vinyl alcohol)-bearing styrylpyridinium (PVA-SbQ) groups are used for fabricating alcohol dehydrogenase in PVA-SbQ for an ampherometric ethanol biosensor.[34],[35] Sol-gel with tetramethoxysilane (TMOS) and tetramethoxysilane (TEOS) is another method in assembling enzymes. The disadvantage of this method is the extreme acidic or alkaline pH conditions and the short shelf life of the matrix.

Polysaccharide based hydrogels including chitosan, alginate and agarose have been used for a long time for entrapment of enzymes on enzyme electrodes. Alginate

gels are biocompatible [36, 37] but enzymes can leach out of the matrix with time leading to loss in sensitivity of the sensor. Chitosan is another example where Tyrosinase[38], glutamate dehydrogenase[39] have been immobilized. Carbon nanotube(CNT)-chitosan composites have been used as well to detect lactate[40, 41], ethanol[42], and cholesterol.[43] CNT is found to increase conductivity of matrix and CNT-chitosan on carbon electrodes have been used with high sensitivities. Agarose is another polysaccharide that dissolves in heat. Enzymes can be mixed with heated agarose solution and cast on electrodes (example: tyrosinase[44]). Here again, due to the porosity of the matrix, enzymes can leach out and to prevent that, enzymes have been crosslinked to beads and immobilized in agarose gels.[45]

1.3.3.2 Adsorption

The easiest means to immobilize proteins onto electrodes is through non-specific adsorption where enzymes are bound through weak hydrogen bonds or van der Waals interactions. The drawback with it is that enzymes desorb from support due to changes in temperature, pH, ionic strength leading to poor life and storage stability. Lactate dehydrogenase was immobilized to polyaniline films by physical adsorption.[46]

1.3.3.3 Crosslinking

Crosslinking via glutaraldehyde is another method by which enzymes can be immobilized. The drawback of this method is that enzymes are non-specifically crosslinked to each other leading to reduced enzyme activity. Conversely, since the crosslinking is covalent there is reduced chance for leaching of enzymes. GOD,

Cholesterol dehydrogenase, tyrosinase etc. have been used in this method to immobilize onto various supports like Nafion-Meldola blue modified screen printed electrodes[47], zinc oxide nanotube-modified electrode.[48]

1.3.3.4 Covalent immobilization

Enzymes have been covalently attached to the solid supports through activation of amine or carboxylic acid groups on solid supports. Activating agents like 1-ethyl-3-(3-dimenthylaminopropyl) carbodiimide (EDC) in conjunction with N-hydroxysuccinamide (NHS) have been used to targeting amine groups in the enzymes. Numerous sensors including sensors for cholesterol[49], glutamate[50] are fabricated using this approach. Self-assembled monolayers containing of long aliphatic carbon chains terminating with thiol groups have been used to self-assemble on solid supports and the terminal group is functionalized with enzymes using some of the previously described chemistries. Conversely enzymes have been engineered with cysteines and covalently assembled onto gold.[51]

1.3.3.5 Affinity

Enzymes have been immobilized on biosensors using affinity between specific functional group/moieties and activated supports. Advantage of this method is the control over enzyme conformation during immobilization onto solid supports. The most common affinity based chemistry used for enzyme immobilization is through biotin-streptavidin chemistry[52] or His peptide tag. Various enzymes have been immobilized using this approach where metal chelators are immobilized on the

electrode surface using some of the above-mentioned materials like PVA-SbQ, polyaniline and polypyrrole and enzymes are reversible bound to metal chelators.

1.3.3.6 Important design considerations for enzyme assembly

The choice of enzyme, immobilization technique, materials used for immobilization, transducer and detection modality all play a vital role in biosensor sensitivity and stability. While physical absorption is the easiest method for immobilization, there is enzyme desorption. Entrapment is the least prohibitive approach for enzyme immobilization but enzymes can escape through the porous matrix. Crosslinking through glutaraldehyde provide tight assembly of enzymes to electrode surface but can be non-selective and reduce enzyme activity. Affinity chromatography based approaches can provide selective crosslinking put generally require engineering of proteins. In addition to this, the type of materials, physical and chemical conditions employed for enzyme immobilization can determine the overall efficiency of enzyme assembly.

All these factors get compounded when multi-enzyme cascades are assembled. Enzyme stoichiometries accounting for relative enzyme activities, spatial arrangements, thermodynamic and kinetic conditions for cascade reactions are all some of the factors that needs to be considered. **Some of the concerns in building multi-subunit complexes are discussed in the Chapter 2 of this work that involves development of modular construction approach by which multi-subunit enzyme complexes can be built on abiotic surfaces in a plug and play fashion.**

Next, I focus on using the modular construction approach detailed in **Chapter 2** of this thesis for integration of biological components with electronic components. To integrate the two class of components, an interface material capable of assembling on abiotic electronic surface and presenting various functional groups for conjugation of bio-components are required. In **Chapter 4,** I focus on virus like particles (VLP) and its use as 3D scaffolds for presenting enzyme cascades on electronic surfaces.

1.4 Virus as interfacial materials at bio-electronic interface

VLPs are a class of biomaterials containing protective coat proteins called capsids that self-assemble from few components into large nanoparticles with distinct size and shapes. Knowledge of the structure of viruses has enabled extensive engineering, both genetic and chemical, to display unique features with precise control over their spatial distributions.

1.4.1 Genetic modification of Viruses

Various genetic modifications are introduced both on the inside and as well as on the outside of both viruses and VLPs. Hepatitis B Virus has been genetically engineered to retain cargoes within the capsids. Cargoes are genetically fused to the termini of capsid subunit that is oriented towards the inside of the capsid.[53] VLPs. have also been genetically modified to display cargoes on the outside (GFP[54] and FLAG tag[55]). However, direct genetic fusion of large cargoes with capsid subunits may affect the overall assembly of capsids.

1.4.2 Conjugation strategies for virus particles

As an alternative to direct genetic fusion, various amino acids are introduced into VLPs that enable conjugation of cargoes post the assembly of the particles. Sortases have been used to covalently attach different proteins together. Bioorthogonal conjugation motifs that are recognized by different sortases are introduced into viral capsid structures for orthogonal conjugation of multiple cargoes.[56] Several amino acids are genetically introduced to enable chemical conjugation of cargoes. Introduction of cysteines at N termini of coat proteins is a preferred choice for sulfhydryl group based conjugation and for gold interactions.[38, 57-59] Lysines for NHS based assembly, aspartic acid for carbodiimide based activation, cysteines for Michael type addition, tyrosine for azo coupling etc. are some of the examples of amino acids being introduced for chemical conjugation.[60] Non-canonical amino acids such as O-methyl tyrosine, *p*-azidophenylalanine, *p*-acetylphenylalanine, *p*-benzoyl-phenylalanine, 3-(2-naphthyl) alanine, *p*-aminophenylalanine are introduced at amber, ocher, opal codons for conjugation.[61-64]

1.4.3 Virus particles as cages

Viruses like Bacteriophage P22 and Cowpea Chlorotic Mottle Viruses (CCMV) have been exploited to act as cages for encapsulating a variety of molecules including drugs and nucleic acids for drug delivery applications and enzymes for nanoscale bioreactors. Upon stimulation with temperature, P22 expands in size and shape and

forms ‘Wiffleball’ structure with small nanometer scale holes in capsids enabling cargoes to move in.[65] CCMV virus capsids can undergo assembly and disassembly in response to pH or ionic strengths incorporating various cargoes.[66]

1.4.4 Biocatalyst application

Enzymes have been co-expressed with coat proteins leading to accumulation of enzymes inside VLPs. Lipases were the first to be displayed on PVX.[67] Later, in one study related to CCMV virus, capsids were engineered with a coiled coil linker that enabled assembly of enzymes PalB to capsid first and later capsids self-assembled into a full particle engulfing the enzymes.[68] P22 phage has been shown to encapsulate alcohol dehydrogenase. Coat proteins and enzymes were co-expressed at the same time and coat proteins engulfed the enzymes during its self-assembly into capsids.[65, 69] Even multi-enzyme complexes have been inserted in this fashion.[70]

1.4.5 VLPs as materials for biodevice assembly

Defined size and shape of the viruses in nanoscale makes viruses attractive for use as a material for biodevice assembly. Mineralization of high aspect ratio virus particles such as Tobacco Mosaic Virus(TMV) and M13 bacteriophage has led to development of nanowires. Self-assembly properties are exploited to assemble nanoscale viruses into mesoscale wire structures [56, 71-73] and for liquid crystal displays.[74, 75] Bio-batteries is another example for viruses being used as materials in conjunction with electronics. Both M13 and TMV have been assembled at anode as

well as cathode for mineralization of carbon, Mn^{2+} and other metal ions and used in Li-ion and Na-ion batteries.[56, 76-80]

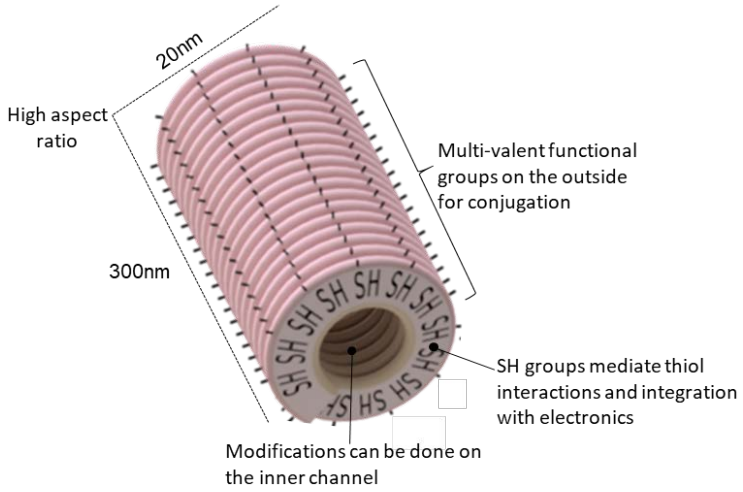

Scheme 1-4 Tobacco Mosaic Virus- Virus Like Particle(TMV-VLP) as materials for enzyme assembly at bioelectronic interface

Nano scale TMV-VLP structures engineered with cysteines at the N termini enable self-assembly onto gold. The C termini of coat proteins can be exploited to genetically engineer functional proteins or peptides. Various cargoes can be loaded on the inside as well as outside of the particle.

1.4.6 Viruses as materials for sensors

Combining the dual properties of viruses as materials for electronic integration as well as genetically modified biomaterial, new biosensors are being designed. A layer of M13 phage on an impedance sensor was used for detection of prostate cancer specific antibodies and antigens.[81] TMV virus particles in combination with polyaniline have been used as a thin film sensor for detection of methanol and ethanol.[82] TMV was also engineered with TNT binding peptides and assembled on

gold surfaces. TNT binding peptides increased the local concentration of TNT at the electrode surface resulting in increased faradaic current.[83]

1.4.7 Enzymes on VLPs for biosensing

With extensive literature available on protein conjugation, enzymes are integrated with virus particles for biosensing. Two enzyme cascade containing glucose oxidase and horse-radish peroxidase has been assembled on the surface of cowpea mosaic virus[84] and TMV for detection of glucose.[85] Capitalizing on virus particles ability to integrate with electronics, multi-enzyme cascades can be assembled on virus particles for fabrication of novel electro-chemical and other sensor types. In this work, I focus on using TMV based virus like particles as 3D scaffolds to present sensor enzymes on electronic surfaces. **I utilized the mTG mediated conjugation approach detailed in Chapter 2 to build a three-enzyme cascade on TMV-VLPs in Chapter 4.**

1.5 Closing the loop from electronics to biology

The critical segment in building closed loop systems is the transduction of information from electronic circuits to biological systems. Functional electrical stimulation (FES), a technique where low levels of electric current are applied across an intact nerve to target and restore impaired body parts is one such example of transduction of electrical information being used to modulate biological system.[86,

87] In this work, I would like to focus on mediating bio-electronic communication outside the purview of neuromodulation.

1.5.1 Bio-electronic communication under microbial context

Under the microbial context, bio-electronic communication may refer to bi-directional electron flow with microbes producing electrical signals in response to a specific stimulus as well as application of electrical signals to microbes to elicit a designed genetic response. Microbial fuel cell (MFC) falls under the first category of bio-electronic communication where microbes produce electric current. MFC's are well characterized systems where microbes consume organic compounds to generate electrons that are passed over to the anode of a battery. [88-90] Some of the well characterized species in MFC's include *Geobacter sulfurreducens* and *Shewanella oneidensis.* Genetic studies have characterized the pathways that enable electron flow and c-type cytochromes are identified to be the major player in electron transport.[91-93] Pili can also help in transfer of electrons to the electrode.[94] Genes that code for the proteins involved in electron transport to the electrodes are genetically engineered into non-electrogenic host such as *E. coli* to make them electrogenic.[95, 96]

1.5.2 Electrogenicity in bio-electronic communication

However, the electron flow in reverse direction from electrodes to cells is not well characterized. Very first report on electrical stimuli responsive promoters in *E.coli* was published in 2001 where current was passed across cells for 30 mins and gene

expression profiles were studied.[97] Around 8 genes were upregulated and 42 were downregulated out of the total 1512 genes. Mild electrical induction in *Saccharomyces cerevisiae* led to elevated intracellular Ca^{2+} concentrations.[98] In the recent past, two synthetic biology devices have been published where electrical signals are used to drive gene expression from electrogenetic promoters.[99, 100] First device involved mammalian cells engineered with aldehyde responsive promoters. Electrical signals were used for electrochemical oxidation of ethanol to aldehyde and drive transgene expression from aldehyde promoters.[100] Second device displayed electrochemical activation of oxidative stress response promoter SoxRS in bacteria to drive transgene expression.[99] More details about the SoxRS system are in **Chapter 5**.

1.5.3 Synthetic transcription factors

A significant capacity addition in the field of electrogenetics would be the ability to target specific genes and regulate host transcriptional regulation using electric signals. Several synthetic transcription factors (TF) that enable controllable and tunable regulation of genes have been established. Zinc-Finger proteins (ZFP's), Transcription factor like effectors (TALEs) and CRISPR-Cas9 systems are some of the TF's that enable transcriptional regulation[101]. However, extensive protein engineering that is required for programming ZGP and TALEs makes them unattractive. On the other hand, the CRISPR-Cas9 based transcriptional factors are easily programmable to target various genes by changing a 20 bp sequence.[102] In **Chapter 5**, **I discuss the**

integration of the CRISPR-Cas9 system with electrogenetic SoxRS system to electrically modulate bacterial transcriptional regulation.

1.6 Summary of aims and contributions

In chapter 2 titled 'Modular Construction of Multi-Subunit Protein Complexes using engineered tags and microbial transglutaminase', I developed a facile method to assemble multi-subunit enzyme complexes for controlling metabolic flux as well as for construction of multifunctional complexes. This chapter was primarily designed and executed by me with the guidance from my advisor Dr. Bentley and was published in Metabolic Engineering[103] and Data in Brief[104].

In chapter 3 titled 'Facile Two-step Enzymatic Approach for Conjugating Proteins to Polysaccharide Chitosan at an Electrode Interface', I developed a transglutaminase based conjugation approach to assemble proteins and enzyme cascades on chitosan coated microchips. This chapter was primarily designed and executed by me with the guidance from my advisor Dr. Bentley and was published in Journal of Cell and Molecular Bioengineering[105].

In chapter 4 titled 'Engineered Tobacco Mosaic Virus -Virus Like Particles (TMV-VLP) as self-assembling 3D scaffolds for multi-enzyme assembly using mTG mediated conjugation', I developed TMV-VLP as self-assembling 3D scaffold to assemble a three-enzyme cascade on microchips. This chapter was primarily designed and executed by me with the guidance from my advisor Dr. Bentley. I engineered the

VLP's and Adam Brown from Culver Lab helped in the initial purification of particles and electron microscopy. Dr. Yi Liu from Payne Lab helped in the setting up of Quartz Crystal Microbalance (QCM) experiments. This chapter will be submitted for publication by March 2018.

In chapter 5 titled 'Integration of CRISPR with electrogenetic promoter systems for transcriptional regulation', I integrated the CRISPR-Cas9 based transcriptional regulation systems with the SoxRS electrogenetic promoter systems. This chapter was primarily designed and executed by me with the guidance from my advisor Dr. Bentley. Kristina Theresa Stephens, a graduate student in the Bentley Lab performed the AI-1 assays in the Appendix 1 and Eric VanArsdale, a graduate student in the Bentley Lab made the chitosan-alginate capsules in the Appendix 1. This chapter will be submitted for publication by March 2018.

Chapter 2 Modular Construction of Multi-Subunit Protein Complexes using engineered tags and microbial transglutaminase

This chapter is adopted from the following publications with permission

Bhokisham N. et al, Modular construction of multi-subunit protein complexes using engineered tags and microbial transglutaminase, Metabolic Engineering, Volume 38, November 2016, Pages 1-9.[103]

and

Bhokisham N. et al, Data on biochemical fluxes generated from biofabricated enzyme complexes assembled through engineered tags and microbial transglutaminase, Data in Brief, Volume 8, 2016, Pages 1031-1035.[106]

2.1 Introduction

Biofabrication is the assembly of biological components such as cells, tissues, proteins, polysaccharides, lipids, nucleic acids etc., using biological means or mimics thereof for the creation of devices and other functional constructs. These biological structures are often integrated within microfluidic and microelectronic systems where they execute an array of functions, including the biosensing of environmental samples [107-109] and toxicity and efficacy testing in lab-on-a-chip devices [19, 110-112]. Advances in genetic and protein engineering have enabled the design and construction of pathways that catalyze a diverse range of reaction products in an efficient manner [113, 114]. Most of these multistep biotransformation processes are located inside the

cells where enabling cofactors and effector molecules are also nearby. These networks, called metabolons, mediate a variety of enzymatic reactions and their construction and assembly can involve extensive metabolic engineering of the host. *In vitro* methods often feature simplified product recovery and minimal substrate toxicity [115, 116], but can suffer by providing limited access to needed co-factors and other effectors. Methods used for the *in vitro* construction of metabolons are many, including co-localization of enzymes via covalent crosslinking and entrapment of enzymes into nanostructures or containers [117, 118]. Additionally, immobilization on solid supports, such as protein scaffolds where enzyme modules are engineered for selective affinity to the scaffolds have appeared [119]. While advantages of crosslinking over entrapment include active site proximity and reduced resistance for substrate or product transport, there are few means to enable domain-specific assembly of component parts. Genetic methodologies can provide control over subunit arrangement and conformation[120], some require long linker peptides as well as extensive selective binding domains.

In this work, I enable metabolon construction by engineering subunits with simple, short linker tags (5-7aa). This linking system exploits the specificity of the crosslinking enzymes for assembly so that the tags provide for orientation of the to-be-assembled subunits. I demonstrate this concept by the assembly of two bacterial quorum sensing (QS) synthases, S-Ribosylhomocysteinase (LuxS) and S-Adenosyl homocysteine nucleosidase (Pfs). I further connected these enzymes to protein G, a *Streptococcal* bacterial protein that binds to the Fc region of IgG [112]. The QS enzymes act to

convert S-Adenosyl homocysteine (SAH) to homocysteine (HCY) and autoinducer-2 (AI-2), a QS signal molecule. I then targeted the protein G-QS enzyme complex to bacterial cells using anti-*E.coli* antibodies leading to biochemical reactions on surface of bacteria and site-specific delivery of the autoinducer to the cells.

In **Figure** 2-1 Schematic of mTG-mediated protein construction. depict the overall scheme for protein assembly. In **Figure** 2-1A, the first subunit is selectively bound to a solid support (Co^{2+} resin) via an N-terminal hexahistidine tag. Then, the second subunit engineered with lysine tags on both termini is covalently grafted using mTG onto the glutamine tag of the first subunit (Q tag). The reaction mechanism is shown in **Figure** 2-1B. Then, in **Figure** 2-1A, I depict linkage of a third subunit comprised of a Q-tag also on the C-terminus for the eventual assembly of many structures covering the bead. In all cases, microbial transglutaminase (mTG) is used to graft adjacent glutamine and lysine residues forming a trans-peptide bond [121-128]. The linker tags engineered onto subunits Pfs, LuxS and Protein G were either hepta-lysine (7aa) and/or penta-glutamine (5aa) [124] and crosslinking was mediated by the addition of microbial transglutaminase (mTG). Schemes for each protein, its tags, and cleavage of the histidine tags are included in **Figure** 2-1C. After using these methodologies to make complexes, I evaluated enzymatic flux to produce AI-2. I note that LuxS can be rate limiting [129, 130]; I altered stoichiometry to generate a Pfs-LuxS-LuxS complex, our hypothesis being that the overall rate might be increased. Finally, as noted above, I added a protein assembly domain, Protein G thereby creating Pfs-LuxS-Protein G complex that could be released from the Co^{2+} resin and further complexed with an

antibody to recognize bacteria. I targeted the released complexes to bacterial cells and elicited quorum-sensing responses from bacterial populations; our hypothesis being a change in phenotype that was correlated to the AI-2 synthesis flux through the complex.

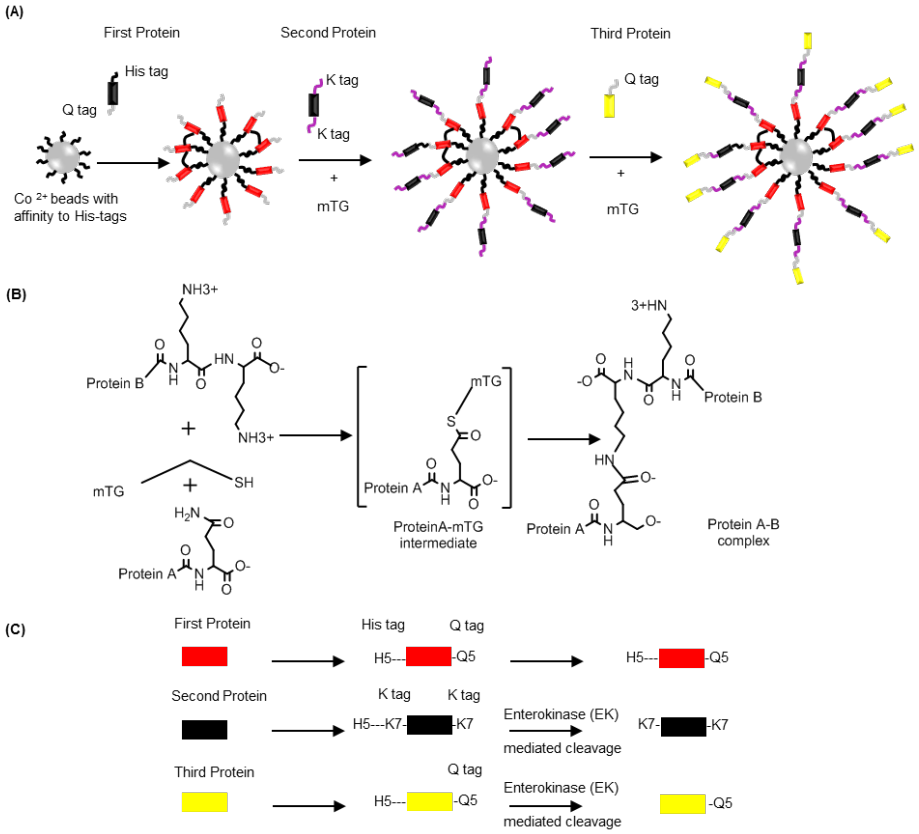

Figure 2-1 Schematic of mTG-mediated protein construction. (A) Scheme depicting construction of three subunit protein complex on beads using engineered tags and mTG. His tags are in black, Q tags in gray and K tags in purple. (B) Scheme for reaction catalyzed by mTG between glutamine of first subunit and lysine of second subunit to form a transpeptide bond between subunits. (C) Engineering subunits with lysine and glutamine tags. All subunits are engineered with His tags and enterokinase (EK) mediated cleavage is used to remove His tags in all subunits except the first subunit used for selective immobilization on the bead.

2.2 Materials and Methods

2.2.1 Plasmids and Strains

All plasmids and strains used in this study are listed in Table 2.1. I performed all cloning and transformations as per standard protocols [131]. Clone designation includes the tag and the employed terminus (e.g., pTrcHisA-7K-LuxS-7K indicates a LuxS vector with a 7-residue lysine tag at both the N- and C- termini, the expressed protein is denoted $_{K}L_{K}$). All primers (Integrated DNA Technologies) used for engineering of proteins in this study are summarized in Table 2.2. All the engineered DNA sequences utilized Xho-1 and EcoR1 restriction sites at 5' and 3' ends of the DNA fragments. For cloning purposes, DNA was ligated with TOPO Blunt II vector (Life Technologies) and transformed into TOP 10 cells. Plasmids were sequenced at the DNA Core Facility of the Institute for Bioscience and Biotechnology Research. For expression, genes were inserted into pTrcHisA plasmid (Lab stocks) and transformed into respective expression hosts. I transformed LuxS containing clones into RK 4353 (*pfs*$^{-}$) for expression of LuxS proteins and the BL21 (*luxS*$^{-}$) for expression of Pfs proteins. A His_6 tag is part of the pTrc plasmid backbone; all expressed proteins have N-terminal His tags. Importantly, all His tagged proteins also contain an enterokinase cleavage site located between the His tag and the K/Q linker tag in the primary sequence (**Figure** 2-1C).

Table 2-1: Strain names and nomenclature

Strain/Plasmid	Relevant Genotype and Property	Reference
Strains		
BL 21 *luxS*$^-$	B strain, F$^-$omp T[dcm] [Ion] hsd S(r_B $^-$, $M_B$$^-$) gal, Δ*luxS*	Lab stocks
RK 4353 *pfs*$^-$	RK 4353 strain, Δ*pfs*(8-226):: *kan*	Lab stocks
CT 104	W3110 strain, Δ*lsrFG*, Δ*luxS*	[132]
Plasmids		
pTrcHisA-LuxS-7K	pTrc derivative, expression of LuxS with lysine tag at C termini, Ap^r	[124]
pTrcHisA-7K-LuxS-7K	pTrc derivative, expression of LuxS with lysine tag at N and C termini, Ap^r	This study
pTrcHisA-LuxS-5Q	pTrc derivative, expression of LuxS with glutamine tag at C termini, Ap^r	[124]
pTrcHisA-Pfs-7K	pTrc derivative, expression of Pfs with lysine tag at C termini, Ap^r	[124]
pTrcHisA-7K-Pfs-7K	pTrc derivative, expression of Pfs with lysine tag at N and C termini, Ap^r	This study
pTrcHisA-7K-Pfs-5Q	pTrc derivative, expression of Pfs with lysine tag at N and glutamine tag at C termini, Ap^r	This study
pTrcHisA-Pfs-5Q	pTrc derivative, expression of Pfs with glutamine tag at C termini, Ap^r	[124]
pET-200 ProteinG-5Q	pET 200 derivative, expression of Protein-G with glutamine tag at C termini	Lab Stock
pCT 06	pFZY1 derivative, containing lsrR and lsrR binding region with T7RPol, Ap^r	[124]
pET-200 DsRed	pET200 derivative, expression of DsRed, Kn^r	Lab Stock

Table 2-2: Primer names and sequences

Primer Name	Sequence	Features
K-LuxS-K (Forward primer)	5'ggcaactcgagaaaaagaaaaagaaaaagaaaccgttgttagatagcttcacag3'	EcoR1 site and K tag
K-LuxS-K (Reverse primer)	5'gccttgaattctatttcttttttcttttttcttttttggcctgcaacttctctttcggc3'	Xho1 site and K tag
K-Pfs-K (Forward primer)	5'ggcaactcgagaaaaaaaaaaaaaaaaaaaaaaatgaaaatcggcatcat3'	EcoR1 site and K tag
K-Pfs-K (Reverse primer)	5'gccttgaattctatttttttttttttttttttttttgccatgtgcaagtttctgc3'	Xho1 site and K tag
K-Pfs-Q (Reverse primer)	5'gccttgaattctattgctgttgctgctggccatgtgcaagttt3'	Xho1 site and Q tag

2.2.2 Protein Purification

I grew the expression hosts in LB media (Sigma-Aldrich) and induced at OD_{600} of 0.4 with 1 mM IPTG (Sigma). After 4 hrs at 30°C, cells were centrifuged and resuspended in 15 mL of 10 mM phosphate buffered saline (PBS), pH 7.4 (Sigma) and sonicated for 15 min. Post sonication, lysed cells were centrifuged, soluble proteins were retained and purified via HiTrap columns (GE Healthcare). Purified proteins were subsequently dialyzed with PBS and stored at -20° C. I selectively removed His tags by incubation with enterokinase overnight at 4° C as per manufacturer's specifications (EK-Away, Invitrogen). To ensure robust transglutaminase reactions, I rewashed all proteins using a second round of Co^{2+} resin. This served as a quality control to ensure His tag removal. Proteins were stored for further use at -20° C.

2.2.3 Conjugation of Engineered proteins using mTG

I aliquoted 20µl of Talon Metal Affinity resin (Clonetech) in a centrifuge tube and centrifuged to remove residual buffer. To the pelleted resin, I added 10 µl His-tagged protein (concentration varied as noted) with C-terminal 'Q' tags. These were mixed well to mediate attachment of 'His' tagged proteins to resin. Next, I added 10 µl of mTG (Ajinomoto, enzyme activity of 12 U/mg) at concentrations to reflect the desired molecular ratio between reacting protein and mTG (indicated as **β)**, and mixed well at RT. Immediately, I also added 10µl of reacting 'K' tagged protein (concentration varied with experiments) to the protein-resin mix and incubated with shaking at room temperature for 60 min. After incubation, I washed the resin 3x with PBS to remove unbound proteins and residual mTG. In cases where a third subunit was attached, I added another round of subject protein with reaction mixtures exactly as before. To elute the conjugated proteins, I treated the resin with PBS+200mM Imidazole for 10 min on ice and later centrifuged to remove the eluted protein complexes from beads.

2.2.4 Measurement of Homocysteine using Ellman's Assay and Cyclic Voltammetry

I measured homocysteine using calorimetric Ellman's assay as described in [112] and electrochemically using cyclic voltammetry (CV) [133].

2.2.5 Construction of Antibody-Protein complexes

I built the Pfs-LuxS-Protein G complexes on beads as described above. To characterize quantities, I added 10 µg of FITC-labelled anti-*E.coli* antibodies (AbD Serotec) to the protein G-enzyme complexes on the beads and incubated at RT for 30 min. I washed three times using PBS to remove non-specifically or unbound antibodies. Later I eluted the antibody-bound Protein G-enzyme complexes from beads as described before and measured their fluorescence using a plate reader (SpectraMax). The final reaction volume was 200 µl for fluorescence measurements.

2.2.6 Flow Cytometry measurements for targeted enzyme reactions

To ascertain deployment capabilities of our constructed complexes, I eluted the Protein G-Pfs-LuxS complexes from beads, incubated them with FITC labelled anti-*E.coli* antibodies for 30 minutes, and quantified them via fluorescence microscopy and FACS. I grew *E. coli* CT104 cells [132] with pCT06 and pET-DsRed plasmids (Table S1) overnight at 30°C (they can respond to AI-2 by inducing DsRed expression [132]). I pelleted 0.1 OD of cells, incubated with 5% BSA for 30 min, and washed three times with PBS. I next incubated the cells with Antibody-Protein G-Enzyme complexes for 30 min and washed 3x with PBS to remove unbound antibodies and enzyme complexes. I pelleted the cells and incubated them with DPBS (Dulbecco's Phosphate buffered saline, Sigma) solution at 37°C without shaking. After 4 hours, I centrifuged the cells

and analyzed using flow cytometry. I used a minimum of 20,000 cells for analysis of each sample. I used FlowJo software for analysis and image generation[112].

2.3 Results

2.3.1 Reactivity of engineered K and Q tags mediated by mTG

I first studied the effect of engineered tags on the crosslinking of proteins freely suspended in buffer. In **Figure** 2-2, I incubated mTG with enzymes LuxS (L) and Pfs (P) without linker tags (Figure 2.2 Panels 1 and 2), LuxS with C-terminal K and Q tags (Panels 3 and 4), and Pfs with C-terminal K and Q tags. I used a **β** of 100 (**β**, the molar ratio of reacting subunit to mTG) and incubated at RT for 0, 15, 30 and 60 minutes (i.e., four lanes are depicted). I stopped the reactions via heat denaturation at 95°C for 5 minutes and assayed crosslinking by SDS-PAGE and Western blot using anti-His antibodies. I note that untagged LuxS and Pfs (L and P, respectively) exist as homodimers in their native states [134, 135] and without mTG treatment appear as monomers on gels under denaturing conditions. With mTG, native L and P formed small quantities of dimers after ~30-60 minutes (Figure 2.2 panels 1 and 2). Next, I incubated 'K' and 'Q' tagged LuxS (L_K and L_Q) with mTG under identical conditions as the native enzymes (Figure 2.2 panels 3 and 4). As noted in Methods, the prefix and suffix indicate tags at N and C termini, respectively. For example, L_K indicates LuxS with 'K' tag at the C terminus. While L_K formed dimers more readily than native L, L_Q actively cross-linked to form oligomers. The arrows indicate dimer, trimer and tetramer bands; the quantity of each increased with incubation time. Interestingly, Pfs with 'K' and 'Q' tags (P_K and P_Q, Figure 2.2 panels 5 & 6) reacted analogously to L_K and L_Q,

but with less oligomerization for the 'K' tag. While only showing two proteins, these data suggest the 'Q' tag is advantageous for mTG-mediated protein oligomerization. That is, 'Q' tagged protein cross-linked to itself more than untagged native proteins and those with 'K' tags.

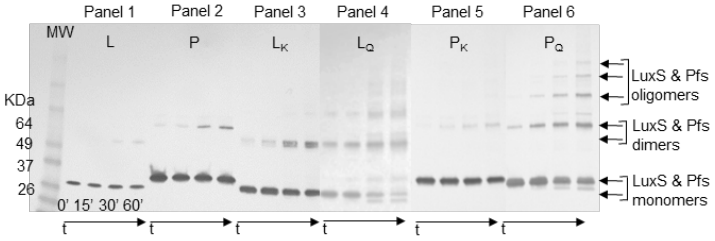

Figure 2-2 mTG mediated crosslinking of enzymes in solution. Western blots indicating the mTG-mediated crosslinking of soluble enzymes (duration, 60 min). Panels 1-6 indicate crosslinking of proteins L, P, L_K, L_Q, P_K and P_Q, respectively. Each panel has 4 lanes indicating 0, 15, 30 and 60 min reactions. Arrows indicate the monomers, dimers and trimers formed.

I next studied how **β** (molar ratio of the subunits to mTG) played a role in determining the extent of crosslinking of the engineered proteins. **Figure** 2-3 depicts mTG-mediated crosslinking of P_Q using mTG with varied **β** at two time points, 15 and 60 minutes. With **β** =1 (same amount of protein as mTG), a smear of P_Q was formed in both samples, whereas with **β** = 100 I observed well-defined dimers and trimers which increased with time. With **β** = 1000, P_Q was relatively unreactive at 15 minutes and formed dimers after 60 min. Similar time and molar ratio profiles of other engineered proteins are provided in **Figure** 2-4. In sum, these results indicate that **β**, the ratio of Q-tagged protein to transglutaminase influences the extent of oligomerization. The

mechanisms by which this appears to function are unclear, but the trends observed could be anticipated (e.g., more enzyme, more crosslinking).

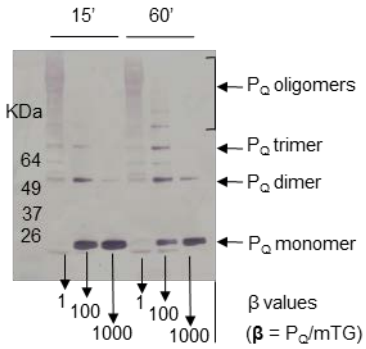

Figure 2-3 Kinetics of mTG mediated crosslinking of P_Q. Western blots indicating progression of crosslinking of soluble P_Q at 15 and 60 min with different **β**'s (**β** is the ratio of P_Q to mTG).

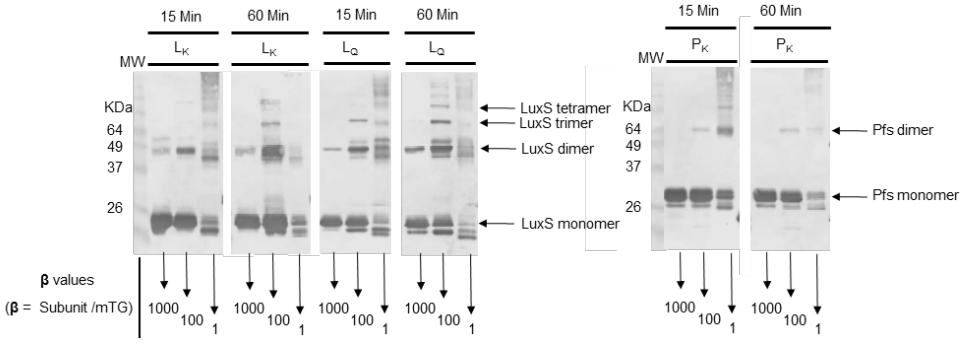

Figure 2-4 Kinetics of mTG mediated crosslinking of L_K, L_Q and P_K. Western blots indicating progression of crosslinking of soluble L_K, L_Q and P_K at 15 and 60 min with different β's (β is the ratio of P_Q to mTG). Three lanes in each panel indicates β of 1000, 100 and 1 respectively. Left panels indicate L_K and L_Q crosslinking at 15 and 60 minutes. Right panels indicate P_K crosslinking at 15 and 60 minutes. Arrows indicate the monomers, dimers and trimers formed. MW indicates molecular weight.

I next tested the kinetics associated with conjugating two different enzymes together and whether the linked AI-2 synthesis pathway could function to make AI-2. In this case, I employed both 'Q' and 'K' tagged proteins. I also note that Pfs-LuxS chimera have been expressed as an intact fusion protein in *E. coli* and when purified and resuspended in buffer with SAH, produces AI-2 [112]. Thus, the test here evaluates whether LuxS and Pfs can be crosslinked using the engineered 'K' and 'Q' to produce AI-2. Both P_Q and L_K were reacted with mTG with a **β** of 100 for 60 minutes (**Figure** 2-5). I found a preponderance of homodimers, rather than heterodimers when cross-linked in solution.

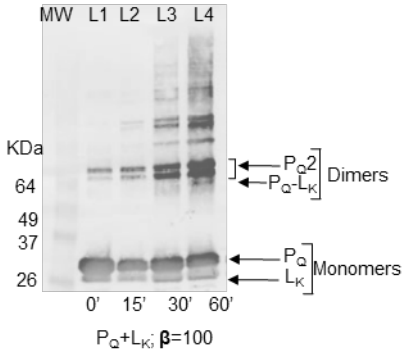

Figure 2-5 Crosslinking of Pfs and LuxS in solution using mTG. Crosslinking of L_K and P_Q mediated by mTG in solution is indicated with four time points (0 to 60 min in lanes L1-L4, respectively).

To explore whether I could promote heterodimer formation and selectively remove homodimers, I first assembled one 'anchor' protein on Co^{2+} affinity resin using the N-terminal His tag, the aim being to restrict access to the N-terminal fusion tag. I then cross-linked the second protein to the first while on the bead using the mTG and

associated fusion tags. For this, the second subunit was treated with enterokinase (EK) to remove N-terminal His tags (Methods), precluding subsequent His-mediated assembly on the Co^{2+} resin. After reaction with mTG for 60 minutes, I washed the beads 3x with PBS to remove unreacted subunits and mTG. I then eluted the cross-linked subunits from beads via ion exchange (Methods) and assayed using Western blots. In lane L1 of left blot in **Figure** 2-6, unreacted P_Q was loaded as control. In lane L2, I reacted P_Q with mTG for 60 min with a **β** of 100 and observed oligomerization as in the case of reactions in solution (**Figure** 2-5). In L3, I show heterodimer formation on the beads by the creation of P_Q-L_K. That is, to the bead bound first subunit, P_Q, a second subunit engineered with 'K' tags were added (in this case $_KL_K$; LuxS with 'K' tags at both N and C termini) along with mTG at **β** of 100. P_Q-$_KL_K$ heterodimers were revealed as a lighter band than the homodimers (e.g., P_Q2). In addition to P_Q-$_KL_K$, I observed P_Q2-$_KL_K$ heterotrimers, all indicating crosslinking of Pfs and LuxS enzymes. Control reactions where the second subunits had no engineered tags yielded no heterodimers indicating the importance of engineered lysine tags to mediate heterodimer formation (**Figure** 2-7). As expected, the lack of mTG for crosslinking also yielded no heterodimers (**Figure** 2-7). Under these crosslinking conditions with **β** = 100, by image analysis I estimate that ~25% of Pfs enzymes were crosslinked to LuxS (**Figure** 2-8). The crosslinking percentage can be improved by employing **β** of 1. However, in this condition the ability to discern heterodimers and homodimers under denaturing SDS gel is diminished (as seen in **Figure** 2-3). To decrease side product formation, I switched the positions of Lys and Gln tagged proteins in our bead-based system

(**Figure** 2-6, blot on the right). I observed a reduction in nonspecific product formation in comparison to when Gln tagged proteins were immobilized on the bead.

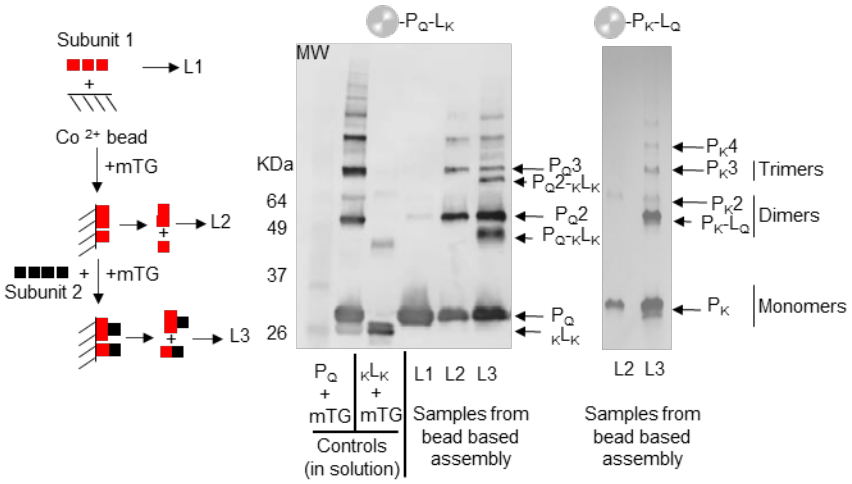

Figure 2-6 Modular construction of multi subunit complexes. **(**Left) Scheme depicting modular construction of protein complexes on beads. (Right) Samples were isolated and analyzed via Western blot (L1, L2 and L3). Controls including soluble PQ and KLK incubated with mTG at a β of 100. (LK indicates LuxS with lysine tag at C-terminus).

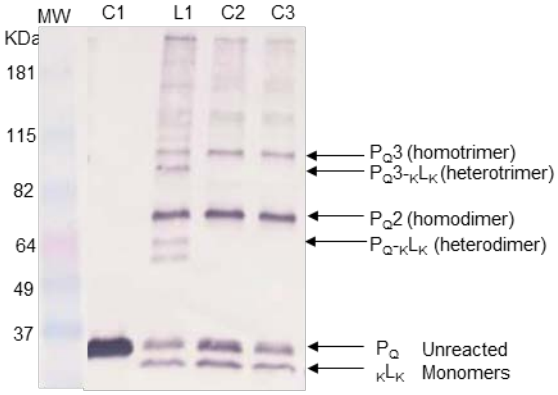

Figure 2-7 Controls of mTG mediated modular construction. Western blot indicating controls for Figure 2-5. Lane C1 contains the PQ without mTG treatment. Lane L1 contains PQ crosslinked to KLK using mTG. Lane C2 contains same as L1

without mTG. Lane C3 contains PQ crosslinked to native LuxS (L) with mTG. Arrows indicate the monomers, dimers and trimers formed. MW indicates molecular weight.

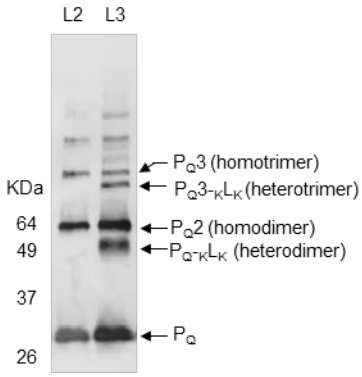

Oligomers	L2 (Mean±SE)	L3 (Mean±SE)
P_Q	46.8 ± .5	39.1 ± 1.1
P_Q2	36.9 ± .2	26.2 ± .4
P_Q3	10.1 ± .2	3.6 ± .1
P_Q4	6.1 ± .1	3.5 ± .03
P_Q5	0	1.75 ± .01
P_Q-$_K L_K$	0	20 ± .4
P_Q2-$_K L_K$	0	5.7 ± .2

Figure 2-8 Estimation of formation of heterodimers through ImageJ. The two lanes L2 and L3 from Figure 2-5 (**Left**) are used to analyze relative percentages of various oligomers using ImageJ. Table (**Right**) indicates the relative percentages of various structures in each lane. Mean and standard error were calculated using 3 measurements from the same blot.

In summary, these results indicated that lysine and glutamine rich tags engineered onto the C- and N-termini of the two AI-2 synthases enabled crosslinking, but additional measures (binding to Co2+ spheres) were needed to guide linkages to form heterodimers. That is, selective immobilization on beads when combined with engineered tags and mTG, lead to somewhat improved formation of heterodimers, but exclusivity was not demonstrated.

2.3.2 mTG mediated control of metabolic flux

I next explored the capability of these assembled enzymes to mediate metabolic flux (in this study, I defined flux as the rate of product generated per unit time by the assembled complexes). Pfs and LuxS are bacterial enzymes involved in the activated methyl cycle and act together to convert S-Adenosyl homocysteine (SAH) into homocysteine (HCY) and (S)-4,5-dihydroxy-2,3-pentanedione (DPD) in a two-step process [136] ultimately yielding autoinducer-2 (AI-2) which is normally secreted by bacteria (**Figure** 2-9). I hypothesized that (i) the engineering tags would not destroy activity, and (ii) that proteins coupled by mTG would retain activity providing complete pathway synthesis. Further, I hypothesized that the proximity of the coupled enzymes could provide efficient substrate utilization.

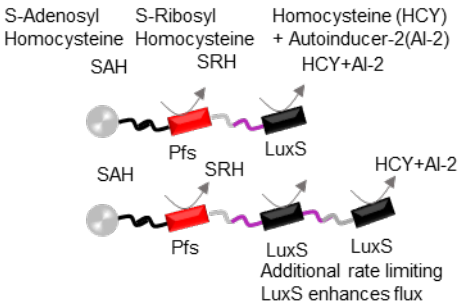

Figure 2-9 Scheme of Pfs-LuxS and Pfs-LuxS-LuxS complexes using mTG to mediate biochemical flux.

In **Figure** 2-10, I immobilized 3µM 'Q' tagged Pfs on Co^{2+} beads as before and crosslinked with 3µM of corresponding 'K' tagged second subunit (L_K) by mTG (as in **Figure** 2-6). In this case, to ensure crosslinking, I incubated reactants at RT for 60

min and **β** = 1. As before, I washed the beads 3x with PBS to remove unreacted enzyme and mTG. I then incubated bead bound enzyme complexes with 1mM SAH at 37°C for 60 min. I measured homocysteine (HCY) using a colorimetric assay (Ellman's sulfhydryl assay, see Methods). Homocysteine levels were markedly different in samples with and without mTG. When coupled with Western oligomerization data, these results indicate that mTG-crosslinked LuxS and Pfs function to make homocysteine.

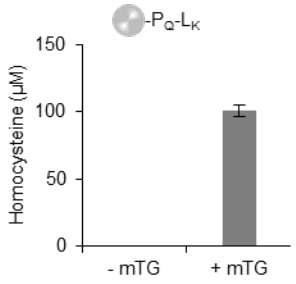

Figure 2-10 Assembly of Pfs-LuxS complex on the bead Pfs-LuxS complex assembled on the bead can mediate flux. Pfs enzyme is assembled on beads and LuxS is crosslinked to Pfs using mTG (with **β** = 1). After wash, the assembled Pfs-LuxS complex is incubated with 1mM SAH and HCY generated is measured biochemically through Ellman's assay after 1 hour incubation at 37°C.

I next studied if I could change the yield of homocysteine by varying the subunit quantities in the crosslinked complexes (**Figure** 2-11). With bead-bound P_Q held constant, I varied the concentrations of L_K and crosslinked exactly as before. After washing 3x with PBS, the beads were incubated with 2mM SAH for 60 minutes and HCY generated was measured. Importantly, I found a linear increase in HCY generated with incubated LuxS concentration, suggesting LuxS rate limitation. As controls, I

performed exactly analogous experiments using native L (without 'K' tag), and there was no significant accumulation of HCY indicating minimal non-specific binding of the LuxS to either the resin or the loaded Pfs. This also indicated that mTG preferentially recognized 'K' and 'Q' tags more than any exposed lysine or glutamine residues on the enzyme subunits. Having demonstrated L_K reacted with Co^{2+} immobilized P_Q, I next studied how bi-tagged LuxS ($_KL_K$, LuxS with 'K' tag at both N and C termini) could crosslink to P_Q. Again, as before, I crosslinked $_KL_K$ with P_Q using mTG. I then provided SAH and observed for HCY generated (**Figure** 2-14). Interestingly, the HCY doubled, perhaps suggesting an advantage to having 'K' residues on each end of the enzyme. Western blots (**Figure** 2-13) indeed showed enhanced crosslinking of $_KL_K$ to P_Q (relative to L_K); correlating with HCY yields determined by Ellman's assay.

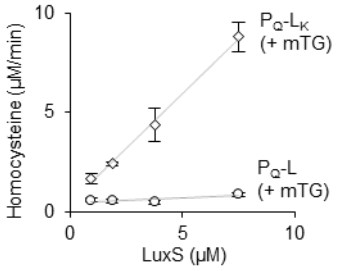

Figure 2-11 Increase in HCY obtained from crosslinking varying concentrations of LuxS to Pfs. Enzymes were incubated with 2mM SAH for 60 mins and HCY was measured using Ellman's assay. Trend lines denote linear best fit.

In **Figure** 2-12, I sought to assemble Pfs-LuxS-LuxS trimers on beads to enhance LuxS activity relative to Pfs, thereby increasing the overall reaction rate. To the P_Q-$_KL_K$ complex initially built on beads, I added L_Q and mTG for a second round of crosslinking exactly as before, expecting that any unreacted lysine tags on $_KL_K$ could crosslink to L_Q. After washing 3x, I provided 1mM SAH, observed for HCY yields using Ellman's assay after incubation for 60 min at 37°C. As anticipated, putative three-subunit complexes enhanced the biochemical flux resulting in increased generation of HCY. Negative controls with non-tagged L exhibited no increase in homocysteine and importantly, an incremental increase in yield was observed as the second incubation with LuxS was performed with higher LuxS concentration (from 1.5 to 3 µM). Subsequent increases in LuxS resulted in no net gain in reaction, suggesting matching of LuxS with Pfs activity. Also, I note that all three subunit complexes were built on the two-subunit complexes from the 3µM LuxS incubation, and in all cases the yields of all three subunit complexes were higher than the corresponding two subunit complexes on which they were built. As controls, I built analogous two and three subunit structures without mTG and all of them generated negligible yields of HCY indicating the crosslinking was mediated by mTG. **Figure** 2-15 depicts HCY generation for an extended duration (240 min) from different Pfs-LuxS complexes. In these data, the three-subunit complex (P_Q-$_KL_K$-L_Q) enabled faster reaction flux than the two-subunit complexes (P_Q-$_KL_K$) which, in turn, were faster than the first P_Q-L_K complex. Controls for these experiments were again structures built without mTG and as expected, controls resulted in negligible reaction.

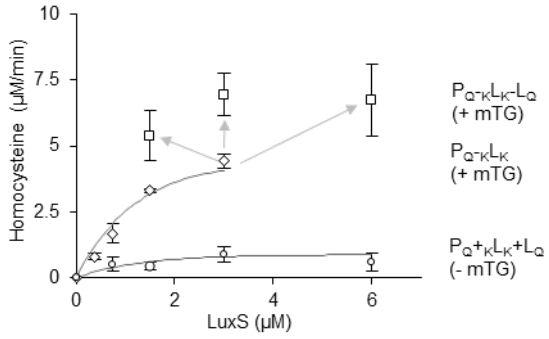

Figure 2-12 Construction of two and three subunit enzyme complexes on beads. Three subunit complexes are built onto two subunit complexes constructed with 3µM LuxS. Assembled complexes were incubated with 1mM SAH for 60 min and HCY was measured using Ellman's assay. Trend lines denote non-linear regression fit using equation $y=y_{max}(1\text{-}\exp(-kx))$.

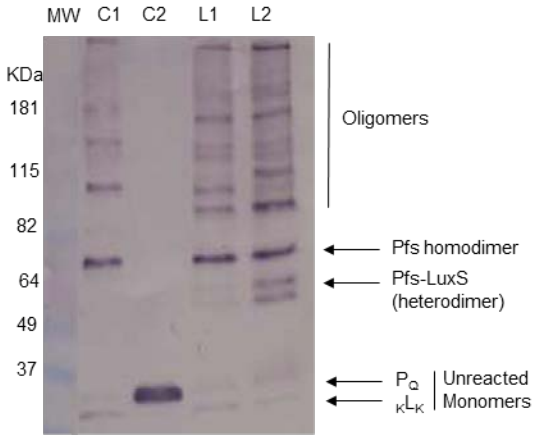

Figure 2-13 Western blot indicating the differences in crosslinking of L_K and $_K L_K$ to P_Q. Lanes C1 and C2 indicate controls. C1 is P_Q assembled on the bead and crosslinked with mTG. Lane C2 is P_Q with L_K without mTG. Lane L1 is P_Q crosslinked to L_K using mTG. Lane L2 is P_Q crosslinked to $_K L_K$ using mTG. Arrows indicate the monomers, dimers and trimers formed. MW indicates molecular weight. Pfs assembled on the bead is engineered with His tag at N termini. Anti-His antibodies are used in western blots to identify Pfs and Pfs linked structures.

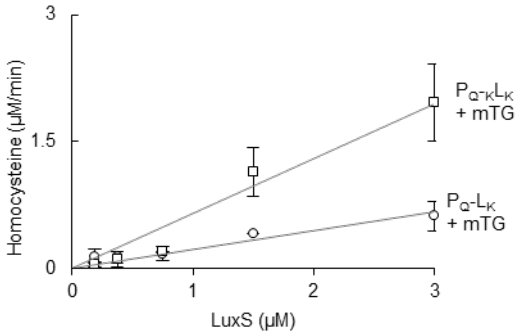

Figure 2-14 Differences in crosslinking between L_K and $_KL_K$ to P_Q. P_Q -$_KL_K$ and P_Q- L_K complexes are assembled on beads and incubated with 1mM SAH for 1 hour at 37°C. Homocysteine generated is measured by Ellman's Assay after 1 hour. Error bars indicate standard deviation with n=3. Regressed lines included denote linear best fit.

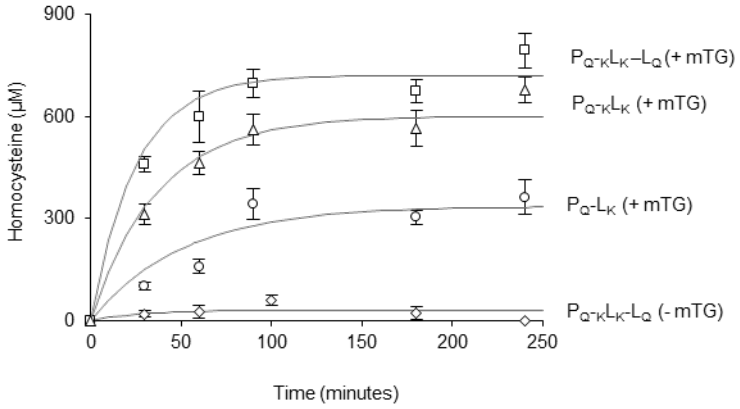

Figure 2-15 Time course measurements of homocysteine from two subunit and three complexes. Time course measurements of homocysteine from two subunit (P_Q-L_K and P_Q-$_KL_K$) and three subunit (P_Q-$_KL_K$ -L_Q) complexes measured by Ellman's

Assay. Error bars indicate standard deviation with n=3. Trend lines denote non-linear regression fit using equation $y=y_{max}(1-\exp(-kx))$.

Interestingly, results from western blots were inconclusive for trimer construction, suggesting non-conformationally assembled enzymes. Thus, in **Figure** 2-16, I examined in more detail, the differences in HCY generated by the addition of third subunit. That is, I built two and three subunit complexes as before but in one case, I replaced the $_{K}L_{K}$ with an *inactive* subunit (**I $_{K}$L$_{K}$**, obtained from periodic freeze thawing). The inactive subunit provided no enzyme activity, but should have retained its crosslinking capability. I built three-subunit complexes with the inactive LuxS as the second subunit exactly as before and compared HCY yields against controls. Specifically, I had a two-subunit inactive complex and a three-subunit complex built on the two subunit inactive complex without mTG. I provided these complexes with SAH and observed HCY in real time using cyclic voltammetry and the results obtained are correlated to homocysteine concentrations [29]. Results indicated that the highest flux was obtained for the Pfs-LuxS-LuxS trimer, as expected. The next highest reaction rate was observed for the Pfs-LuxS dimer. Fluxes generated from the 3-subunit complexes built with an inactive second subunit LuxS (w & w/out mTG) were lower than the flux generated by two-subunit complexes built with active LuxS. It is noteworthy that the Pfs-inactive LuxS-LuxS construct exhibited almost exactly one half the activity of the Pfs-LuxS-LuxS construct. Additional tests were performed with varied Pfs (data not shown) where Pfs-Pfs-LuxS complexes were built and the flux

generated from the Pfs-Pfs-LuxS complexes were lower than the Pfs-LuxS complex. I note, however, that in these cases the maximum activity was obtained by the addition of 6 μM LuxS and this was similar to the maximum activity observed for the Pfs-LuxS construct built with 3 μM LuxS, again suggesting LuxS rate limitation. In sum, these results could be rationalized by at least two factors: (1) the extra spacing (either partially inactive LuxS or Pfs between active Pfs and LuxS enzymes contributes to a reduced reaction rate; and/or (2) there is less binding of third subunits to second subunits than of second subunits to first subunits. Results from **Figure** 2-12 illustrate that the addition of the third subunit depends on its concentration, thus some level of optimization is needed to maximize linkage to the second subunit and even after optimization, results may not show as much linkage as a second subunit to its first.

Thus, data in **Figure** 2-10 - **Figure** 2-16 demonstrate that I built two and three subunit crosslinked complexes on beads using engineered ‘Q’ and ‘K’ tags and mTG. The complexes assembled were shown to display altered reaction kinetics based on the number of rate-limiting enzymes. In addition, I found that as the number of desired enzymatic subunits to be crosslinked was increased, the per enzyme reaction rate decreased, suggesting need for further examination and/or a limitation of this approach.

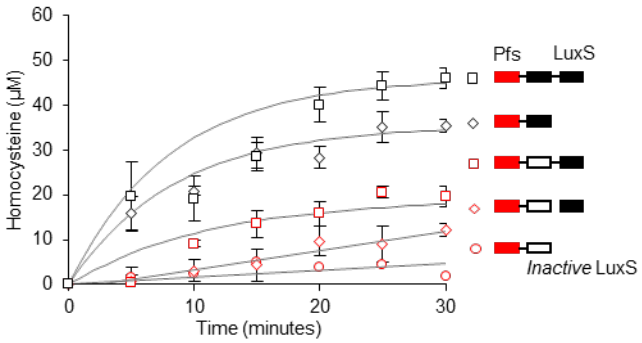

Figure 2-16 Real time HCY generated from two and three subunit complexes measured electrochemically through cyclic voltammetry. Complexes involving *Inactive* $_{K}L_{K}$ are indicated with red markers while complexes with active LuxS are indicated with black markers. Error bars in all cases represent standard deviation with n = 3. Trend lines for data in red circles and diamonds denote linear best fit. Trend lines for rest of the data are generated through non-linear regression fit. Non-linear regression fit is obtained using equation $y=y_{max}(1-\exp(-kx))$.

2.3.3 Assembly of multi-functional complexes using mTG

Beyond linkage of biosynthetic enzymes, I next studied whether mTG mediated cross-linking could be used for the construction of multi-functional protein complexes, again in a flexible manner. In addition, I wanted to explore further the limitations found by sequentially attaching two LuxS enzymes. I constructed a Pfs-LuxS complex (as before) but then coupled this with *Streptococcal* protein G [137]. Protein G has the ability to bind the Fc region of IgG. I suggest this enables the assembly of covalently tethered complexes with targeting antibodies, enabling the localized generation of reaction products. In our case, I first sought to create a Pfs-LuxS-Protein G complex

that could be coupled with anti-*E. coli* antibodies in order to direct the enzymes to the surface of *E. coli* (**Figure** 2-17) for localized AI-2 synthesis.

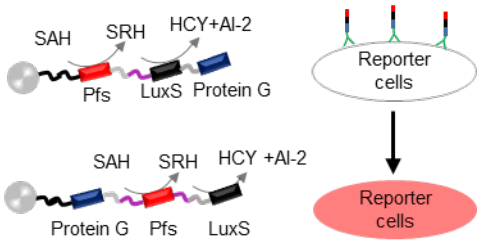

Figure 2-17 Scheme depicting construction of multifunctional complexes on beads. Pfs-LuxS-ProteinG complexes are assembled on beads and transplanted to reporter cells to mediate varied metabolic response.

I first studied whether protein G could be crosslinked to Pfs-LuxS complexes using the same linking motif ('L' and/or 'Q' tags). That is, I sought to create Pfs-LuxS-Protein G complexes comprised of P_Q, $_KL_K$ and G_Q (protein G engineered with 'Q' tag at C terminus). I loaded P_Q on the beads and crosslinked the second subunit ($_KL_K$) using mTG for 60 min at RT with **β** = 1. After washing the beads 3x with PBS, I crosslinked G_Q as before. I used Dylight 633-labeled protein G for visualization. Beads were again washed 3x to remove unbound protein G. Analogous to the LuxS-capped complexes, controls for these tests were two subunit complexes, incubated with labeled G_Q but without mTG. I eluted the assembled complexes from beads and measured fluorescence (**Figure** 2-18). I found the fluorescence from complexes built with mTG was proportional to the concentration of G_Q added, again suggesting crosslinking limitation with protein G (as with LuxS previously). Interestingly, however, a doubling

of protein G yielded a doubling of fluorescence, suggesting that incremental protein G was fully linked to the two subunit complexes. Analogous controls built without mTG had negligible fluorescence indicating lack of G_Q crosslinking. Importantly, these results support our hypothesis that the third subunit, G_Q, was bound to two-subunit complexes on the beads.

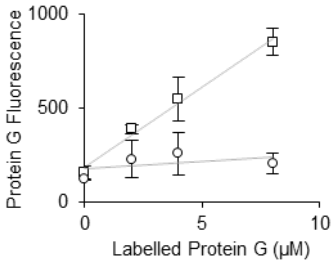

Figure 2-18 Construction of Pfs-LuxS-Protein G complex. Assembly of Pfs-LuxS-ProteinG complex is shown by crosslinking Protein G labelled with Dylight 633 fluorescent dye to Pfs-LuxS complexes on the bead. Assembled complexes are eluted from beads to measure fluorescence using plate reader. Trend lines denote linear best fit.

To further evaluate assembly, I added 10 μg of FITC-labelled antibodies to these three-subunit complexes (unlabeled in this case). After incubation for 30 minutes, I washed the beads 3x with PBS to remove unbound IgG and eluted the protein complexes from beads via ion exchange. I measured fluorescence of the complexes "loaded" with the labelled antibodies (**Figure** 2-19) and found a linear increase with antibody until ~5 μM, when the fluorescence appeared to saturate. Corresponding controls consisted of the same incubations but without mTG; there was minimal fluorescence in all samples indicating the absence of protein G crosslinking and the

lack of antibody assembly. These data support our original hypothesis that IgG bind protein G that, in turn, are the terminal addition to P_{Q}- $_{K}L_{K}$ complexes. Moreover, the additional antibody was nearly stoichiometrically similar to the added protein G (e.g., antibody, provided in excess, was bound in proportion to the added protein G until 8µM, when fluorescence became saturated). Being a 'third' subunit, these data suggest that a progressive inefficiency of subunit addition may not have been a primary factor for the decreased flux observed in **Figure** 2-16(albeit this addition is not enzymatically mediated).

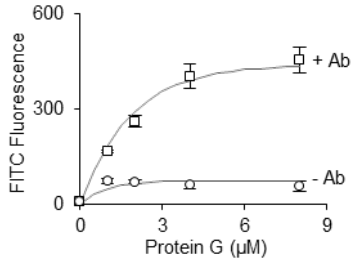

Figure 2-19 Binding of antibodies to Protein G in Protein-Enzyme complex. Antibody binding to the Pfs-LuxS-Protein G complex is measured by loading the Pfs-LuxS-Protein G complex on the beads with FITC-labelled antibody. Assembled protein-antibody complexes are later eluted to measure the FITC fluorescence in plate reader. Trend lines denote non-linear regression fit using equation $y=y_{max}(1-\exp(-kx))$.

I then tested whether the assembled three-subunit ($P_{Q\text{-}K}L_{K}\text{-}G_{Q}$) complexes retained enzymatic activity. Three-subunit complexes were assembled on beads using mTG exactly as before. Control tests were performed on two-subunit complexes without protein G ($P_{Q\text{-}K}L_{K}$). I provided the bead bound complexes with substrate 1mM SAH, incubated for 60 minutes at 37°C and measured HCY. I found $P_{Q\text{-}K}L_{K}\text{-}G_{Q}$ complexes

resulted in 4-fold lower homocysteine levels than $P_{Q\text{-}K}L_K$ complexes (without protein G), suggesting that addition of Protein G to $_KL_K$ resulted in a significant decrease in enzymatic activity ($p < 0.05$) (**Figure** 2-20). I then replaced protein G with EGFP (E_Q, EGFP with Q at C terminus) to test whether this effect was subunit specific; the decrease in HCY was similar (**Figure** 2-21) suggesting crosslinking of an additional subunit to LuxS in a Pfs-LuxS two-subunit complex resulted in reduction in enzyme activity. Recall that our previous tests suggested that LuxS was limiting, so I suspected the additional subunit might have interfered with the first LuxS activity (e.g., linked on both termini). I then changed the relative positions of the subunits creating a $G_Q\text{-}_KP_K\text{-}L_Q$ complex where LuxS was added at the end. Thus, I assembled G_Q first and created $G_Q\text{-}_KP_K\text{-}L_Q$ using mTG exactly as before. In this configuration, HCY yields from $G_Q\text{-}_KP_K\text{-}L_Q$ were lower but not significantly different from $P_{Q\text{-}K}L_K$ ($p > 0.05$) (**Figure** 2-20) indicating that the subunit re-arrangement had rescued the original enzymatic activity. The slight decrease could have been attributed to decreased linkage of LuxS as a third subunit. Overall, these data highlight the flexibility of our modular construction approach for building multi-subunit complexes through enzyme mediated termini-specific linkage.

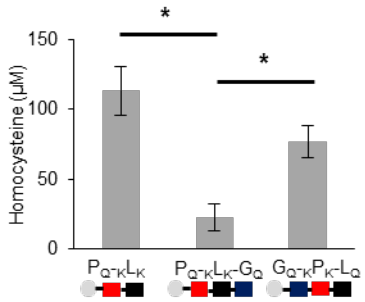

Figure 2-20 Effect of sequence of crosslinking of enzymes on enzyme complex activity. Change in order of crosslinking leads to altered enzymatic activity. Assembled enzyme-Protein G protein complexes are incubated with 1mM SAH for 1 hour at 37°C and HCY yields generated is measured using Ellman's assay. One tailed unpaired student t test is performed between samples (* indicates $p < 0.05$).

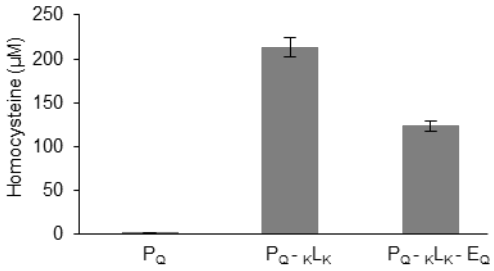

Figure 2-21 Effect of addition of non-enzyme components to enzyme complexes. Addition of EGFP leads to decrease in enzyme activity of Pfs-LuxS complex. Assembled protein complexes (Pfs-LuxS and Pfs-LuxS-EGFP) were incubated with 1mM SAH for 2 hours at 37°C and HCY generated was measured using Ellman's assay. Error bars indicate standard deviation with n=3.

2.3.3.1 Deployment of Multifunctional Complexes

I next tested if I could 'build' and 'transplant' our protein complex to antibody-targeted sites where they could carry out enzymatic reactions. I built $P_{Q\text{-}K}L_{K\text{-}}G_Q$ and $G_{Q\text{-}K}P_{K\text{-}}L_Q$ complexes on the beads using mTG, as before. I eluted these protein complexes from the beads and incubated with FITC labelled anti-*E.coli* antibodies. After 30 minutes, I added the enzyme-antibody complexes to *E. coli* CT104 reporter cells (these cells respond to AI-2 with DsRed fluorescent protein expression [132]). I note that AI-2 is a byproduct generated with HCY in equimolar amounts by the enzyme complexes. After an incubation time of 30 minutes, I washed the cells 3x with PBS to remove unbound protein-antibody complexes and suspended the cells in DPBS (Dulbecco's Phosphate Buffered Saline) solution containing 1mM SAH at 30°C for 4 hours without shaking. I used FACS to analyze the bacterial populations for their DsRed fluorescence. Controls for these experiments were the cells incubated with protein complexes but without the anti-*E.coli* antibodies. Representative fluorescence microscopy images of the experimental and control bacterial populations are provided in **Figure** 2-23 in [105]. Notably, populations incubated with antibody coupled enzyme complexes displayed ~15-fold more fluorescence overall than controls indicating that antibody bound complexes attached to bacterial cells, they were active, and synthesized AI-2 was delivered to the cells wherein they responded by altered gene expression (**Figure** 2-22). Between the populations coupled with antibodies and enzyme complexes, there were significant differences in Mean Fluorescence Intensities (MFI).

That is, populations with Ab-G_{Q}-$_{K}P_{K}$-L_{Q} complexes had 6-fold higher mean fluorescence intensity than the populations with P_{Q}-$_{K}L_{K}$-G_{Q}-Ab (**Figure** 2-22). The differences in AI-2/HCY yields from complexes G_{Q}-$_{K}P_{K}$-L_{Q} and P_{Q}-$_{K}L_{K}$-G_{Q} measured in **Figure** 2-22 correlated well with bacterial population's MFI in **Figure** 2-22. These results indicate that differences in enzyme activity that stem from the order of assembly were replicated by changes in gene expression of the cells exposed to the same complexes.

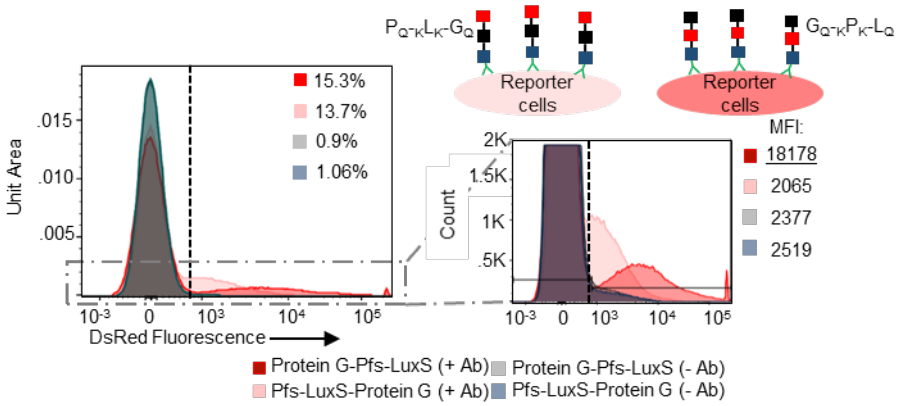

Figure 2-22 Flow cytometry analysis of reporter cells deployed with ProteinG-enzyme complexes. Deployment of multi-functional complexes to E. coli CT104 (reporter) cells and flow cytometry analysis to measure DsRed fluorescence from reporter cells. Cells fluorescing from coupling of Pfs-LuxS-Protein G and Protein G-Pfs-LuxS complexes are compared. Control populations were incubated with enzyme-Protein G complexes without antibodies. MFI indicates the mean fluorescence intensities. Error bars indicate standard deviation for a sample size of n = 3.

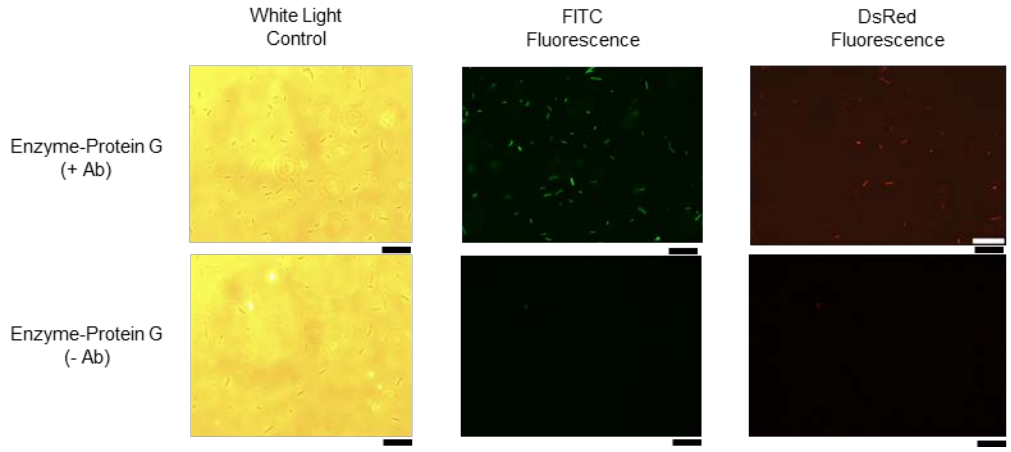

Figure 2-23 Fluorescence microscopy images of reporter cells deployed with ProteinG-enzyme complexes. Fluorescence microscopy images of DsRed protein expression in E. coli CT104 reporter cells used in **Figure** 1.22. Top row images: Cells incubated with Enzyme-Protein G complexes coupled with antibodies. Bottom row images: Cells incubated with Enzyme-Protein G complexes without antibodies. Antibodies are labelled with FITC. Scale bar: 50 µm.

2.4 Discussion

In this work, I demonstrate a facile method for the assembly of multi-subunit protein complexes using engineered N- and C-terminal ‘Q’ and ‘K’ tags that are coupled using mTG on solid supports. I built a two-enzyme metabolon involving bacterial QS enzymes Pfs and LuxS and displayed control of metabolic flux across these enzymes. Through this method, I was also able to build a multi-functional Pfs-LuxS-Protein G complex that was eluted from assembly beads and used for specific targeted enzyme applications. I displayed modularity and versatility in construction by switching of positions of the subunits in the multi-subunit complexes.

2.4.1 Insights on structural variation using transglutaminase based conjugation approach:

In enzyme based protein conjugation approaches, there is a strong inverse correlation between the specificity of conjugation and the quantity of specific conjugation products. Several different conjugation tags have been designed specifically for the mTG mediated conjugation chemistry to generate specific heterodimers and in most cases, the conjugation tag is comprised of a single lysine or a glutamine residue to facilitate specific conjugation[126]. However, in these cases, very low amounts of specific heterodimers were formed and various purification methodologies like size exclusion chromatography or salt precipitation needs to be employed to isolate these specific structures. To enhance conjugation, the number of lysines and glutamine residues can be increased in the conjugation tags at the expense

of specificity. The balance between the percentage of conjugation and the specificity of conjugation needs to be ascertained on a case by case basis keeping in mind the relevant context and application for which the conjugation is employed.

For construction of enzyme cascades under the biodevice context, I heuristically created conjugation tags comprising of seven lysine and five glutamine residues to facilitate enhanced conjugation of enzymes. Addition of mTG to Lys and Gln engineered proteins in solution resulted in more homodimer formation rather than heterodimers (**Figure** 2-5) and hence to drive heterodimer formation, I adopted bead based conjugation approach. Under this approach, I optimized several factors that contributed to reduction of side products including **β** (the ratio between subunit and mTG), the position of K and Q tagged proteins in the bead based crosslinking process, and the duration of crosslinking. Firstly, **β** had a positive correlation with the extent of crosslinking overall. While I employed **β** of 100 for crosslinking to get 25% heterodimerization in **Figure** 2-8, I also observed decreased yield of crosslinked protein. On the other hand, I could decrease the **β** from 100 to 1 and obtain higher levels of protein conjugation, but at the cost of increased construct heterogeneity (**Figure** 2-3).

Secondly, positions of Q and K tagged proteins also provide a basis for control. While the 'Q' tags caused self-oligomerization when treated with mTG, I did not observe the same with lysine ('K') tags (**Figure** 2-2). This behavior of Q tags can be attributed to the two-step reaction catalyzed by mTG, where first, the glutamines in the 'Q' tag can readily interact with mTG to form an intermediate complex that can then

attack the lysines nearby. Considering that the proteins tested here exist as dimers, there is increased propensity to target lysines of their own leading to homo-oligomerization than target other enzymes or proteins. For the proteins engineered with 'K' tags, the glutamines present on the proteins are inaccessible to mTG, thereby making them inert to intra-crosslinking [138]. Hence, when positions of Q and K tagged proteins are switched, with K tag on the bead and Q tag in solution, the K tag is inert to mTG leading to reduced side products. Once the soluble Q tagged second subunit is added, mTG can react with its glutamine tag and mediate crosslinking. However, the percentage of crosslinking can remain low because the mTG-Gln intermediate complex can potentially crosslink to any soluble lysine, get washed away, or get hydrolyzed to form glutamate. Other conditions including temperature (not shown) and duration of crosslinking (**Figure** 2-3) play a role; these factors should be considered to control the variety of products formed using mTG based conjugation chemistry.

2.4.2 Insights on characterizing flux across enzymes complexes built modular construction approach:

In this study, I define flux as the amount of homocysteine generated per unit time by the assembled enzyme complexes. In **Figure** 2-21, addition of Protein G to the LuxS in the Pfs-LuxS complex resulted in reduction of flux generated by the protein complex. Enzyme activity was partially resuscitated by re-configuring the arrangement of protein complexes with addition of Protein G in the first layer and LuxS in the last

layer of the multi-subunit protein complex. A 4-fold reduction in flux when LuxS is in the second layer of multi-subunit complex can be attributed to inability of LuxS to form homodimers in the second layer of the multi-subunit complex. LuxS exists in a homodimeric form in solution and its enzyme activity is dependent on its dimeric structure.[139] Improvement in flux observed upon re-configuration of the structures with LuxS in the last layer can be attributed to enhanced steric flexibility of LuxS to form homodimeric complexes.

The reduction in flux can also be attributed to structural variability in the products generated using the mTG mediated conjugation approach detailed in the section above. Formation of tetramers and trimers in the conjugation process can impede the natural orientation of these enzyme components resulting in loss of enzyme activity. The effect of structural variability on flux can be moderated by including flexible linker tags between globular structure of protein components and the conjugation tags to enhance steric flexibility of the individual protein components in the multi-subunit structure. The lack of clarity on the type and quantity of products formed further impedes the ability to determine effective enzyme concentrations (Et) that are factored by the percentage of enzymes conjugated and the impact of immobilization on enzyme activity. Inability to accurately calculate Et makes this approach difficult to employ in substrate channeling studies.

In this work, I also demonstrated control of metabolic flux by the addition of rate-limiting LuxS (**Figure** 2-11 and **Figure** 2-12). The increased flux obtained from each round of additional crosslinking was apparently linear however and instead appeared

to saturate with the number of added proteins (**Figure** 2-12 and **Figure** 2-16). Our approach was helpful in constructing multi-functional complexes (**Figure** 2-17) and this not only proved beneficial as I changed the orientation of complexes finding resuscitation of enzymatic activity, making them both effective and multifunctional, but also provided insight into the decrease in flux obtained per unit enzyme. That is, since the addition of Protein G and EGFP decreased the activity of LuxS, the rate-limiting factor, I hypothesize that addition of subsequent LuxS subunits may also decrease the preceding LuxS subunit's activity, thereby leading to overall decrease in per unit enzyme activity with each round of crosslinking. It would be interesting to study how these complexes perform in comparison to multiple gene fusions.

The use of Co^{2+} beads provided control over crosslinking orientation and helped create 'deployable' complexes. Since I assembled enzymatic complexes that were involved in generation of QS responses, by controlling the sequence of crosslinking and orientation of the subunits, I could mediate and control small molecule communication between an assembled abiotic complex and cells leading to altered metabolic outcomes. I note this lysine and glutamine tag/transglutaminase methodology can be used to fabricate protein complexes that retain function of each assembled subunit.

In addition to building complexes that have utility in solution, as demonstrated by altering QS communication *in vitro*, I expect this methodology will find utility in assembling biological components in conjunction with cells and tissues in lab-chip or animal-on-a-chip systems. Biological components embedded with electronics can

sense, report and modulate the tissues and cells of interest [112]. Developing methodologies to assemble enzyme cascades in these systems would be valuable in providing greater access and even control. Hence I believe that the solid phase synthesis approach can be translated to microfluidic and microsystem environments where multiple components can be flowed in and immobilized to each other [118], rather than existing techniques that utilize harsh immobilization chemistries, or valves, pumps, and printing methodologies.

Chapter 3 Facile Two-step Enzymatic Approach for Conjugating Proteins to Polysaccharide Chitosan at an Electrode Interface

This chapter is adopted from the following publication with permission

Bhokisham, N.et al. Cel. Mol. Bioeng. (2017) 10: 134. https://doi.org/10.1007/s12195-016-0472-5 [105]

3.1 Introduction

Biofabrication enables assembly of biological components including proteins, polysaccharides, DNA, cells etc. onto electronic devices to create microscale systems that mediate seamless interaction between the two[140-143]. While biological components are naturally evolved with capabilities to 'sense' and 'perceive' (e.g., cells) or 'act' (e.g., enzymes, cells), biology's molecular information flow is incompatible with electronics. Also, electronic devices are designed to process and communicate information to and from the user, typically not with the biological system. Biofabricated devices are developed by integrating biologic and electronic components and the devices have immense potential for bi-directional information transfer, affecting a wide range of fields from biosensing, lab on chip systems, bio-batteries and biofuel cells to personalized diagnostic devices[144]. A second generation of biofabricated devices have been developed that not only combine the above mentioned characteristics but also display elements of 'control' and 'actuation'[133] of biological components through electronic signals.

One of the critical components for integration of biological and electronic systems is the interface material. It is desired to functionalize the surface of electronic components with reactive groups that can easily interact with biological components[144] and, importantly, in a way that precludes non-specific binding of materials at the electrode interface. Non-specific binding can be pronounced, eroding function and sensitivity in biosensors, for example. Various materials such as carboxy methylated-dextran, polyethylene glycol (PEG)-containing hydrogels[145], self-assembled monolayers of alkane thiols[146], chitosan-*N*-poly(ethylene oxide)[147] have been developed to lower non-specific binding of proteins and increase sensitivity. I am interested in chitosan, a deacetylated polysaccharide from chitin, as a facilitator of biological assembly onto microelectronic devices, such as biosensors, and MEMS devices. Because chitosan's solubility is easily controlled (via pH), it can be partitioned into various forms including hydrogels and coated on electrodes. In our work, chitosan enables electrode-based interrogation of cell signaling[112, 148, 149] as well as conveyance of molecular information to and from electrodes[133, 150].

Proteins and enzymes have been coupled to chitosan using a tyrosine based chemistry (see **Figure 3-1**) mediated by tyrosinase[151]. However, tyrosinase oxidation of phenolic groups to quinones can be slow[152, 153]. In addition, the abundance of positive charges due to the amine groups on the surface of chitosan, a property that makes chitosan viable in a multitude of applications, can also lead to nonspecific binding of proteins[154]. The combination of both nonspecific binding and slow tyrosinase-mediated conjugation chemistry leads to a scenario of a low 'signal to

noise' ratio for protein conjugation particularly when attempting rapid assembly. In our previous work, tyrosinase mediated coupling was shown to yield satisfactory 'signal to noise', but conjugation reactions were carried out overnight.

In an attempt to accelerate this process and enhance 'signal to noise', I modified chitosan first using the tyrosinase-mediated coupling of a Lys-Tyr-Lys (KYK) tripeptide transforming the available primary amine to a pair of primary amines each on essentially a 4-carbon linker, then employed a microbial transglutaminase (mTG) to link proteins engineered with glutamine-rich tags[155] to peptide-chitosan complex. Importantly, mTG is a crosslinking enzyme with ~100 fold higher enzyme turnover number than tyrosinase[153, 156]. In this work, I specifically focus on the 'signal to noise' ratio of these two approaches to assemble proteins onto chitosan (see **Figure 3-1**): the tyrosinase-mediated approach involving conjugation of proteins directly to chitosan and the two-step approach involving coating the surface of chitosan with KYK peptides using tyrosinase and direct conjugation of proteins to KYK peptides through transglutaminase. I further characterized the transglutaminase-catalyzed approach by assembling a two-enzyme cascade onto gold chips coated with peptide modified chitosan. As model enzymes, I used S-Adenosylhomocysteine nucleosidase (Pfs) and S-Ribosylhomocysteine lyase (LuxS), both part of the activated methyl cycle in bacteria[157]. While Pfs converts S-Adenosylhomocysteine (SAH) to S-Ribosylhomocysteine (SRH), LuxS converts SRH to homocysteine (HCY) and (S)-4,5-dihydroxy-2,3-pentanedione (DPD), a precursor to autoinducer-2 (AI-2), a quorum sensing (QS) signal molecule. The net reaction rate is determined here by quantifying

the level of homocysteine, an easily measured sulfhydryl-containing byproduct of AI-2 synthesis. Using these methodologies, surfaces can be developed with tailored biochemical flux.

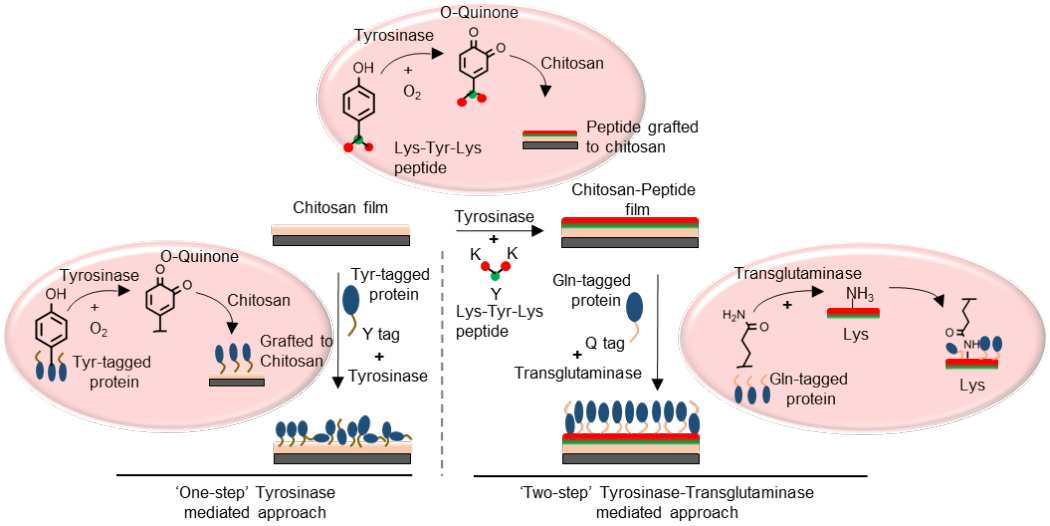

Figure 3-1: Enzymatic assembly of engineered proteins onto chitosan films

Enzymatic assembly of engineered proteins onto chitosan films. Left: a "one-step" tyrosinase mediated conjugation approach that utilizes mushroom tyrosinase to "activate" a tyrosine rich tag engineered onto the C-terminus of the assembled protein. Tyrosinase converts the phenolic functional group of tyrosine to an ortho-quinone which subsequently binds to the primary amine of chitosan (via Michael addition). Right: Two-step approach utilizing the initial "coating" of chitosan films with Lys-Tyr-Lys (KYK) peptides using tyrosinase (as on left), followed by conjugation of proteins engineered with C terminal glutamine-rich tags onto the KYK peptides using a microbial transglutaminase.

3.2 Materials and Methods

3.2.1 Preparation of chitosan films in 48 well plates

I prepared chitosan films using 1.5% chitosan (Sigma Aldrich) solution at pH 5.6, dissolved in HCl. 200 µls of chitosan solution was added to each well of the 48 well plate and vacuum dried at 65 °C for 24 hours. After incubation, I washed the films thrice with PBS (Phosphate buffered saline; Sigma Aldrich), pH 7.5 and neutralized by immersing the films with 1M NaOH (Sigma) for 45 minutes at RT. Later I washed the films again 3X with PBS and used for experiments.

3.2.2 Electrical deposition of chitosan onto gold chips

I immersed clean gold chips in 1.5% chitosan solution and applied a current of $4A/mm^2$ for 2 minutes to each chip. Later I air dried the gold chips and used for experiments.

3.2.3 Conjugation of Lys-Tyr-Lys (KYK) peptide to chitosan films

I prepared 1mM KYK peptide (Sigma Aldrich) solution using Phosphate Buffered Saline, pH 7.5 (PBS, Sigma Aldrich). I added 100 µl of KYK peptide solution along with tyrosinase from mushroom (Sigma Aldrich) at a concentration of 50U/ml in 50 mM potassium phosphate buffer, pH 6.5.I incubated the films with peptide solution at RT for overnight and later washed 3X with PBS and used for experiments.

3.2.4 Conjugation of engineered proteins using tyrosinase and microbial transglutaminase

I used proteins engineered with tyrosine [158] (for one-step conjugation approach) and glutamines [106] (for two-step conjugation approach). For one-step tyrosinase mediated conjugation of proteins to chitosan films, I added tyrosine engineered proteins and tyrosinase (dissolved in 50 mM potassium phosphate buffer, pH 6.5) at either 3.5 U/µl or 11 U/ µl concentrations and incubated for 1hr at RT. For two-step transglutaminase mediated conjugation to peptide modified chitosan films, I added glutamine engineered proteins and incubated for 1 hr at RT with 0.00132 U/µl of mTG, purified from *Streptoverticillium mobaraense* (Ajinomoto) and dissolved in Phosphate buffered saline, pH 7.5 (Sigma Aldrich).

3.2.5 Ellman's DTNB assay

I prepared Ellman's DTNB stock solution containing 50 mM sodium acetate, 2 mM DTNB (Sigma Aldrich) using water. I prepared assay solution containing 100 µls of 1M Tris-Hcl, pH 8, 50 µls of DTNB solution and 800 µls of water. I mixed 50 µls of solution containing homocysteine with 950 µls of assay solution and measured absorbance at 412nm.

3.3 Results

3.3.1 Lys-Tyr-Lys peptide prevents non-specific binding to chitosan

I compared levels of non-specific binding of enzymes to chitosan films and peptide (KYK)-modified chitosan films (**Figure 3-2**). I used S-Ribosylhomocysteine lyase (LuxS) as a model enzyme to measure non-specific binding of enzymes to chitosan. For this purpose, I engineered LuxS at its C terminus with either a penta-tyrosine tag (indicated as $LuxS_Y$) or a penta-glutamine tag (indicated as $LuxS_Q$). All proteins are engineered with hexahistidine tags at the N-termini[106]. As controls, I also used native LuxS (with hexahistidine tag for purification) to measure non-specific binding. I note that both native and engineered LuxS's displayed similar enzyme activities per molecule (data not shown). For these experiments, chitosan films were cast into 48 well plates. To each well, I added 200 µl of 1.5% chitosan solution, pH 5.6 and vacuum dried at 65 °C for 24 hours. Dried films were later neutralized with 1M NaOH for 45 mins at RT. Post neutralization, chitosan films were washed 3X with PBS (Phosphate Buffered Saline, pH 7.4) and used for experiments. To modify chitosan films with KYK peptide, I incubated neutralized films with 1mM Lys-Tyr-Lys (KYK) peptide and tyrosinase at 50U/ml concentration overnight at RT[155]. Post incubation, films were washed 3x with PBS. In **Figure 3-2**, to study levels of non-specific binding, I added 15µM of native (LuxS) and engineered LuxS ($LuxS_Y$ and $LuxS_Q$) to empty and KYK peptide coated chitosan films. Additional controls consisted of enzymes loaded with 70

and 200 µg per 100µls (10.6 µM and 30.3 µM, respectively) of bovine serum albumin (BSA, a common blocking agent). Post incubation at RT for 60 mins, I washed the films 3X with PBS. I measured LuxS bound to films by measuring the enzyme activity; quantified by the sulfhydryl generation from LuxS byproduct, homocysteine. I added 190 µls of 1mM S-Adenosyl Homocysteine (SAH) and 10 µls of 20 µM enzyme S-Adenosyl homocysteine nucleosidase (Pfs) and incubated the films for 60 mins at 37C. Pfs converts SAH to SRH and SRH is converted to homocysteine (HCY) by LuxS. Since LuxS is the rate limiting factor in this two-step reaction, HCY generated by LuxS is directly proportional to amount of LuxS on the chitosan film[105]. After incubation, I measured HCY levels using Ellman's assay (sulfhydryl assay).

In the left most panel of **Figure 3-2**, there was significant homocysteine generation (>0.01 µM/min/mm^2) indicating significant non-specific binding to chitosan. There was no apparent difference due to the glutamine or lysine tags, nor was there a consistent influence due to BSA in the ranges of concentrations used (10-30µM). Note that I co-incubated with BSA, I did not block with BSA first then add LuxS; the effect of BSA here was to demonstrate the capacity of binding sites for LuxS and to mimic the addition of either the tyrosinase or the transglutaminase which were added at similar levels. Interestingly, I observed the HCY levels from the peptide modified chitosan film to be 5 times lower on average than the HCY levels from the empty chitosan films (p value < 0.001). Again, there was no competitive advantage due to the addition of BSA at the conditions tested. Finally, I note both native and engineered LuxS were identical in their non-specific binding profiles. These results

clearly demonstrated that addition of KYK peptide to the chitosan film reduced 5-fold the quantity of enzymatic activity bound to the films. In separate experiments (not shown here), I found the peptide when incubated in solution with the LuxS enzyme without chitosan present had no influence on enzyme activity. In sum, our results are consistent with the hypothesis that less enzyme was non-specifically bound in the presence of the KYK peptide.

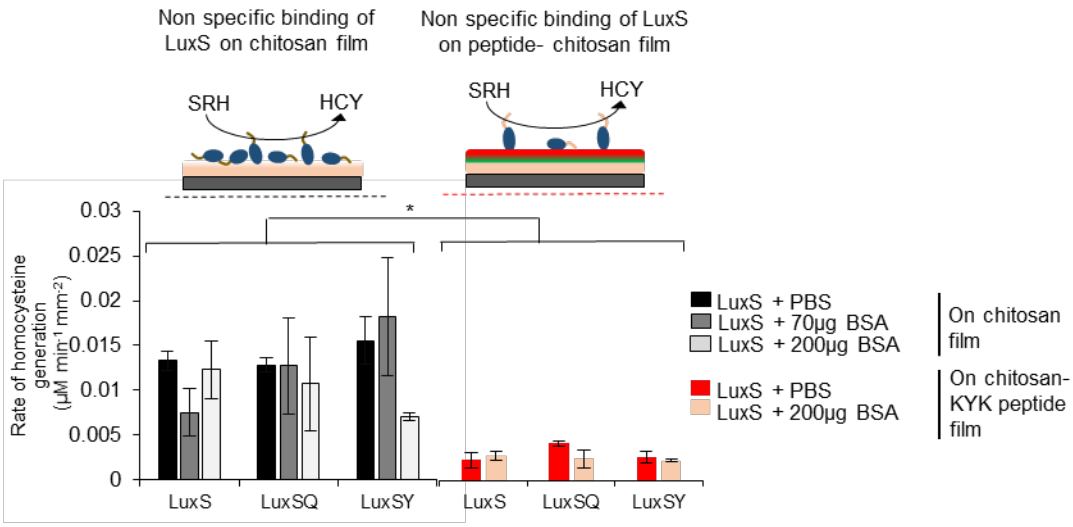

Figure 3-2: Lys-Tyr-Lys peptide prevents non-specific binding to chitosan

Non-specific binding profiles of LuxS, $LuxS_Q$ and $LuxS_Y$ onto chitosan film and chitosan-KYK peptide films. Blocking protein bovine serum albumin (BSA, 70µg BSA/100µl) was used; this level is the molar equivalent to 3.50U/µl of Tyrosinase; 200µg/100µl of BSA is the molar equivalent to 1.1U/µl of tyrosinase and 60µM mTG. Error bars indicate n = 3. * indicates $p < 0.00001$ using student's t test.

3.3.2 Enzyme activities of soluble $LuxS_Y$ with tyrosinase and microbial transglutaminase

As depicted in **Figure 3-3**, I studied the role of conjugation enzymes (tyrosinase and microbial transglutaminase) on enzyme activity of LuxS. In our previous work[112, 149, 158, 159], I demonstrated that Pfs was stable and that equimolar mixtures of Pfs and LuxS exhibited less activity than a Pfs-LuxS fusion. In part this was due to substrate channeling [160], but could have also been attributed to diminished LuxS activity. Here, $LuxS_Y$ was incubated at RT for 60 minutes with following solutions: 1) phosphate buffered saline, pH 7.5; 2) microbial transglutaminase (at 00132 U/µl concentration) dissolved in phosphate buffered saline, pH 7.5; 3) potassium phosphate buffer, pH 6.5 and 4) tyrosinase (11 U/µl concentrations) dissolved in potassium phosphate buffer, pH 6.5. After incubation, 2 µM of Pfs and 1 mM SAH was added and incubated at 37°C for 20 minutes. After incubation, Ellman's assay was performed to measure amount of homocysteine generated. Results indicated that incubations with both conjugation enzymes: microbial transglutaminase and tyrosinase exhibited reductions in LuxS activity. Tyrosinase at 11U/µl dissolved in potassium phosphate buffer, pH 6.5 had the greatest reduction.

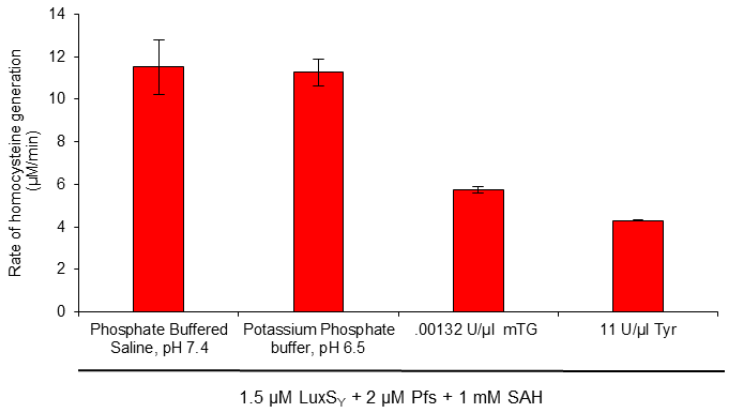

Figure 3-3: Enzyme activities of soluble $LuxS_Y$ with tyrosinase and microbial transglutaminase

Effect of tyrosinase and microbial transglutaminase incubation on activities of $LuxS_Y$. $LuxS_Y$ was incubated with phosphate buffered saline, pH 7.4, potassium phosphate buffer, pH 6.5, tyrosinase (11 U/µl) and microbial transglutaminase (.00132 U/µl) for 60 minutes at RT. After incubation, 2 µM of Pfs and 1 mM SAH was added and incubated at 37°C for 20 minutes. After incubation, Ellman's assay was performed to measure amount of homocysteine generated. Error bars indicate n = 3

3.3.3 mTG catalyzed approach significantly improves 'signal to noise' for enzyme conjugation onto chitosan

I next compared the one-step tyrosinase-mediated conjugation approach with the transglutaminase-catalyzed approach to measure the ratio between 'signal' from enzyme mediated specific conjugation and 'noise' from non-specific binding.

For the tyrosinase-mediated approach, I used tyrosinase to crosslink $LuxS_Y$ to empty chitosan film. After the chitosan film was assembled and neutralized, I added 15 µM of $LuxS_Y$ along with tyrosinase (dissolved in potassium phosphate buffer, pH 6.5) and incubated for 60 mins at RT. In **Figure 3-4**A, I used two tyrosinase conditions, 3.5 U/µl and 11 U/µl. In previous work, I found 3.5 U/µl was sufficient for coupling tyrosine tagged proteins to chitosan films[133, 161]; 11 U/µl was the highest available concentration. After the 60 min incubation, I washed the chitosan film 3X with PBS

and measured the enzyme activity as described earlier. In both cases, LuxS enzyme activity was significantly lower than the control without tyrosinase indicating that nonspecific binding of $LuxS_Y$ to chitosan was surprisingly greater than with tyrosinase mediated conjugation This reduction in activity of conjugated LuxS from chitosan films was due, in part, to a reduction of per unit enzyme activity of LuxS that is mediated by the tyrosinase itself (**Figure 3-3**) and the potential interference of non-specific binding due to tyrosinase (as compared to BSA). Overall, the ratio of LuxS activity from tyrosinase mediated conjugation to non-specific binding was 0.33. I had previously demonstrated that tyrosinase linkage works well for two more stable proteins (GFP and Pfs) relative to non-conjugation controls, however in those studies the conjugation times were between 12-16 hours[149, 162]. At a conjugation time of 60 mins, LuxS enzyme activity from specific conjugation was lower than the nonspecific binding controls.

I next measured the analogous 'signal to noise' ratio for the two-step method. In **Figure 3-4**B, I added 15 μM of $LuxS_Q$ and 0.00132 U/μl of mTG to the peptide modified chitosan film. As a control, I used $LuxS_Q$ without mTG. I incubated the proteins at RT for 60 min and washed the films 3x with PBS. After washing, I measured activity using Ellman's assay. I observed (1) that, as in **Figure 3-4**, there was minimal activity assembled onto the peptide modified chitosan films not treated with transglutaminase and (2) that enzyme activity from mTG-crosslinked proteins resulted in 6-fold more activity than the tyrosinase-mediated case. Again, all conditions, concentrations, wash steps, etc., were identical. The only differences were the actual

proteins assembled (Q vs Y tag) and the enzymes used to crosslink (tyrosinase vs transglutaminase). In solution, just like tyrosinase, I observed a decrease in per unit enzyme activity of LuxS (**Figure 3-3**) upon incubation with mTG, but this decrease was less than incubation with tyrosinase. Overall, the signal to noise ratio exceeded 20-fold that of the negative controls.

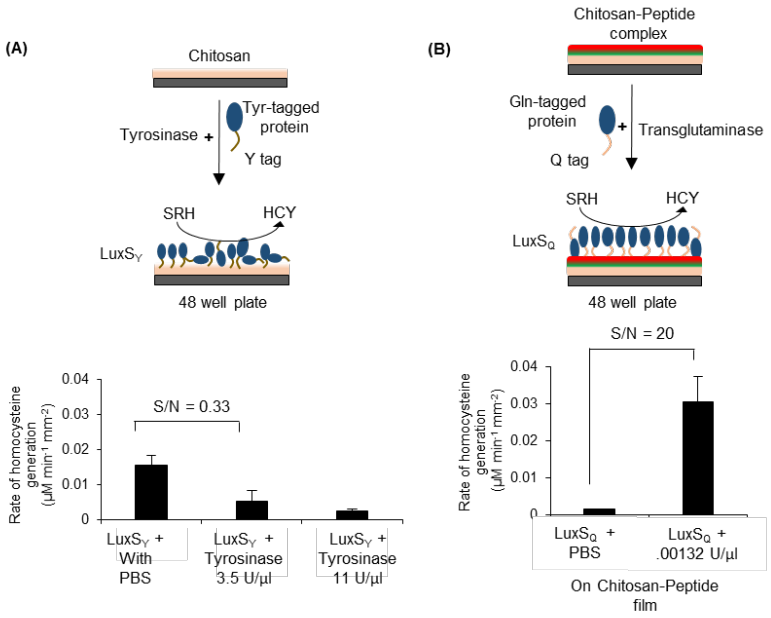

Figure 3-4: mTG catalyzed approach significantly improves 'signal to noise' for enzyme conjugation onto chitosan

Comparison of tyrosinase mediated conjugation of tyrosine engineered LuxS ($LuxS_Y$) to chitosan films with the two-step transglutaminase (mTG) catalyzed conjugation of glutamine engineered LuxS ($LuxS_Q$) to peptide-chitosan films. **(4A)** Tyrosinase mediated conjugation of $LuxS_Y$ onto chitosan films. Controls indicated are for $LuxS_Y$ without tyrosinase. **(4B)** Transglutaminase mediated conjugation of $LuxS_Q$ to the chitosan-KYK peptide films. Controls include $LuxS_Q$ incubated with chitosan-peptide films but without mTG. "S/N" indicates signal to noise ratio, where "Signal" is LuxS activity from enzyme mediated conjugation and "Noise" is LuxS activity from nonspecific binding. Error bars indicate n = 3.

3.3.4 Characterization of transglutaminase-catalyzed approach to conjugation onto chitosan

Having demonstrated that transglutaminase-catalyzed approach was potentially superior to the tyrosinase-mediated approach, I sought to further characterize the transglutaminase-catalyzed methodology. That is, in **Figure 3-5** I varied the concentrations of $LuxS_Q$ added to the conjugation reactions. I prepared peptide modified chitosan films as described earlier and in addition, I also blocked the films with 5% BSA for 1 hour. After incubation, I washed the films 3x with PBS to prep for subsequent enzyme assembly. I added varying amounts of $LuxS_Q$ to peptide-modified chitosan films and crosslinked the enzymes to films by mTG. The molar ratio between LuxS and mTG was constant at 1:3 for all cases. I discovered heuristically this was a good ratio for assembly. Controls consisted of identical experiments without mTG. After conjugation at RT for 60 mins, I washed the films 3x with PBS and measured enzyme activity. I observed that there was a monotonic increase in HCY generated with increased $LuxS_Q$ concentration. There were no significant differences among the negative controls, as expected.

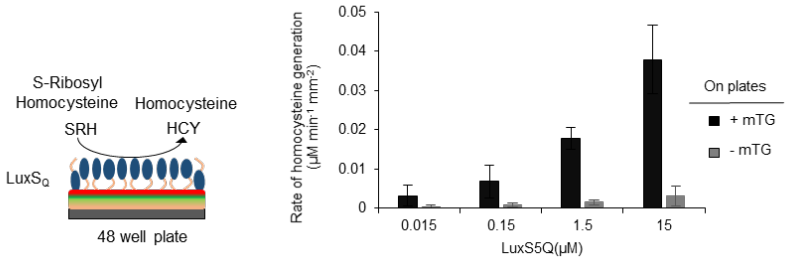

Figure 3-5: Characterization of transglutaminase-catalyzed approach to conjugation onto chitosan.

Capacity for binding $LuxS_Q$. Activities exhibited from different concentrations of LuxS conjugated with chitosan films using the two-step microbial transglutaminase approach. Controls indicated include $LuxS_Q$ without mTG. Error bars indicate n = 3.

3.3.5 Assembly of EGFP to peptide modified chitosan films on gold chips

In Figure 3-6, I demonstrate the two-step approach of protein conjugation onto gold chips using fluorescent protein, EGFP, engineered with glutamines at its C termini (indicated as E_Q). I electrically deposited chitosan onto gold chips (Methods) and crosslinked 1mM KYK tripeptide to chitosan using 50U tyrosinase at RT overnight. After incubation, I washed the gold chip 3X with PBS to remove unreacted peptide and tyrosinase. I then conjugated EGFP (0.5 mg/ml E_Q) to the peptide modified chitosan via incubation with 30 μM mTG at RT for 60 min. After incubation, I washed the gold chip 3X with PBS. As controls, I performed the same reactions without mTG. Fluorescence microscopy images are included that indicate conjugation of E_Q to peptide modified chitosan (experimental samples with mTG exhibited green fluorescence while the mTG negative controls had negligible green fluorescence). Data confirm minimal non-specific binding.

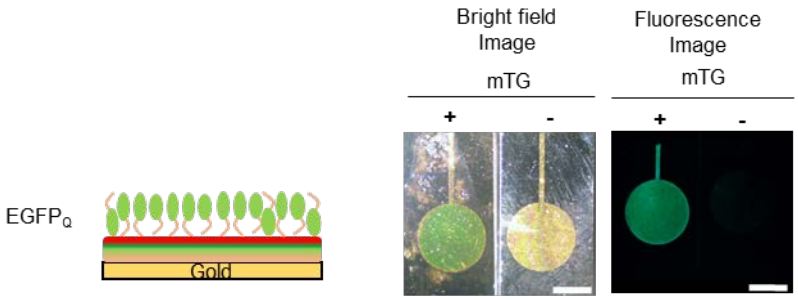

Figure 3-6: Assembly of EGFP to peptide modified chitosan films on gold chip.

Assembling of $EGFP_Q$ on chitosan using 'two-step' mTG mediated approach. KYK peptide was first crosslinked to chitosan using tyrosinase (Methods) and EGFP engineered with glutamines at C termini (Methods) was crosslinked to KYK peptide using mTG (Methods). Scale bar: 2mm.

3.3.6 Assembly of two enzyme metabolic pathway to peptide modified chitosan on chips

Having demonstrated the specificity of two-step approach, I next assembled two enzymes onto peptide modified chitosan and mediated flux between the two enzymes. For this purpose, I used both enzymes Pfs_Q and $LuxS_Q$. That is, I generated Pfs engineered with penta-glutamine tag at C terminus (indicated as Pfs_Q) for this purpose. For conjugation, I used chitosan films both casted on plates as well as electrically-deposited chitosan films on gold chips and conjugated the KYK peptide to the chitosan films. (Scheme in **Figure 3-7** and Methods). Later, both films were blocked with 5% BSA for 60 minutes. After incubation, films were washed 3x with PBS and used for experiments. To demonstrate assembly onto gold chips, I assembled green fluorescent protein (E_Q) using the transglutaminase-catalyzed approach (**Figure 3-6**). To demonstrate assembly of the enzyme cascade, I first added varying

concentrations of $LuxS_Q$ to peptide modified chitosan using mTG (molar ratio of LuxS: mTG of 1:3). After a 60 min incubation, both the plates and chips were washed 3X with PBS. Under similar conjugation conditions, the second enzyme, $Pfs_{Q,}$ was crosslinked to chitosan-peptide-$LuxS_Q$ film (again with a molar ratio of Pfs: mTG of 1:3). After this second round of conjugation, plates and gold chips were washed again 3X with PBS and incubated with 1mM SAH. After 2 hours of incubation at 37°C, the HCY generated was measured by Ellman's assay. HCY levels generated from enzymes assembled to both plates and chips are indicated in **Figure 3-7B**. Consistent with previous results, I found up to ~20 fold increases in biochemical flux through the assembled pathways. I also note that there were relatively minor differences due to the electrodeposited (denoted "On chips") versus the cast chitosan films (denoted "On plates"), although the deposited activities were somewhat higher. In all cases, the HCY

generated from negative control experiments were insignificant.

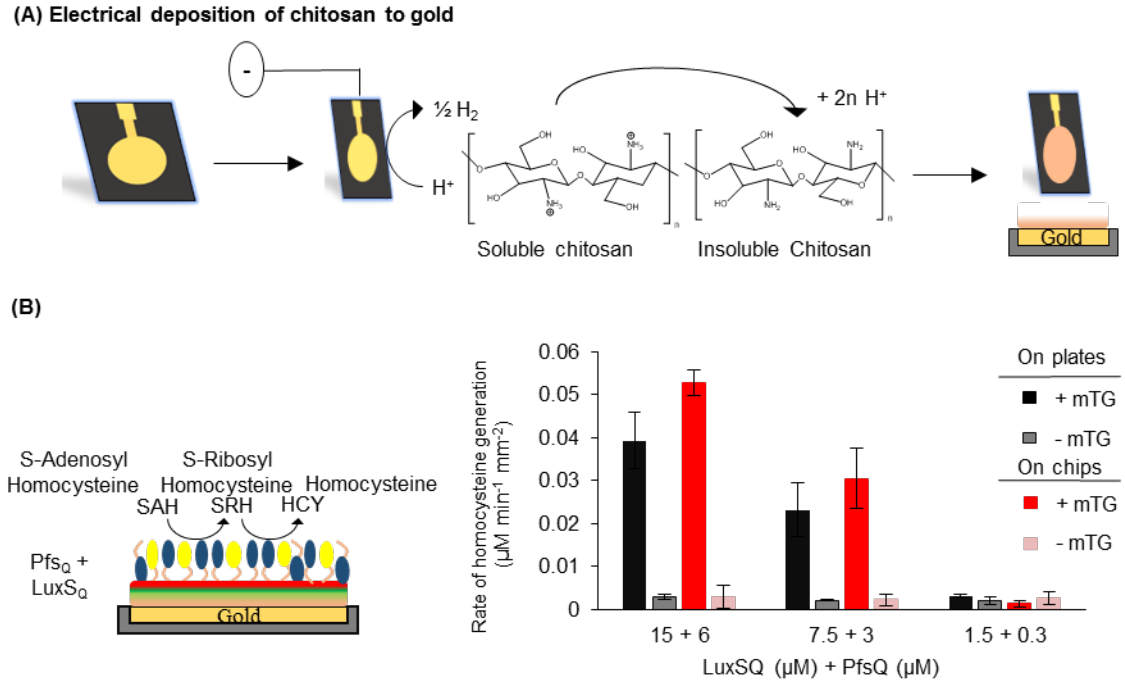

Figure 3-7: Assembly of two enzyme metabolic pathway to peptide modified chitosan on chips.

(A) Schematic indicating electrical deposition of chitosan films onto gold chips[157, 161]. **(B)** Conjugation of LuxS and Pfs, representing a two enzyme metabolic pathway to peptide-chitosan films on gold chips and on microtiter plates. Controls include Pfs and LuxS enzymes incubated with KYK peptide chitosan films (as in **Fig. 3**) but without mTG. Error bars indicate n = 3.

3.4 Discussion

In this study I compared two different biofabrication approaches for the assembly of proteins onto chitosan films. First, a tyrosinase-mediated approach involving conjugation of tyrosine engineered proteins to chitosan was examined for specificity and non-specific binding. In previous work, I demonstrated assembly of tyrosinase linked proteins on chitosan [158] but did not address the non-specific interactions between the enzyme (Pfs) and chitosan. In addition, our previous studies focused on Pfs and GFP, which are more stable than LuxS. The two-step approach here involving tyrosinase mediated coating of chitosan film with Lys-Tyr-Lys tripeptide followed by direct conjugation of glutamine engineered proteins to peptide modified chitosan film using transglutaminase was simple, and exhibited far less background activity.

The reasons for *reduced* nonspecific binding is confounding given that I modified the surface of chitosan with peptides containing more positively-charged free amines. Beyond charges on the surface, there might be other factors at play that influence the extent of nonspecific binding of proteins to chitosan. The thickness of the modified chitosan films and the method of deposition of these films have been reported to play a role in nonspecific binding. Specifically, reduced binding was attributed to reduced mobility of the different chitosan films[147]. In our case, the addition of tripeptide might have reduced the mobility of the chitosan films resulting in reduced non-specific binding. Also, poly-lysine molecules, owing to their charge, have been

shown to bind to metal oxides[163]. There is a remote possibility that tripeptides containing lysines bound to the surface of gold, preventing non-specific binding of proteins to gold, however, given the thickness of the films, it is quite unlikely to have played a major role. Analogously, should the peptide bind both gold and chitosan, reduced mobility could be envisioned.

Alternatively, proteins have been known to undergo refolding upon contact with a charged surface[164]. In this study, since the non-specific binding is reported indirectly through enzyme activity on the surface of the biosensors, LuxS, the rate limiting factor in the two enzyme QS pathway might have refolded upon contact with a tripeptide leading to reduced enzyme activity. Perhaps this was a contributing factor. In either case above, additional experiments would be needed to evaluate the mechanistic causality of the reduced non-specific binding.

In sum, the two-step assembly process entails an extra step of modifying chitosan films with peptides prior to crosslinking with engineered proteins, thereby increasing the overall fabrication time. However, by switching from the use of empty chitosan films to peptide-modified films for crosslinking, I could transition from the low k_{cat} tyrosinase to mTG for final assembly. In biosensor and other fabrication processes, the assembly of the enzyme onto the biosensor surface is the crucial time sensitive step. Here, I could accelerate crosslinking from 12 hours to 1 hour using mTG and peptides. Also, given the relatively low requirement for mTG (1.3U/ml), I believe crosslinking times can be reduced even further. Parenthetically, since the peptide

modified films are relatively stable, the peptide modification of chitosan might be done ahead of time and kept ready for enzyme crosslinking.

From a biofabrication standpoint, I have displayed construction of a two enzyme metabolic pathway on chips wherein enzymes/biomaterials can be specifically crosslinked within a short duration across a wide concentration range of 15 μM to 15 nM and with minimal nonspecific binding at all concentrations. I envisage using this methodology for the fabrication of biomaterials in bioMEMS devices, sensors and lab chip devices, some of which have already been shown. [112, 133, 161] In general, by combining the pH-controlled solubility of chitosan with peptide-mediated reduced non-specific binding, peptide-chitosan complexes created here using transglutaminase are likely to find utility in antigen-antibody and immunodetection assays and other sensing applications on chips and within devices.

Chapter 4 Engineered Tobacco Mosaic Virus -Virus Like Particles (TMV-VLP) as self-assembling 3D scaffolds for multi-enzyme assembly using mTG mediated conjugation

Sections from this chapter will be submitted for publication by January 2018

4.1 Introduction

Electronic components with signal processing and communication capabilities have been integrated with biomaterials for development of interesting devices and applications.[107, 108] The challenge in building these devices is the construction of 'bio-electronic' interface to enable assembly of biocomponents on abiotic electronic surfaces and mediating communication across the interface. In general, biomaterials are one of the best examples of bottom-up assemblies with several simple biological components self-assembling into multi-component structures such as DNA origami[165, 166], protein origami[167], liposomes[168, 169], viruses[170], enzymes[171] etc. Various bio-inspired materials such as gold binding peptides[172, 173], graphite binding peptides[174, 175] that self-assemble into a 2D monolayer at bio-electronic interface have been engineered.

However, biosensor fabrication typically requires facile assembly of biocomponents at high molecular densities and there is a need to develop 3D interfacial scaffolds with high aspect ratios as well as those with the capability to display desired conjugation chemistries for integration of biocomponents. Virus like particles (VLP),

a class of biomaterials derived from coat proteins of viruses are increasingly being used purely as materials for bio-device assembly.[170] Well established structures of VLPs have enabled genetic engineering of coat proteins to display multivalent conjugational moieties on the surface of the VLP with well-defined periodicities. Individual coat proteins can self-assemble into hierarchical assemblies with different shapes and dimensions from nanoscale to mesoscale.[71, 176] Finally, introduction of cysteines into VLPs has enabled VLPs to self-assemble onto the gold surface and be used as interfacial materials at bio-electronic interface.[38, 57, 58]

Capitalizing on the dual nature of virus like particles as materials for bio-device integration, as well as easily modifiable biomaterial for biocomponent assembly[177], new biosensors are being designed using virus and virus like particles as interface material. M13 bacteriophage has been used as scaffold material in an impedance sensor for detection of prostate cancer specific antibodies and antigens.[81] Tobacco Mosaic Virus (TMV) in combination with polyaniline have been used in a thin film sensor for detection of methanol and ethanol.[82] TMV-VLP has also been genetically engineered to display functional peptides for TNT[83] and anti-body detection.[55] With extensive literature available on protein conjugation, enzymes have been integrated with VLPs for biosensing. Two-enzyme cascades containing glucose oxidase and horse-radish peroxidase has been assembled on the surface of cowpea mosaic virus[84] and TMV for detection of glucose.[85, 178]

Capitalizing on VLP's ability to integrate with electronics, facile assembly of multi-step enzyme cascades on VLPs can increase the scope of electrochemical

biosensors and other types for biosensing. In this work, I engineered a self-assembling 3D scaffold comprised of VLP to display assembly of multi-step enzyme cascades on electrode surfaces. Firstly, I engineered a self-assembling monolayer of TMV-VLP to display glutamines on the outer surfaces of the VLPs. I utilized the engineered glutamines for conjugation of biocomponents via mTG mediated conjugation chemistry.[105] Through our earlier described modular construction approach for assembly of bio components via mTG mediated conjugation[106], I displayed layer-by-layer assembly of multi-component assembly on VLP monolayer on gold surfaces. In addition, I used the VLP particle and mTG mediated conjugation approach to display assembly of a novel three enzyme synthetic cascade to sense intermediates in methyl cycle: S-adenosylmethionine, S-adenosylhomocysteine and homocysteine on the surface of a gold chip.

In **Figure 4-1**, I depict the overall scheme of enzyme assembly where TMV-VLP coat proteins are engineered with Gln **(a)** and expressed in bacteria. Engineered coat proteins self-assemble into long rod-shaped VLP **(b)**. In the second step, a first layer of enzyme engineered with Lys at both the N and C termini are conjugated to Gln in VLPs using microbial transglutaminase **(c)**. In the third step, a second layer of enzymes engineered with Gln at the C termini are conjugated to the first enzyme through another round of mTG mediated conjugation **(d)**. Finally, VLPs functionalized with enzyme cascades can be assembled on gold surface and integrated with electronic devices **(e)**.

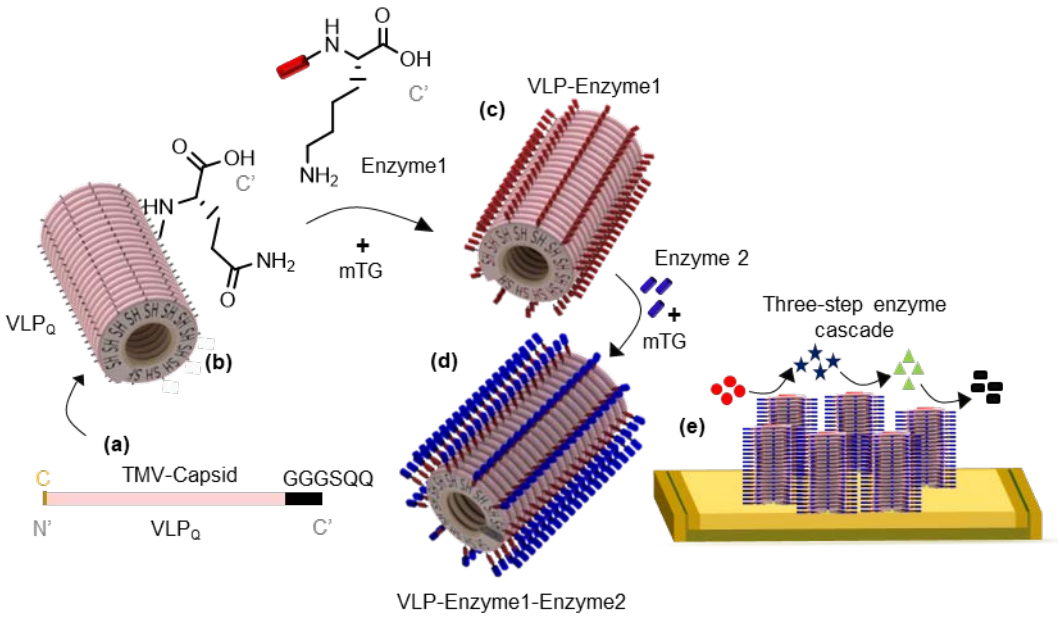

Figure 4-1Engineered Tobacco Mosaic Viruses-Virus Like Particles (TMV-VLP) as 3D scaffolds for enzyme cascade assembly onto microchips.

(a) TMV capsid subunit engineered with 1 Cys at the N termini and 2 Gln's at the C termini. **(b)** Self-assembly of capsids into VLP_Q with cysteines exposed at the 3' end of the particle and glutamines on the outer surface. **(c)** Enzymes engineered with Lys at the C termini or the N termini or both are conjugated to VLP_Q using microbial transglutaminase. **(d)** Second layer of enzymes are conjugated to the first layer of enzymes through another round of mTG mediated conjugation. **(e)** Multi-enzyme cascades are assembled on the surface of the microchip using VLP_Q as 3D scaffolds.

4.2 Materials and Methods

4.3 Strains and Plasmids

All plasmids and strains used in this study are listed in **Table 4-1.** I performed all cloning and transformations as per standard protocols[131]. Primers (Integrated DNA Technologies) used for engineering of proteins are summarized in **Table 4-2.** pET28a-TMV1Cys plasmid (obtained as a gift from Dr. James N. Culver) was used as template for all VLP engineering done in this study.

Table 4-1: List of Plasmids

Plasmid	Relevant genotype/property	Reference
pET28a-TMV1Cys (referred as TMV1Cys	TMV capsid protein engineered with Cys at 1st amino acid position	[179]
TMV-10aa-QQQQQ	TMV1Cys engineered with 10aa linker and 5 Gln's at C'	This study
TMV-GSGSQQ	TMV1Cys engineered with 4aa linker and 2 Gln's at C'	This study
TMV-GSGSQQQ	TMV1Cys engineered with 4aa linker and 3 Gln's at C'	This study
TMV-GGGSQQ (Referred to as VLP_Q)	TMV1Cys engineered with 4aa linker and 2 Gln's at C'	This study
TMV-GGGSQQQ	TMV1Cys engineered with 4aa linker and 3 Gln's at C'	This study
pTrc-Tam-7Lys	Tam engineered with 7 Lys's at the C termini	This study
pTrc-7Lys-Tam-7Lys	Tam engineered with 7 Lys's at both the N and C termini	This study
pTrc-Pfs-7Lys	Pfs engineered with 7 Lys's at the C termini	[103]

pTrc-7Lys-Pfs-7Lys	Pfs engineered with 7 Lys's at both the N and C termini	
pTrc-LuxS-7Lys	LuxS engineered with 7 Lys's at the C termini	
pTrc-LuxS-5Gln	LuxS engineered with 5 Gln's at the C termini	
pET200-HGLPT-5Gln	Fusion Enzyme with both Pfs and LuxS and engineered with Gln tag at the C termini (FE_Q)	[180]
Strain	**Relevant genotype/property**	**Reference**
BL 21 *luxS*$^-$	B strain, F$^-$omp *T[dcm] [Ion] hsdS(r_B^-, M_B^-) gal*, Δ*luxS* (For LuxS and Tam expression)	Lab stocks
RK 4353 *pfs*$^-$	RK 4353 strain, Δ*pfs*(8-226):: *kan* (For Pfs expression)	Lab stocks
BL21 CodonPlus (DE3)	*E. coli B F$^-$ompT hsdS(r_B^-, M_B^-) dcm$^+$ Tet^r gal endA Hte [argU ileY leuW Cam^r]* (For VLP expression)	Lab stocks

Table 4-2: List of Primers

Primer name	Sequence (5'-3')	Features
TMV1Cys Forward primer	taattttgtttaactttaagaaggggatatacatatgtcgtgttatagcattaccaccccg	Nde-1 restriction site, overlaps with pET28a and the N termini of TMV1Cys
10 aa linker-QQQQQ Reverse Primer	gctcgagttattgctgttgctgctgactgcctccaccgccgctgccacctccgcggttgccggaccagaggt	Xho-1 restriction site, overlap with pET28 and C termini TMV1Cys, 10aa linker-QQQQQ sequence
TMV-GSGSQQ Reverse Primer	tcagtggtggtggtggtggtgctcgagttactgctgagaaccagaaccggttgccggaccagagg	Xho-1 restriction site, overlap with pET28 and C termini TMV1Cys, and GSGSQQ sequence
TMV-GSGSQQQ Reverse Primer	tcagtggtggtggtggtggtgctcgagttactgctgctgagaaccagaaccggttgccggaccagaggt	Xho-1 restriction site, overlap with pET28 and C termini TMV1Cys, and GSGSQQQ sequence
GGGSQQ Reverse primer	tcagtggtggtggtggtggtgctcgagttactgctgagaaccaccaccggttgccggaccagaggt	Xho-1 restriction site, overlap with pET28 and C termini TMV1Cys, and GGGSQQ sequence

GGGSQQQ Reverse primer	tcagtggtggtggtggtgctcgagtta ctgctgctgagaaccaccaccggttgccg gaccagaggt	Xho-1 restriction site, overlaps with pET28 and C termini TMV1Cys, and GGGSQQQ sequence
Tam-7K Forward Primer	cactcgagatgtctgactggaaccc	Xho-1 restriction site, overlaps with pTrcHisA and Tam gene in *E. coli*
Tam-7K Reverse Primer	tggaattctatttctttttctttttctttttctcca tacgccgggc	Eco RI restriction site, 7 Lys, overlaps with pTrcHisA and Tam gene in *E. coli*
7K-Tam-7K Forward Primer	cactcgagaaaaagaaaaagaaaaaga aaatgtctgactggaacccctctttatatct acac	Xho-1 restriction site, 7 Lys, overlaps with pTrcHisA and Tam gene in *E. coli*
7K-Tam-7K Reverse Primer	tggaattctatttctttttctttttctttttctcca tacgccgggcaacaataaacag	EcoRI restriction site, 7 Lys, overlaps with pTrcHisA and Tam gene in *E. coli*

4.3.1 Protein expression and purification:

I grew the expression hosts for enzymes Tam, Pfs, LuxS and FE (fusion of Pfs and LuxS) in LB media (Sigma-Aldrich) and induced at OD_{600} of 0.4 with 1 mM IPTG (Sigma). After 4 hrs at 30°C, I centrifuged the cells and suspended in 15 mL of 10 mM phosphate buffered saline (PBS), pH 7.4 (Sigma-Aldrich). To lyse the cells, I performed sonication for 15 min and centrifuged again at 20,000g for 20 mins to remove soluble proteins. To purify his-tagged enzymes, I performed immobilized metal ion chromatography via HiTrap columns (GE Healthcare) and subsequently dialyzed the purified enzymes with PBS and stored at -20°C. I selectively removed His tags of all $_{K}Enzyme_{K}$'s (enzymes engineered with Lys tags at both the N and the C termini) used in this study by incubation with enterokinase overnight at 4°C as per

manufacturer's specifications (EK-Away, Invitrogen). Enzymes were stored for further use at -20°C.

4.3.2 Tobacco Mosaic Virus-Virus like Particle (TMV-VLP) Purification and visualization:

I transformed plasmids containing engineered TMV-VLPs into BL21 CodonPlus (Agilent) for protein expression. I grew the strains in LB media at OD_{600} of 0.4 induced with 1mM IPTG for protein expression. After induction for 24 hrs at 30˚C, I pelleted the culture and suspended in 2.5 mL of Bugbuster (EMD Millipore), 2µL of 1M DTT (Sigma) and 1 µL of Lysonase (EMD Millipore) and gently shaken for 45 min at room temperature. After incubation, I added 10% (v/v) of chloroform to each tube, vortexed and centrifuged at 4000 rpm for 20 minutes. I separated the supernatant and pelleted in an ultracentrifuge at 30000 rpm for 60 min at 4ºC. Later, I re-dissolved the pellets in 2 ml of 0.1M phosphate buffer, pH 7 by gently shaking the pellets for overnight at 4ºC and transferred into 10% - 40%sucrose gradients in 0.1M phosphate buffer, pH 7 and centrifuged at 22500 rpm for 60 min at 4ºC. I extracted the TMV-VLPs in the gradient and centrifuged again at 30000 rpm for 60 min. Finally, I re-dissolved the VLP pellet in 0.1M phosphate buffer, pH 7 and used them for further experiments. To visualize the TMV-VLP particles, I loaded 0.5µg of VLPs onto transmission electron microscope grids and coated the VLPs with 2% aqueous uranyl acetate and visualized using transmission electron microscope at 80kV.

4.3.3 Nickel Plating for Scanning electron microscopy

For the plating procedure, I prepared palladium stock solution containing 0.01g Na_2PdCl_4 in 1.5 mL methanol and nickel stock solution containing 0.6g $NiCl_2$ hexahydrate, 0.45g glycine, 1.5 g sodium tetra borate and 0.77g dimethylamine borane complex in 25 mL H_2O. I covered 5mm^2 gold chips (Platypus Technologies) with 25µg of VLP_Q in solution and incubated for overnight at 4ºC. Following overnight incubation with VLPs, I washed the chips with 30 mL of PBS and submerged in a 30X dilution of palladium stock solution for 30 minutes at RT. After 30 min incubation, I washed the chips with PBS and submerged the chips in 2X dilution of nickel stock solution. After 30 min, I washed the chips again and dried for 5 mins and used for scanning electron microscopy.

4.3.4 Assembly of VLPs onto gold chips

I added 25µg of VLPs onto 10 mm^2 gold chips and incubated the chip at 4°C for overnight. After incubation, I washed the chips with 30 mL of 0.1M phosphate buffer, pH 7 to remove unbound VLPs on gold chips. Later, I blocked the chips with 100 µL of 5% bovine serum albumin (BSA) solution and incubated at 37°C for 60 min. After incubation, I washed the chips again and used for further experiments.

4.3.5 Conjugation of EGFP to VLPs in a Layer by Layer assembly

I conjugated $EGFP_K$ (EGFP engineered with lysines at the C termini) to VLP_Q by addition 7.5 µM $EGFP_K$ and 10 µM microbial transglutaminase (mTG) to VLP_Q's assembled on gold chips. Control experiments without mTG were performed as well.

All the solutions were mixed well and spread to cover the entire area of the 10 mm^2 and chips were incubated at RT for 60 min. After incubation, I washed the chips with 0.1M phosphate buffer, pH 7 and used further for fluorescence microscopy.

4.3.6 Measurement of Homocysteine using Ellman's Assay and Cyclic Voltammetry

I measured homocysteine using calorimetric Ellman's assay as described in Fernandes et al [112] and electrochemically using cyclic voltammetry as described in Gordonov et al.[133]

4.4 Results

4.4.1 Engineering and assembly of engineered VLPs

I first intended to assemble a TMV-VLP particle engineered with glutamines on the outer surface. I used a TMV1Cys Virus Like particle (VLP) engineered with one Cys residue at the N termini of each TMV capsid subunit enabling the VLP to self-assemble as a monolayer on gold.[179] I intended to create a Gln engineered VLP (VLP_Q) that forms a monolayer on the gold surface and conjugate enzymes to the engineered Gln's in the VLP_Q monolayer via mTG mediated conjugation chemistry.[106]

In this pursuit, I engineered the TMV1Cys VLP with a 10aa flexible linker peptide and a penta-glutamine tag at the C termini of coat protein (**Table 4-1)**. However, I was unable to express and purify a fully assembled VLP_Q particle (data not shown) and hence, I replaced the long 10aa linker with a short 4aa linker and reduced the number of Gln residues from 5 to either 2 or 3 (**Table 4-1**). With fewer glutamine residues and shorter linker sequences, I successfully expressed and purified VLP_Q's in bacteria (**See 4.3.2**). **Figure 4-2a** depicts a 4-20% denaturing SDS-PAGE gel containing aliquots from various stages of the purification process of a TMV-VLP particle engineered with GGGSQQ sequence at C termini (referred further as VLP_Q). Results indicated that I could successfully purify ~17Kda coat protein of the virus particle.

Next, to verify if the engineered VLPs assembled into a complete filamentous rod like structure, I used transmission electron microscopy (**See4.3.2**). TEM image of purified particles (**Figure 4-2b**) indicated that VLP_Q's assembled into complete rod like structures. When interacted with a gold surface, Cys residue at the N termini enables formation of self-assembled monolayer (SAM) of VLP. To verify if the engineered VLP_Q's can self-assemble into a monolayer, I covered a ~5 mm^2 gold chip with 0.25mg/ml solution of VLP_Q and incubated the chips at 4^0C for overnight., Next day, I washed the chips with water and coated the particles with nickel **(See 4.3.3)** and performed scanning electron microscopy. **Figure 4-2c** indicated that VLP_Q's self-assembled to form a monolayer on gold, as expected.

In conclusion, I engineered the VLP particles with glutamine residues at C termini and purified fully assembled particles in bacteria. I also displayed that the Gln engineered particles formed a self- assembled monolayer on gold surface.

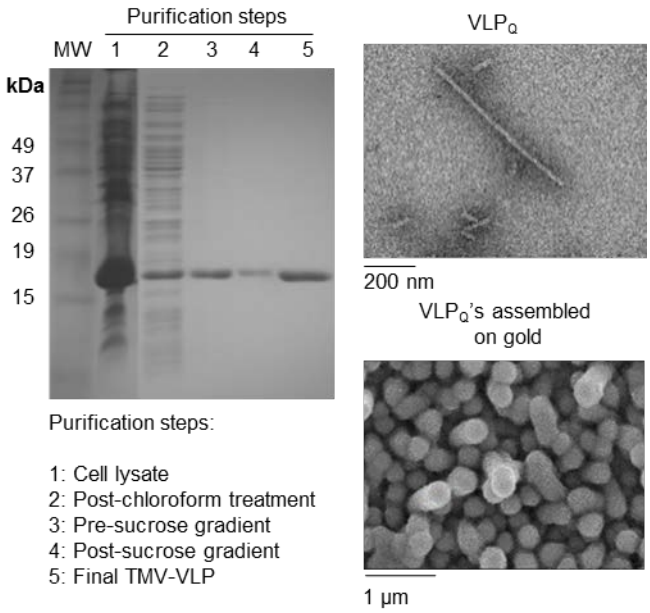

Figure 4-2 Purification and Assembly of engineered VLP_Q

(a) 4-20% SDS PAGE gel indicating different stages of the VLP_Q purification process. **(b)** TEM image indicating the fully assembled TMV-VLPs engineered with glutamines (VLP_Q); Scale: 200 nm. **(c)** SEM image indicating VLP_Q assembled on the surface of gold coated microchip; Scale: 1 µm.

4.4.2 Conjugation of proteins onto engineered VLPQ via mTG mediated conjugation chemistry

After displaying the assembly of the VLP_Q monolayer on the gold surface, I next ascertained if the engineered Gln residues in VLP_Q can be utilized for conjugation of proteins using microbial transglutaminase (mTG). To this end, I used an enhanced green fluorescent protein engineered with 7 lysines at the C termini (denoted as $EGFP_K$) and conjugated it to the VLP_Q using mTG (**Figure 4-3**).

As qualitative evidence, I first used fluorescence microscopy to determine the assembly of $EGFP_K$ to VLP_Q's. I assembled a VLP_Q monolayer onto 10mm^2 gold chips

(**See 4.3.4**) and conjugated 7.5 µM $EGFP_K$ to VLP_Q's using 10 µM microbial transglutaminase (mTG). After incubation at RT for 60 min, I washed the chips with 0.1M Phosphate buffer, pH 7 and air dried the gold chips. As controls, I also performed experiments without mTG. Fluorescence microscopy images **Figure 4-3b** indicated that in the presence of mTG, $EGFP_K$ is conjugated to VLP_Q while the negative controls displayed negligible fluorescence.

Next, to quantify the amount of $EGFP_K$ conjugated to the VLP_Q monolayer on gold chips, I performed *ex situ* quartz crystal microbalance (QCM), **Figure 4-3c**. Initially, I measured the resonant frequency (F_{Cell}) of each individual gold coated quartz crystal sensor (ICM, Oklahoma, USA) used in the QCM experiments. Later, I assembled the VLP_Q monolayer on the sensor (area: 2 mm^2) using 25 µg of VLP_Q. After incubation at 4˚C for overnight, I removed the excess VLP_Q's by washing with Super Q water, vacuum dried the sensor chips at RT for 60 min and measured the resonant frequency again (F_{VLP}). I observed a shift in frequency corresponding to the addition of the VLP_Q monolayer and determined the frequency change (ΔF_1) between F_{Cell} and F_{VLP}. Next, I added 7.5 µM $EGFP_K$ and 10 µM microbial transglutaminase (mTG) to the VLP_Q monolayer and incubated at RT for 60 min. Post incubation, I washed the crystals again with Super Q water; vacuum dried the sensors and measured the frequency again ($F_{mTG/EGFP}$). Post conjugation, I noted a yet another shift in the frequency (ΔF_2) between F_{Cell} and $F_{mTG/EGFP}$ indicating conjugation of the $EGFP_K$ to VLP_Q monolayer. As expected, control experiments without mTG or $EGFP_K$ showed negligible frequency change. Using the Saurbrey's equation[181], I correlated ΔF_1 and

ΔF_2 to the amount of material assembled on the sensor at each step of the assembly process. I estimated that ~100 ng of VLP_Q's was assembled on the sensor surface (0.2 cm^2) and ~1.15ng of $EGFP_K$ was conjugated per 1 ng of VLP_Q on the sensor, indicating ~47% coverage of VLP_Q surface with $EGFP_K$. Both conjugation controls had ~0.1ng of proteins assembled per 1 ng of VLP_Q's indicating a 10-fold difference between mTG mediated conjugation and nonspecific binding of EGFP on sensors.

These qualitative and quantitative results indicated that proteins engineered with lysines can be conjugated to the VLP_Q monolayer using mTG mediated conjugation chemistry.

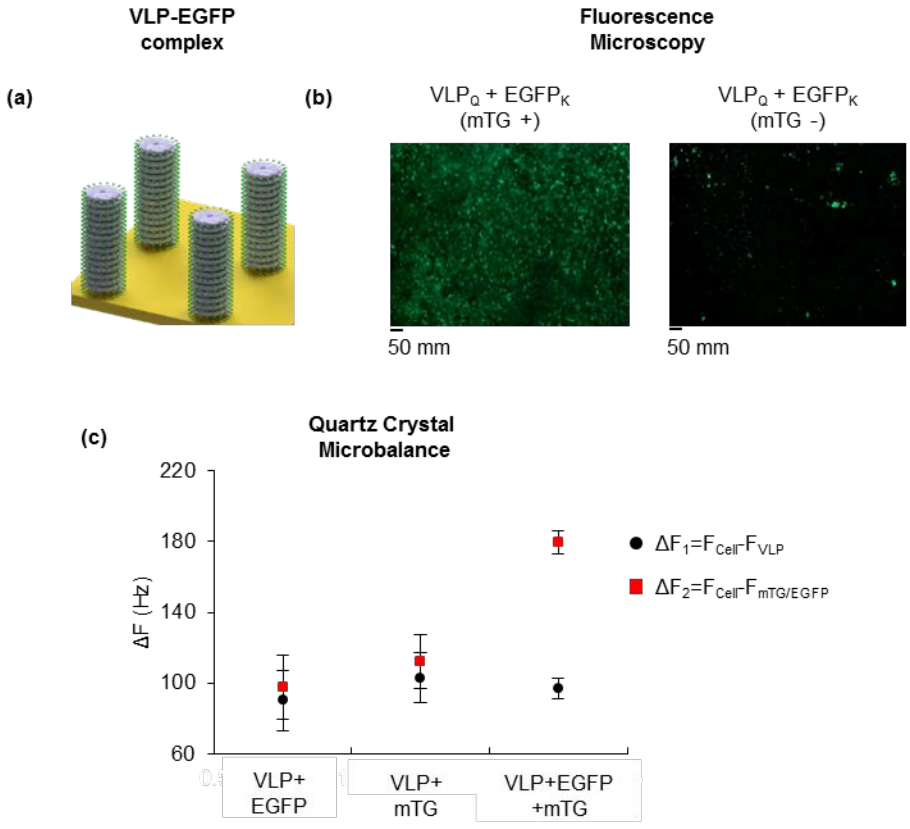

Figure 4-3 Qualitative and Quantitative evidence for protein assembly onto VLP_Q via mTG mediated conjugation

(a) Assembly of $EGFP_K$ (EGFP engineered with Lys tag at C termini) onto VLP_Q monolayer on chips using microbial transglutaminase and engineered tags. **(b)** Qualitative fluorescence microscopy images of $EGFP_K$ conjugated to VLP_Q; Scale: 50 mm **(c)** Quantitative quartz crystal microbalance data indicating conjugation of $EGFP_K$ to VLP_Q in the presence of mTG. Resonant frequency of empty sensor (F_{cell}), after addition of VLP_Q (F_{VLP}) and after conjugation of EGFP to VLP ($F_{mTG/VLP}$) is measured. Change in the frequency due to addition of VLPs onto sensors ($\Delta F1$) are indicated by black circles. Change in the frequency due to the assembly of proteins onto VLPs are indicated by red squares ($\Delta F2$). Error bars indicates standard deviation across three independent sensors used for each condition.

4.4.3 Conjugation of enzymes to mTG

After displaying conjugation of proteins to the VLPs, I intended to display assembly of enzyme cascades on the VLP_Q monolayer assembled on gold chips. To display this, I assembled a three-enzyme synthetic cascade for conversion of S-adenosylmethionine (SAM) and S-adenosylhomocysteine (SAH) to homocysteine (HCY), all part of methyl cycle. I employed three *E. coli* enzymes namely 1) trans-aconitate methyl transferase (Tam) for conversion of S-adenosylmethionine (SAM) to S-adenosylhomocysteine (SAH)[182]; 2) S-adenosylhomocysteine nucleosidase (Pfs) for conversion of SAH to S-ribosylhomocysteine (SRH)[130] and 3) S-ribosylhomocysteinase (LuxS) for conversion of SRH to homocysteine (HCY) and autoinducer-2(AI-2), a quorum sensing (QS) enabling molecule[129] (**Figure 4-4a**). While Pfs and LuxS are part of the activated methyl cycle in bacteria, Tam is not known to be involved. However, *tam* is part of *lsr* quorum sensing operon and is directly regulated by AI-2, the QS molecule produced in the cascade.[108]

Since I had already characterized Pfs and LuxS in earlier chapters of this thesis, here I first studied Tam. I cloned *tam* gene out of *E. coli* genome, engineered with 7 Lys amino acids at C termini (denoted as $T_{K)}$ and purified the enzyme (See Methods). To determine whether Tam can convert SAM into HCY, I added 3 µM concentrations of each soluble with 1mM SAM and incubated for 60 min at 37°C. After incubation, I measured amounts of HCY generated using a calorimetric assay (Ellman's sulfhydryl assay, See Methods) (**Figure 4-6)**. I also characterized an electrochemical method using cyclic voltammetry to detect HCY **(Figure 4-7)**. Results indicated that there was a 100% conversion from SAM to HCY. Going further, I assumed 3 µM enzyme concentration and 60 min incubation at 37°C as non-rate limiting conditions for reactions involving soluble enzymes.

Next, I individually immobilized each enzyme of the cascade onto the VLP_Q monolayer and determined their relative enzyme activities in immobilized state. I used Tam, Pfs and LuxS enzymes engineered with 7 lysines at both the N and the C terminus (denoted as ${}_KT_K$, ${}_KP_K$ and ${}_KL_K$ respectively) and conjugated them to VLP_Q monolayer. In all experiments, I first assembled the VLP_Q monolayer onto the gold surface by incubating 25 µg of VLP_Q's onto 1 cm^2 gold chips and performed blocking and washing steps as detailed before.

Firstly, I conjugated LuxS, the last enzyme in the three-enzyme cascade onto VLP_Q monolayer assembled on gold chips. I added 20 µM and 50 µM concentrations of L_K along with 10µM of mTG for conjugation and incubated for 60 min at RT. As conjugation controls, I also performed the same reactions without mTG. After

incubation, I washed the chips with Phosphate buffer and provided 1mM SAH and soluble Pfs (at 3 μM concentration) in 10mM Phosphate Buffered Saline, pH 7.4 (PBS) to the VLP-LuxS monolayer on chips. After incubation at 37°C for 2 hours, I measured the amount of HCY generated through Ellman's assay. Results indicated that with increasing concentrations of LuxS conjugated to VLP_Q monolayer there was increasing amounts of HCY generated with 50 μM conjugation condition yielding 20% conversion from SAH to HCY. (**Figure 4-4b**). These results confirmed with earlier results that LuxS was the rate-limiting factor among Pfs and LuxS enzymes. [106] Conjugation controls without mTG had negligible HCY generations. As an additional control, I also conjugated L_K onto empty-VLP monolayer lacking the engineered glutamines at the C termini of TMV capsids(TMV1Cys). Interestingly, there was small yet significant HCY generation from empty-VLP monolayer in comparison to its own conjugation control indicating enzyme conjugation to native glutamines in the TMV capsid. However, HCY yields from empty-VLP monolayer was still lower than yields from VLP_Q monolayer indicating enhanced protein conjugation due to engineered glutamines in VLP_Q.

Next, I conjugated Pfs, the second enzyme in the enzyme cascade. I conjugated 20 μM of P_K onto VLP_Q monolayer under similar conjugation conditions as before. After conjugation, I washed the chips and added 1mM SAH and 3 μM of soluble LuxS in PBS. After 2 hours of incubation at 37°C, I measured HCY yields. Results indicated 85% conversion of SAH to HCY indicating that P_K had higher enzyme activity than LuxS. Significantly, even the conjugation controls without mTG gave ~65%

conversion of SAH to HCY (**Figure 4-4c**). These results again indicated that Pfs was not the limiting factor. I repeated similar conjugation experiments for Tam, the first enzyme in the cascade. After conjugation, I provided 1mM SAM as substrate for Tam along Pfs and LuxS (each 3 μM) and incubated for 2-hour incubation at 37°C. I measured HCY yields and the results indicated 20% to 30% conversion of substrate SAM to HCY. Conjugation controls without mTG had negligible HCY yields (**Figure 4-4d).** I also independently immobilized all the enzymes in the cascade onto the VLP monolayer on gold surface and characterized the km, Vmax and kcat values for each enzyme **(Figure 4-8).**

In sum, I studied the relative enzyme activities of all three enzymes when conjugated independently to VLP_Q monolayer through mTG mediated conjugation. Second enzyme in the cascade, Pfs had the highest enzyme activity in comparison to Tam and Pfs. Under the conjugation conditions used, Tam displayed a marginally higher enzyme activity than LuxS.

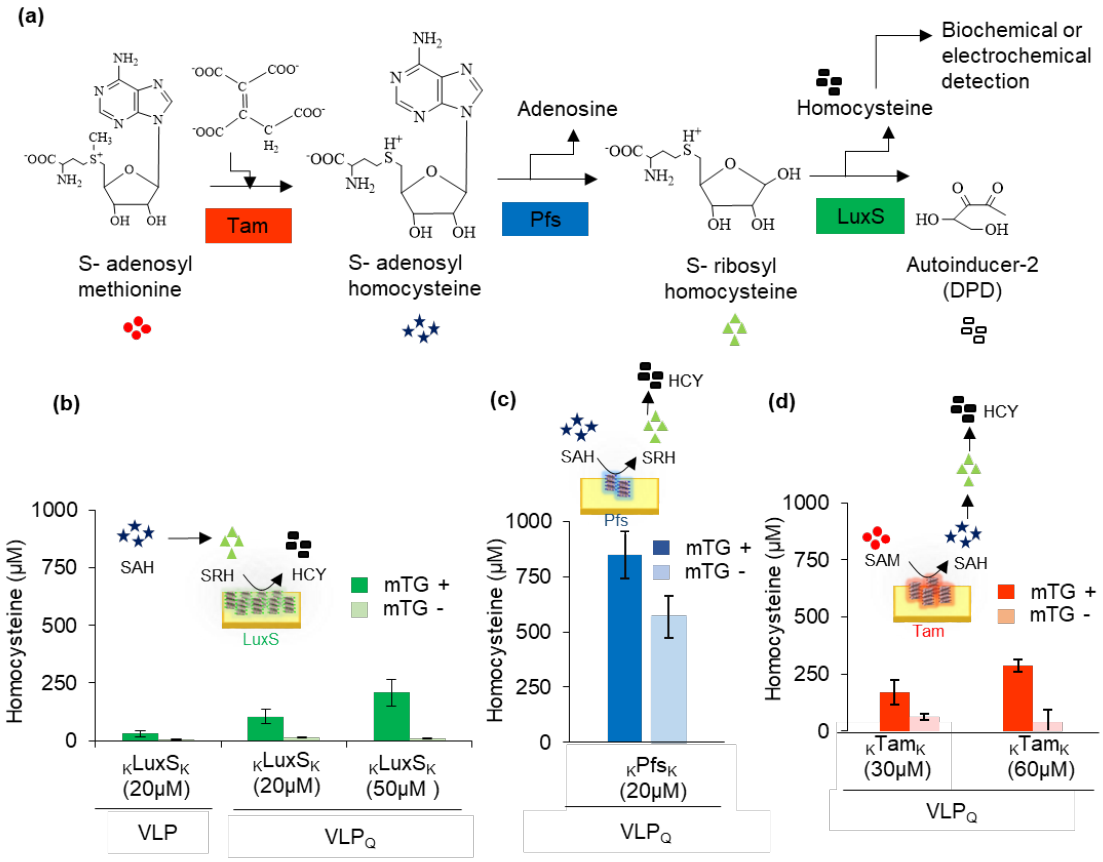

Figure 4-4Assembly of enzymes involved in conversion of S-adenosylmethionine (SAM) to Homocysteine (HCY) onto microchips.

(a) Three enzyme synthetic cascade for conversion of S-adenosylmethionine (SAM) to Homocysteine (HCY). Tam converts SAM to S-adenosylhomocysteine (SAH). Pfs converts SAH to S-ribosylhomocysteine (SRH). LuxS converts SRH to homocysteine (HCY) and Autoinducer-2. **(b, c and d)** Each individual enzyme engineered with Lysine tags (7 Lys at both the N and the C termini) are conjugated separately to VLP_Q assembled on the surface of microchips. These immobilized enzymes are provided with 1mM SAM (for Tam) and 1mM SAH (for Pfs and LuxS) and the other remaining enzymes for HCY generation at non-rate limiting conditions (3 μM of each enzyme). Reaction is incubated at 37°C for 2 hours and the amounts of HCY generated was quantified using Ellman's assay.

4.4.4 Layer by Layer assembly of enzymes onto VLPQ

After displaying the assembly of individual enzymes of the cascade onto VLP_Q monolayer, I intended to display layer-by-layer assembly of multiple enzymes on VLP_Q monolayer. To display multi-layer assembly, I first constructed a two-enzyme cascade comprising of Pfs and LuxS for the conversion of SAH to HCY. For this, I adopted our earlier described modular construction approach of assembling multiple enzyme components using mTG (**Figure 4-5a,b**).[105, 106]

To mediate construction, I used Pfs engineered with 7aa lysine tags at both the N and the C termini ($_KP_K$) and LuxS with 5aa Gln tags at the C termini (L_Q). As with single enzyme assembly, I first assembled the VLP_Q monolayer onto 10 mm^2 gold chips as before. Then, I added 30 µM $_KP_K$ and 10µM mTG for Pfs conjugation onto to the VLP_Q monolayer. After conjugation for 60 min at RT, I washed the chips again and performed another round of mTG mediated conjugation as before to conjugate different concentrations of L_Q (30 and 90 µM) onto the assembled VLP_Q-$_KP_K$ complex. After conjugation and wash steps, I provided 1mM SAH in PBS for 2 hrs at 37°C and measured the HCY yields through Ellman's assay. I observed that with the increasing concentration of LuxS there was an increase in HCY generation indicating again LuxS as the rate limiting factor among Pfs-LuxS (**Figure 4-5c**). More importantly, HCY yields obtained from conjugation of LuxS in the second layer was lower than the HCY yields obtained from conjugation of LuxS in the first layer of assembly (**Figure 4-4b**). These results confirmed with our earlier results with layer by layer assembly where per unit enzyme activity decreases with increasing layers of enzymes.[106]

Next, I intended to assemble a three-enzyme cascade comprising Tam, Pfs and LuxS for conversion of SAM to HCY. To overcome the kinetic limitations with both Tam and LuxS being rate limiting and the fabrication limitations with the layer-by-layer approach (see page 114, **Figure 4-10**), I used genetically fused enzymes to reduce the number of layers required for the three enzyme assembly (**Figure 4-5d**). For this, I employed a fusion enzyme containing equimolar concentrations of Pfs and LuxS for conversion of SAH to HCY.[112] This fusion enzyme was also engineered with 5 Gln residues at the C termini (denoted FE_Q) to enable conjugation via mTG[180]. I engineered Tam, the first enzyme in the cascade with 7 Lys residues at both the N and the C termini (labelled as $_KT_K$) and used $_KT_K$ as the first layer of enzymes to conjugate onto VLP_Q. I assembled the VLP_Q monolayer onto 10mm^2 gold chips as before and added 120 µM of $_KT_K$ along with 60 µM mTG onto VLPs. To enable increased conjugation, I increased the conjugation time from 60 min to 2 hours at RT. After incubation, I washed the chips as before and conjugated 50 µM FE_Q to VLP-$_KT_K$ complex with another round of mTG mediated conjugation. After conjugation for 2 hours, I washed the chips again and added substrates 1mM SAM and SAH separately and incubated the chips at 37˚C for 2 hours. HCY yields indicated that there was 22% conversion of SAM to HCY and 33% conversion of SAH to HCY (**Figure 4-5e**). Differences in conversion between SAM and SAH on chips could be attributed to lack of diffusion of substrate SAM and TAA, the methyl acceptor for Tam into the first layer of enzymes. Controls experiments containing just Tam assembled in the first layer on chips with Pfs and LuxS in solution gave ~75% conversion (**Figure 4-10**). Decrease

in percentage of conversion of SAM to HCY from 75% in controls to 22% again indicated reduction in per unit enzyme activity of FE assembled in second layer. Considering that I added low concentrations of second layer enzymes (50 μM) in comparison to the first layer of enzymes (120 μM) for conjugation, I could increase the concentrations of second layer enzymes to generate higher percentages of conversion of SAM to HCY

In sum, I displayed that I could use the mTG mediated conjugation approach to build a three-enzyme cascade on VLP_Q monolayers assembled on the gold surface. Enzyme activity decreased with increasing layers in the layer by layer assembly process and to circumvent this problem, I used genetically fused enzymes to minimize the number of layers required for a three-enzyme assembly. Alternatively, the possibility of fusing all the three enzymes into a single fusion protein to assemble as a single layer onto VLP_Q's needs to be explored.

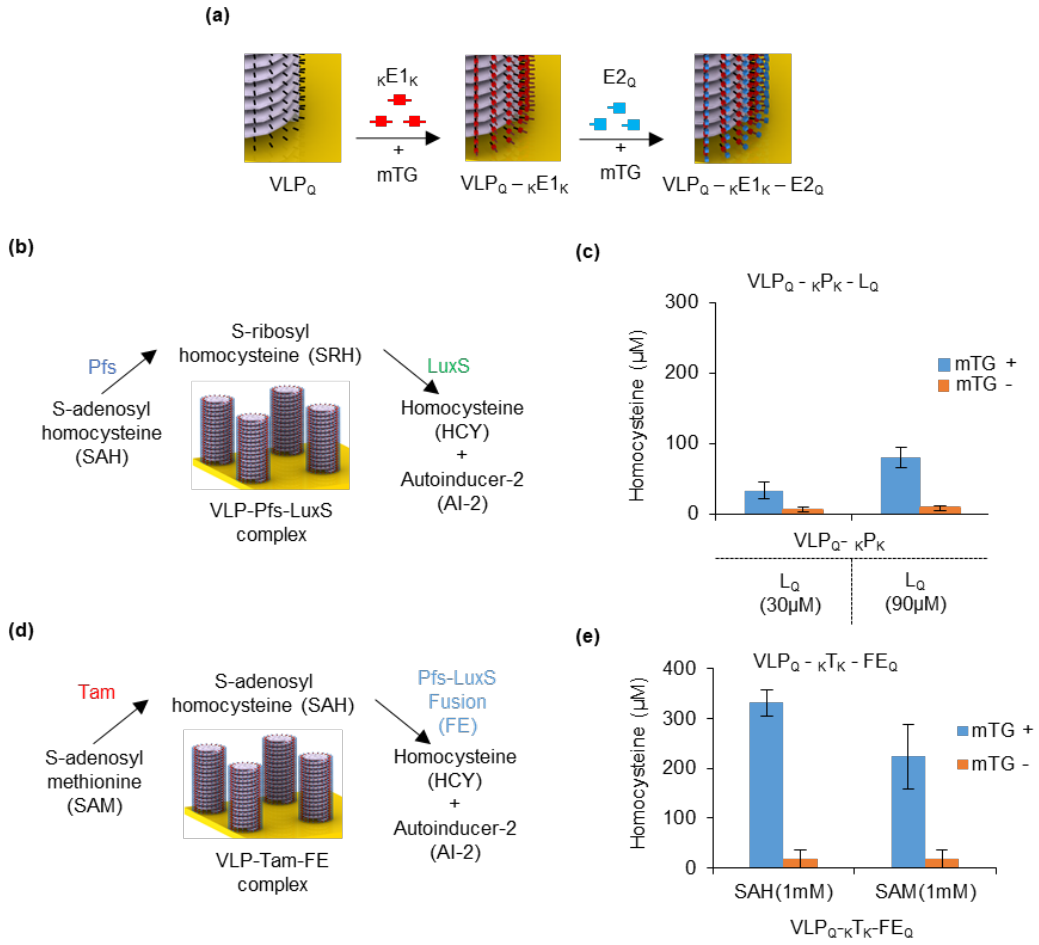

Figure 4-5 mTG mediated layer by layer assembly of three enzyme cascades onto gold chips

(a) Scheme of layer-by-layer assembly of enzymes onto VLPs using transglutaminase chemistry. The first enzyme in the assembly, engineered with Lys tags at both the N and the C termini, is conjugated to VLP first through mTG. Unreacted Lys tag in the first layer is conjugated to second layer of enzymes engineered with Gln tags at the C termini. **(b)** Scheme of VLPs conjugated to Pfs and LuxS in a layer-by-layer process and the biochemical reaction catalyzed by the two enzymes assembled on chips. **(c)** Biochemical data from VLP_Q-$_KP_K$-L_Q complex assembled on chips. Enzyme complex is reacted with 1mM SAH and incubated for 2 hours and HCY is measured using Ellman's assay. **(d)** Assembly of three enzymes Tam, Pfs and LuxS in two layers onto VLP_Q. First layer comprised of Tam engineered with Lys tags at both the N and the C termini and second layer comprised of Pfs-LuxS fusion protein engineered with Gln tag at the C termini (FE_Q) **(e)** Biochemical data from VLP_Q-$_KT_K$-FE_Q complex. Enzyme

complexes are reacted with 1mM SAM as well as 1mM SAH and incubated for 2 hours and HCY is measured using Ellman’s assay.

4.5 Conclusion

In conclusion, I have developed a self-assembling 3D scaffold that displays desired functional groups for biocomponent functionalization on the sensor surface. In association with 3D scaffolds, I also adapted a bio-conjugation framework using which I built a three-enzyme cascade 'layer-by-layer' onto the VLP_Q monolayer assembled on the gold surface. Combining the scaffold material and conjugation framework, I assembled a synthetic enzyme cascade at the electronic surface to convert methyl cycle intermediates (SAH and SAM) into homocysteine that can be detected through calorimetric and electrochemical means.

The novelty of this approach is that I utilized bio-based materials and techniques for hierarchical assembly of interfacial materials and synthetic cascades on electronic surfaces. In addition to several conjugation chemistries that have been genetically engineered into VLPs for conjugation of cargoes, I have added mTG mediated conjugation chemistry for protein assembly onto VLPs and employed the facile and rapid mTG chemistry for multi-component assembly with nanoscale spatial resolutions.

The significance of the work is that the process of integration of biological components with electronics is simplified due to self-assembly of interfacial material. 3D scaffolds in combination with conjugation chemistry enables integration of more complex enzyme systems at the electrode interface to detect new biochemicals using

electrochemical means. TMV-VLP as 3D scaffolds are bio-compatible to human body and can be used as interface materials in *in situ* biosensors as well. Synthetic enzyme cascades assembled on the surface of the chip can be developed into a fully functioning biosensor for SAM and SAH detection. Stoichiometries of each individual enzymes needs to be optimized further to improve the response time and various sensor parameters like sensitivity, detection limit and linear range needs to be characterized for a fully functioning SAM biosensor.

4.6 Supplementary information

4.6.1 Enzyme activity of Tam in solution

After I purified the Tam enzyme (**See 4.3.1**), I ascertained whether the purified enzyme was active. I added all the three enzymes in the cascade, Pfs, LuxS and Tam (3 µM each) and added 1mM SAM as substrate for Tam along with 20 mM trans-aconitic acid (TAA), the methyl acceptor for Tam in 0.4M HEPES buffer, pH 7.5 and incubated at 37°C for 60 min. After incubation, I measured the amounts of HCY generated by Ellman's assay (**Figure 4-6**). I observed 100% conversion from SAM to HCY. Controls without Pfs and LuxS had no HCY.

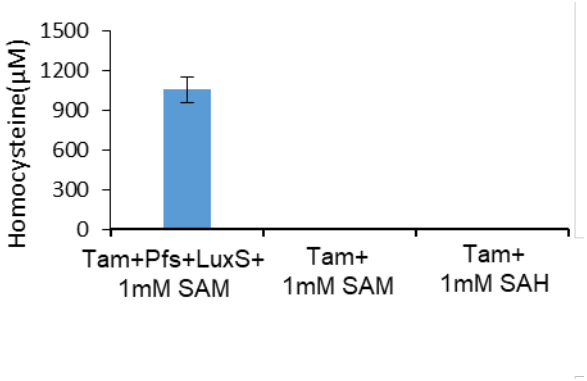

Figure 4-6 Enzyme activity of Tam in solution

Measurement of conversion of SAM to HCY by soluble enzymes Tam, Pfs and LuxS (3 µM concentrations for each enzyme) using Ellman's assay. Controls included just Tam with 1mM SAM as well as 1mM SAH.

4.6.2 Electrochemical detection of HCY from SAM

I had earlier used cyclic voltammetry (CV) to determine concentrations of HCY from SAH.[103] Here, I employed CV using a standard gold electrode (CH Instruments) to determine concentrations of HCY obtained from SAM. I incubated 1mM SAM along with 3 µM each of Tam, Pfs and LuxS in solution and after 2 hours of incubation at 37°C I performed Ellman's assay to measure HCY concentrations via Ellman's assay. Based on the concentrations obtained from Ellman's assay, I prepared various dilutions of HCY and performed CV's (Cyclic Voltammogram in **Figure 4-7a**). I measured the total charge that was accumulated at the working electrode and built a standard curve correlating charge to HCY concentrations (**Figure 4-7b)**. Based on the standard deviation of the blank sample (-2.1µC), I estimated the LOD of the technique to be ~100µM homocysteine.

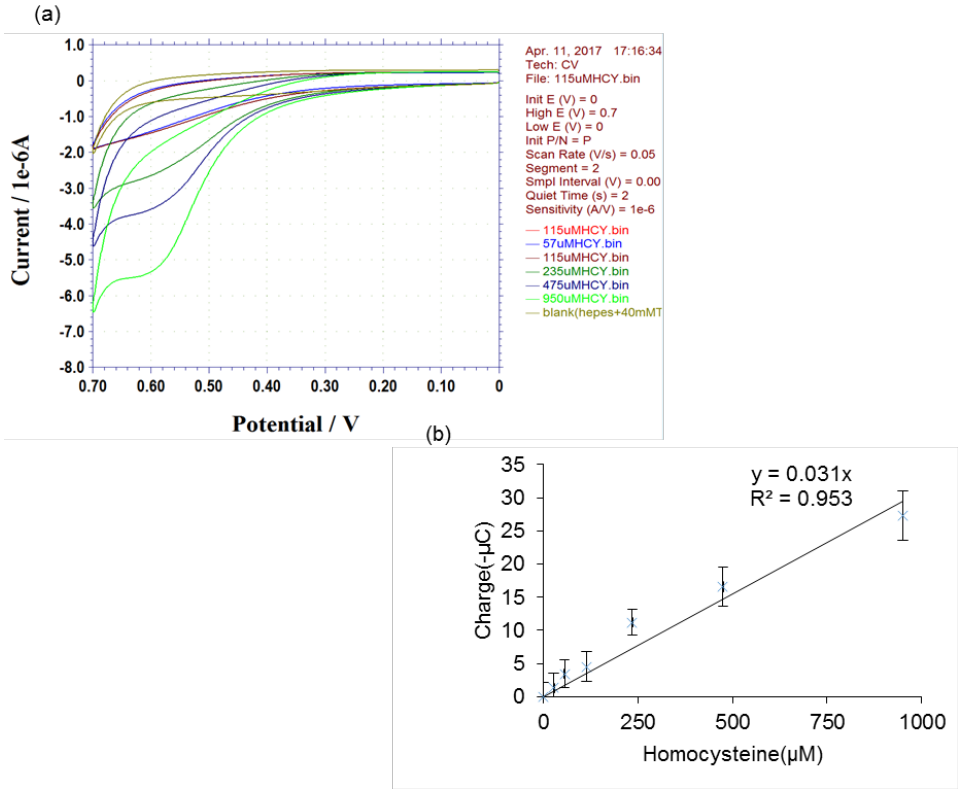

Figure 4-7 Electrochemical detection of HCY

(a) Cyclic voltammetry based detection of HCY from SAM. I swept potentials from 0 V to 0.7 V and back and measured the amount of current that is generated with various concentrations of HCY in solution. **(b)** Standard curve correlating the charge accumulated in CV vs HCY concentrations, n=2.

4.6.3 Michaelis-Menten kinetics on immobilized enzymes

I intended to determine the km and Vmax values for each enzyme in the synthetic cascade when immobilized onto the VLP_Q monolayer on the gold surface. To enable this, I used a gold coated 48 well plate (UMD FabLab) for the assembly of VLP_Q's. I assembled the VLP_Q monolayer onto the gold surface by incubating 25 μg

of VLP_Q's onto 1.4 cm^2 wells in the 48 well plates. To the assembled VLP_Q monolayer, I added 23 µM of each cascade enzyme separately along with 30 µM of mTG. All cascade enzymes were engineered with Lys tags at both the N and the C termini. After 1hour incubation at RT, gold coated 48 well plates were washed with 0.1M phosphate buffer, pH 7.4 and incubated with varying concentrations of substrate SAM along with other soluble enzymes in the cascade required for generation of HCY at non-rate limiting concentrations (3 µM). Rate of HCY generation (V) with various concentrations of the substrate SAM ([S]) were determined for each immobilized enzyme and plotted against substrate concentrations and fitted into Michaelis-Menten model in GraphPad software to determine km and Vmax values **(Figure 4-8)**. kcat value for each enzyme was estimated by using 0.234 µM as effective enzyme concentration (Et) under following assumptions 1) assuming 50% coverage of VLP_Q monolayer with each enzyme, and 2) assuming the efficiency of conjugation for each enzyme onto VLP_Q monolayer was the same under constant mTG conditions.

(a)

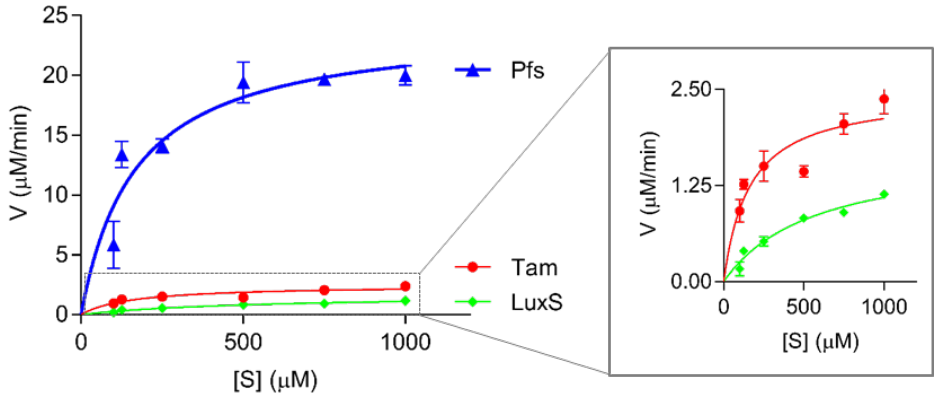

(b)

	Tam	Pfs	LuxS
Km (µM) (Mean±SE)	155±43.6	165.3±41.2	533.5±121.7
Vmax ($\mu M.min^{-1}$)	2.483	24.3	1.701
kcat (min^{-1}) (Mean±SE)	10.6±0.9	103.7±7.8	7.25±0.78

Figure 4-8 Plot of substrate-velocity for km and Vmax estimation.

Determination of km, Vmax and kcat values for each enzyme in the cascade immobilized on the VLP_Q monolayer. 23 µM of each enzyme in the cascade was immobilized onto the VLP_Q monolayer and provided with varying concentrations of substrate S-adenosylmethionine (SAM). Other enzymes in the cascade required for HCY generation were provided at non-rate limiting concentrations (3 µM) in solution. **(a)** Plot of various substrate SAM concentrations ([S]) used and the velocity of homocysteine (HCY) generation (V) with all the three enzymes Tam, Pfs and LuxS for each SAM concentration employed. **(b)** Table indicating km, Vmax and kcat values for each of the immobilized enzyme obtained by fitting [S] and V values for all enzymes into Michalis- Menten model using GraphPad.

4.6.4 Conjugation of Enzymes to VLPs in solution

As an alternative to layer-by-layer assembly, I intended to first conjugate enzymes to VLPs and then directly assemble the VLP-enzyme conjugates onto gold chips. To mediate conjugation of enzymes to VLPs in solution, I added 100 µg of VLP_Q, 400 µg of $Enzyme_K$ and 16 µM mTG in a total reaction volume of 600 µls and incubated at RT for 2 hours with gentle shaking. To isolate VLPs and VLP-enzyme conjugates from the rest of the mixture, I performed ultracentrifugation at 112000g for two hours and re-dissolved the pellet in 100 µL of Phosphate Buffer, pH 7.0 by gentle shaking at 4°C for overnight. To characterize the enzyme activities of conjugates, I added various amounts of all the three VLP-enzyme conjugates onto $10mm^2$ gold chips and incubated at 4˚C for overnight. Post incubation, I washed the gold chips with phosphate buffer, pH 7 and provided 1mM substrate (SAM for Tam and SAH for both Pfs and LuxS) and other enzymes required for HCY generation. After 2-hour incubation at 37˚C, I measured HCY yields and results indicated that Pfs conjugates were the most active followed with LuxS and Tam conjugates **(Figure 4-9a**). As controls, I also performed relative enzyme activity measurements on VLP-enzyme conjugates in solution prior to adding on gold chips (data not shown). As expected, enzyme activities of conjugates in solution were higher than conjugates assembled on gold but the relative trends among the three enzyme-VLP conjugates were the same.

However, I did not use this method for conjugation of VLPs and enzymes due to the formation of large VLP-enzyme aggregates (data not shown) and very low

recovery of conjugates from ultracentrifugation process. Hence, layer-by-layer approach was preferred to assemble the enzymes on chip.

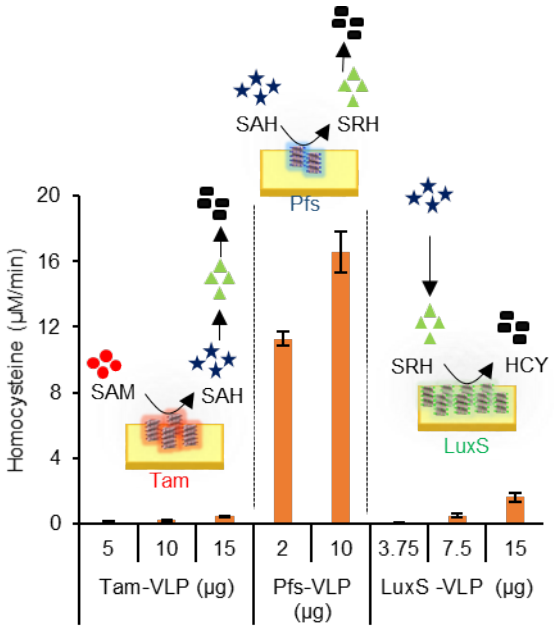

Figure 4-9 Measurement of relative enzyme activity of VLP-enzyme conjugates

VLPs and enzymes were first conjugated in solution and purified. Relative enzyme activities of various VLP-enzyme conjugates on chips are displayed. VLP-LuxS and VLP-Pfs conjugates were provided with 1mM SAH and VLP-Tam conjugates were provided with 1mM SAM as substrates and incubated at 37°C for 2 hours. Other enzymes required for HCY generation are provided in solution at 3 μM concentration, n=3.

4.6.5 Assembly of a three-enzyme cascade comprising individual Tam, Pfs and LuxS onto VLP monolayers

I intended to assemble all the three individual enzymes Tam, Pfs and LuxS onto VLPs in a layer by layer fashion. However, since there was a reduction in enzyme activity with increasing layers in the layer by layer approach (**Figure 4-5c**), I intended

to perform the three-enzyme cascade in two chips of equal sizes (10 mm^2) placed side by side. I performed four conditions with different enzyme arrangements in each.

In condition 1, I had 120 µM of $_KT_K$ conjugated to VLP_Q monolayer on gold chips and provided other two enzymes Pfs and LuxS (3 µM each) in solution. In condition 2, I had 120 µM of $_KT_K$ conjugated to VLP_Q monolayer on gold chips as the first layer of enzymes and P_Q (20 µM) conjugated to $_KT_K$ in the second layer. I also provided LuxS (3 µM) in solution. In condition 3, I had $_KT_K$ and P_Q on VLP_Q monolayer, just like condition 2. In addition, I also had L_K (60 µM) conjugated to the VLP_Q monolayer in a second chip. In condition 4, I had 120 µM of $_KT_K$ conjugated to VLP_Q monolayer in chip 1 and VLP_Q-$_KP_K$- L_Q in chip 2. In all these conditions, I provided 1mM SAM as substrate, incubated at 37°C for 2 hours and HCY yields measured using Ellman's assay.

Results indicated that condition 1 with $_KT_K$ conjugated to VLP_Q monolayer had highest HCY yields with ~75% conversion of SAM to HCY. Condition 2 containing Tam and Pfs in a single chip had marginally lower yields than in condition 1 with ~60% conversion. HCY yields from conditions 3 and 4 with LuxS in a second chip was lower than 20% indicating LuxS limitation in the cascade. To overcome these fabrication and kinetic limitations, I adopted a genetic fusion strategy to combine Pfs and LuxS into a single protein (labelled as Fusion enzyme, FE) and conjugated to Tam on VLP monolayer (**Figure 4-5e** and **Section 4.4.4)**.

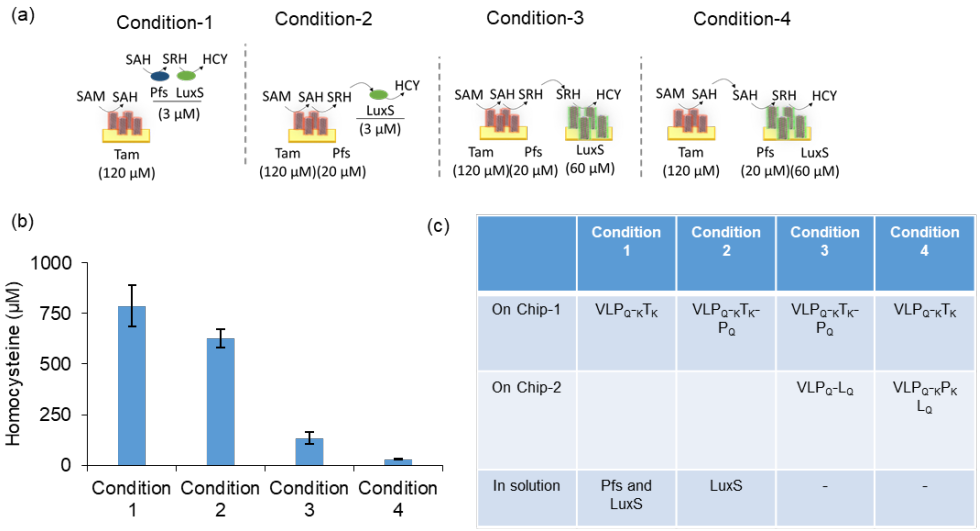

	Condition 1	Condition 2	Condition 3	Condition 4
On Chip-1	$VLP_{Q-K}T_K$	$VLP_{Q-K}T_{K-}P_Q$	$VLP_{Q-K}T_{K-}P_Q$	$VLP_{Q-K}T_K$
On Chip-2			VLP_Q-L_Q	$VLP_{Q-K}P_K L_Q$
In solution	Pfs and LuxS	LuxS	-	-

Figure 4-10 Assembly of a three-enzyme cascade comprising individual Tam, Pfs and LuxS onto VLP_Q monolayers.

Scheme **(a)** depicts various conditions used for the assembly of three enzymes in one and two chip configurations. Condition 1 had just one chip with Tam immobilized on the VLP monolayer. Condition 2 had 1 chip with both Tam and Pfs. Condition 3 had two chips, with Tam and Pfs in one chip and LuxS in the second chip. Condition 4 had two chips, with Tam in one chip and Pfs and LuxS in second chip. **(b)** Relative HCY yields from all 4 conditions after incubation with 1mM SAM for 2 hours at 37°C. Other enzymes required for HCY generation are provided in solution at 3 μM concentration, n=3.

Chapter 5 Integration of CRISPR with electrogenetic promoter systems for transcriptional regulation

Sections from this chapter will be submitted for publication by March 2018

5.1 Introduction

5.1.1 Concept of electrogenetics

The term *electroceuticals* was coined by the pharmaceutical company GlaxoSmithKline, refers to the application of electrical impulses to stimulate nerves and muscles for alleviation of pain[183], movement disorders[184], urinary functions[185], wound healing[186] etc. However, these are examples of systems level perturbations in human body targeting nerves and muscles and the potential of targeting specific genes in the host system using electrical signals for modulating transcriptional regulation is largely unexplored.

Synthetic biology, an interdisciplinary field involving assembly of standardized biological parts to replicate basic engineering functions like logic Boolean gates, band pass filters, oscillatory functions etc. in biologic systems[187], has produced two electrogenetic promoter systems. First system involves a bacterial promoter system in mammalian cells that responds to electrochemical conversion of ethanol to aldehyde with expression of SEAP (secreted embryonic alkaline phosphatase).[100] Second system is an oxidative stress response promoter SoxS that responds to Pyocyanin (PYO), an oxidative stress inducing molecule in bacteria. SoxS promoter activity is controlled by electrochemical recycling of Ferricyanide and

Pyocyanin(PYO) and has been used for electrical activation of Quorum Sensing (QS) and chemotaxis in bacteria.[99]

In both the electrogenetic systems described above, specific transgenes were produced from electrogenetic promoters. In this work, I propose to enhance the capabilities of electrogenetic systems by integrating synthetic transcriptional factors (TF) with electrogenetic promoters. To achieve this goal, I planned to integrate the CRISPR-Cas9 system based TF's with the *E coli* SoxS promoters and upon electrochemical induction, TF's can be produced to target specific genes in the bacterial host system and regulate transcription. Both components of our system, the electrogenetic SoxS promoters and the CRISPR-Cas9 based synthetic TF's are introduced in the next few sections.

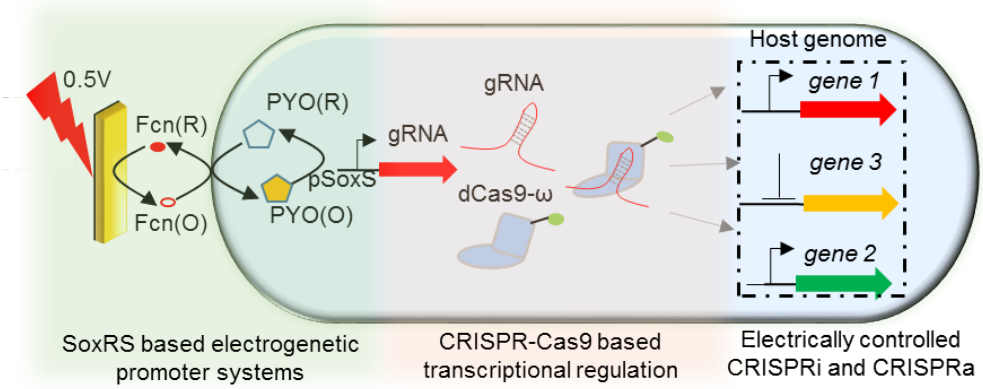

Scheme 5-1 Connecting electrogenetic promoter SoxS with CRISPR for bacterial transcriptional regulation.

SoxRS based electrogenetic promoter systems can be electrically induced using Ferricyanide (Fcn) and Pyocyanin (PYO). The CRISPR-Cas9 based transcriptional regulation system comprising of transcriptional activator dCas9-ω and gRNA can target any specific gene in the genome and modulate transcription. Combining the two systems can lead to electrical control over host transcriptional regulation.

5.1.2 Electrogenetics based on SoxRS system

The SoxRS system is one of the two-primary oxidative-stress defense response mechanisms in bacteria and comprises of two components, SoxR, the repressor for SoxRS system and SoxS, a MerR family transcription factor. Both *soxR* and *soxS* are expressed from overlapping SoxRS promoters and in the absence of oxidative stress, SoxR represses the SoxRS promoters. Upon exposure to oxidative stress, SoxR de-represses the SoxS promoter resulting in ~100-fold upregulation of SoxS. SoxS is the primary mediator of host defense mechanism to oxidative stress[188] and directly upregulates transcription of ~15 genes including superoxide dismutases (*sodA* and *sodB)*, fumarate hydratase (*fumC*), glucose-6-phosphate dehydrogenase (*zwf*) among others. All of them are related to reduction of oxidative stress in bacteria.

In a previous work from our group, the SoxRS system was re-purposed into an electrogenetic device where the oxidative stress response promoter SoxS is activated through Pyocyanin (PYO) and Ferricyanide (Fcn (O)) to express specific genes of interest.[99] PYO, a phenazine class antibiotic produced by *Pseudomonas aeruginosa*, can oxidize the SoxR repressor leading to de-repression of SoxS promoters. Upon oxidation of SoxR, the now-reduced PYO can be recycled again by electron transfer across the electron transport chains with oxygen as the final electron acceptor in aerobic conditions. Intracellular PYO recycling can also be mediated by redox active electron acceptors like Ferricyanide (Fcn (O)) and Ferrocyanide (Fcn (R)) whose redox state can be controlled by application of an electric potential through an electrode. Under anaerobic conditions, by electrically controlling the conversion of Fcn (R) to Fcn (O),

the redox capacitance of the system to accept electrons can be controlled leading to control over intracellular PYO recycling and in turn the SoxS promoter activity.

5.1.3 CRISPR-Cas9 based synthetic transcriptional factors (TF's) for transcriptional regulation

CRISPR (Clustered Regularly Interspaced Short Palindromic Repeats)-Cas9 is an adaptive immune system in bacteria that is used for defense against viruses. The *S pyogenes* CRISPR-Cas9 system comprises of two components: Caspase 9 (Cas9), a nuclease capable of inducing double stranded breaks in the DNA and the crRNA (CRISPR RNA) that directs the Cas9 to a specific location in the genome. In general, when a virus infects bacteria, a small part of the DNA from the invader's DNA is incorporated into the CRISPR array of the host bacteria as spacers and transcribed into a CRISPR RNA (crRNA). In type II CRISPR systems, crRNA forms a complex with the trans activating RNA (tracrRNA) and recruits the Cas9 to target the complementary target DNA.[189] Alternatively, crRNA and tracrRNA can also be replaced with a single short guide RNA (gRNA) sequence to direct the Cas9 to a specific location.[190]

The CRISPR-Cas9 system is re-purposed as an efficient genome editing tool and used for creating knock-ins, knock-outs and single strand breaks (nicks) at specific sites in a variety of host genomes. The Cas9 which is a nuclease protein has also been modified to eliminate its nuclease activity (labelled as dead Cas9 or dCas9). The dCas9 can be directed to genes of interest to silence genes in the genome (referred to as CRISPRi).[191, 192] Alternatively, dCas9 has been fused to transcriptional activators such as VP16[193] and ω subunits[194] to recruit transcriptional machinery at desired

sites and activate transcription (referred to as CRISPRa). In addition, the CRISPR-Cas9 system can also be easily multiplexed to simultaneously target different sites. For example, the type II CRISPR system in *S pyogenes* can naturally processes the CRISPR array into several different crRNAs that direct Cas9s to multiple locations. Alternatively, self-cleaving ribozyme processing systems such as hammerhead (HH)[195] and hepatitis delta virus (HDV)[196] have also been used to self-cleave a single transcript into multiple gRNAs.[101]

In an electrogenetic context, the CRISPR-Cas9 system can be utilized to electrically target a specific location in the genome to either edit, silence or activate transcription by insertion of a 20-base pair gRNA spacer sequence into electrogenetic promoters. In this study, I intend to integrate the CRISPR-Cas9 system with SoxRS based electrogenetic promoters to electrically modulate bacterial host gene transcription.

5.1.4 Goals of this work

Due to the presence of well-established eukaryotic transcriptional activators such as VP64, p53 etc., transcriptional activation achieved through CRISPRa is in the range of several thousand fold in eukaryotic systems.[197] However, in the microbial context, CRISPRa is largely unexplored. Bikard et al had originally displayed CRISPRa in bacteria with transcriptional activation of up to 23-fold using ω subunit of RNA polymerase as transcriptional activator. The ω subunit is the non-essential component in bacterial RNA polymerase and its function includes stabilizing the RNA polymerase complex at the target promoter regions[198, 199] as opposed to

mammalian transcriptional activators that actively recruit transcriptional factors for assembly of RNA pol II at target sites. Hence, there is a strong need to develop efficient transcriptional activators in bacteria. Here, I studied whether increase in number of transcriptional activators (ω subunits) can lead to enhanced CRISPRa.

Additionally, there is a need to create tunable and controllable CRISPRa systems for better integration with the existing synthetic biology tool set. In this study, I characterized various factors such as promoter and copy numbers of plasmids expressing CRISPR components; mode of spacer delivery through the short gRNA system and the tracrRNA: crRNA hybrid system; effect of mutations in the seed region of spacers on the effect of CRISPRa to obtain tunable, controllable CRISPRa. In addition, I also integrated the CRISPRa system into electrogenetic SoxS promoters to obtain an electrically tunable CRISPRa.

One of the major challenges in synthetic biology is to make the assembled biological parts function uniformly across a vast variety of chassis strains.[200] Such challenges exists with the previously described electrogenetic systems as well.[99] Since, the electrochemical activation exploits the oxidative stress mechanisms in native bacteria, the native host oxidative stress defense mechanism are removed. I explored to see if CRISPR-Cas9 mediated temporal and reversible silencing of *soxS* might lead to better electrogenetic activation of SoxS promoters in wild type strains.

5.2 Materials and Methods

Table 5-1: Table of strains and plasmids

Strain	Relevant Genotype and Property	Reference
NB101	ZK126[201] Δ*rpoZ*	This study
NB2031	ZK126[201] Δ*rpoZ*, Δ*luxS*	This study
JEN202	MG1655, Δ*rpoZ*	[194]
GC4468	Δ(argF-lac)169 λ IN(rrnD-rrnE)1 rpsL179(strR)	[202]
DJ901	DlacU169 rpsL DsoxRS901(GC4468 Δ*soxRS*)	[202]
Plasmids	**Relevant Genotype and Property**	**Reference**
pWJ89	pZS*24-MCS1, PAM-rich 5' UTR region, J23117, *gfp-mut2*	[194]
pWJ66	pACYC184(CmR) with tracrRNA, *cas9*(D10A, H840A)-ω, repeat-BsaI spacer-repeat	[194]
p108gRNA	108-spacer in pgRNA-bacteria (Addgene plasmid # 44251) with pBR322 origin, Amp^r, J23119 promoter	This study
pControl gRNA	Control spacer in pgRNA-bacteria (Addgene plasmid # 44251) with pBR322 origin, Amp^r, J23119 promoter	This study
pdCas9-ω	ω was inserted into C termini of dCas9 in pdCas9-bacteria (Addgene plasmid # 44249), p15A, pLtetO-1, Cm^r	This study
pdCas9-2ω	Two ω's was inserted into C termini of dCas9 in pdCas9-bacteria (Addgene plasmid # 44249), p15A, pLtetO-1, Cm^r	This study
pdCas9-3ω	Three ω's was inserted into C termini of dCas9 in pdCas9-bacteria (Addgene plasmid # 44249) , p15A, pLtetO-1, Cm^r	This study
pdCas9-ω_{ssRA}	ssRA protein degradation tag added to the C termini of ω in pdCas9-ω	This study
pIntdCas9-ω	pdCas9-ω with engineered Tet promoter and dCas9 RBS sites	This study
pIntdCas9-ω_{ssRA}	ssRA protein degradation tag added to the C termini of ω in pIntdCas9-ω	This study
pNC-gRNA-1, 3 &5	p108gRNA with single point mutations in the seed region of 108 spacer	This study
pTrc-108gRNA	108gRNA sequence inserted in pTrcHisA plasmid(Invitrogen)	This study
pSoxS-108gRNA	108gRNA sequence inserted into SoxS promoter in pTT01[99]	This study
pSC-S108	SoxS-108gRNA, $pSC101^*$, Kan^r	This study
pMC-GFP	pWJ89 with pBR322 and Amp^r instead of $pSC101^*$ and Kan^r	This study
pMC-LasI	*lasI* instead of *gfpmut2* in pMC-GFP	This study
pMC-LuxS	*luxS* instead of gfpmut2 in pMC-GFP	This study
pMC-phiLOV	*phiLOV* instead of gfpmut2 in pMC-GFP	This study
pS-1, 2	SoxS specific gRNA spacers (S1 and S2) inserted into pgRNA-bacteria (Addgene plasmid # 44251) with pBR322 origin, Amp^r, BBa_J23119 promoter	This study
pTT01	*phiLOV* under SoxS promoter, pBR322, Amp^r	[99]
pNB01	SoxS specific S1 gRNA under BBa_J23119 promoter in pTT01	This study
pNB02	S1 gRNA under SoxS promoter in pTT01	This study
pNB03	HH-S1gRNA-HDV-HH-108gRNA-HDV under SoxS promoter, pBR322, Amp^r	This study

pNB04	HH-ControlgRNA-HDV-HH-108gRNA-HDV under SoxS promoter, pBR322, Amp^r	This study

Table 5-2: Table of Primers

Primer Name	Sequence (5'-3')	Features
p108gRNA		
N1	tccggcctgcagccagttttagagctagaaatag caag	Amplifies 108spacer with pgRNA-bacteria [for p108gRNA]
N2	tcttccacaacacgcactagtattatacctaggact g	Amplifies 108spacer with pgRNA-bacteria [for p108gRNA]
pControlgRNA		
N3	aagctcaaaggtctcgttttagagctagaaatagc aag	Amplifies Control spacer with pgRNA-bacteria [for pControlgRNA]
N4	ccgagactggtctcaactagtattatacctaggac tg	Amplifies Control spacer with pgRNA-bacteria [for pControlgRNA]
pTrc- ω, pTrc- 2ω and pTrc- 3ω		
N5	gctagcctcgagggtggtggttcagcacgcgtaa ctgttcaggac	Nhe-1, Xho-1; amplifies ω subunit-1
N6	tgcagatcttgaaccaccaccacgacgaccttca gcaatagc	Bgl-2; amplifies ω subunit-1
N7	tcaagatctgcacgcgtaactgttcaggac	Bgl-2; amplifies ω subunit-2
N8	gcgaattcagaaccaccaccacgacgaccttca gcaatagcgg	GGGS linker, EcoR-1; amplifies ω subunit-2
N9	gaattcgcacgcgtaactgttcaggac	EcoR-1; amplifies ω subunit-3
N10	aagcttttaacgacgaccttcagcaatagcg	Hind-3; amplifies ω subunit-3
pdCas9- ω, 2ω, 3ω		
N11	gaaggtcgtcgttaaggatctccaggcatcaaat aaaacgaaagg	Stop site; amplifies vector pdCas9 [for pdCas9-ω, 2ω, 3ω]
N12	aacagttacgcgtgctgaaccaccaccgtcacct cctagctgactcaaatcaatgc	GGGS linker, overlaps ω, amplifies vector pdCas9[for pdCas9- ω, 2ω, 3ω]
pdCas9- ssRA		
N13	gctaggaggtgacggtggtggttcagca	Amplifies ω subunit-3 [for pdCas9-ω_{ssRA}]
N14	atgcctggagatccttaagcagccagagcgtagt tttcgtcgttagcagcacgacgaccttcagc	Amplifies ω subunit-3 with ssRA tag and stop codon [for pdCas9-ω_{ssRA}]
pdIntCas9- ω and pdIntCas9- ω_{ssRA}		
N15	Atcggcacaaatagcgtcgg	Amplifies pdCas9 excluding pLtetO-1 [for pIntdCas9-ω and pIntdCas9-ω_{ssRA}]
N16	cattagagctgcttaatgaggtcgg	Amplifies pdCas9 excluding pLtetO-1 [for pIntdCas9-ω and pIntdCas9-ω_{ssRA}]
pTrc-108gRNA		
N17	aattaaagaggtatatattaagcgtgttgtggaag atcc	Amplifies 108gRNA, overlaps pTrcHisA [for pTrc-108gRNA]
N18	tctcatccgccaaaacagccaaaaaagcaccga ctcgg	Amplifies 108gRNA, overlaps pTrcHisA [for pTrc-108gRNA]
N19	ggatcttccacaacacgcttaatatatacctctttaa tt	Amplifies pTrcHisA, overlaps 108gRNA spacer-scaffold [for pTrc-108gRNA]

N20	ccgagtcggtgctttttggctgttttggcggatgaga	Amplifies pTrcHisA, overlaps 108gRNA spacer-scaffold [for pTrc-108gRNA]
pSoxS-108gRNA		
N21	catgtttgacagcttatcatcgatattaaaaaagcaccgactcggt	Amplifies 108gRNA, overlaps pTT01 [for pSoxS-108gRNA]
N22	tgaaaagaggcagatttgcgtgttgtggaagatccg	Amplifies 108gRNA, overlaps pTT01 [for pSoxS-108gRNA]
N23	cggatcttccacaacacgcaaatctgcctcttttca	Amplifies pTT01, overlaps 108gRNA spacer-scaffold [for pSoxS-108gRNA]
N24	accgagtcggtgctttttaatatcgatgataagctgtcaaacatg	Amplifies pTT01, overlaps 108gRNA spacer-scaffold [for pSoxS-108gRNA]
pSc-S108		
N25	ctacgctctggctgcttaaggatcccatggtacgcgtgctagagg	Amplifies pSC101, Kan^r backbone (pWJ89) [for pSc-S108]
N26	ttttcgtcgttagcagctttgtatagttcatccatgccatgtgtaatcccag	Amplifies pSC101, Kan^r backbone(pWJ89) [for pSc-S108]
N27	aaatctgcctcttttcagtg	Amplifies SoxR-pSoxS-108gRNA [for pSc-S108]
N28	atcgatgataagctgtcaaa	Amplifies SoxR-pSoxS-108gRNA [for pSc-S108]
pMC-GFP		
N29	tacaagagccataagaacctctacaaactctttttgtttatttttctaaatacattcaaatatgtatc	Amplifies Amp-pBR322 cassette [for pMC-GFP]
N30	caggatgaggatcgtttcgccgcgttgctggcgtttttc	Amplifies Amp-pBR322 cassette [for pMC-GFP]
N31	aggttcttatggctcttg	Amplifies pWJ89 excluding pSC101, Kan^r [for pMC-GFP]
N32	gcgaaacgatcctcatcc	Amplifies pWJ89 excluding pSC101, Kan^r [for pMC-GFP]
pMC-LasI		
N33	ggatcccatggtacgcgtg	Amplifies MC-GFP excluding *gfpmut2* [for pMC-LasI]
N34	ctagatttctcctctttaaaggaattcgc	Amplifies MC-GFP excluding *gfpmut2* [form MC-LasI]
N35	tttaaagaggagaaatctagatgatcgtacaaattggtcgg	Amplifies *lasI* [for pMC-LasI]
N36	gcacgcgtaccatgggatcctcatgaaaccgccagtcg	Amplifies *lasI* [for pMC-LasI]
pMC-phiLOV		
N37	tttaaagaggagaaatctagatgattgaaaaaagctttgtgattac	Amplifies *phiLOV* [for pMC-phiLOV]
N38	gcacgcgtaccatgggatccttacacatgatcgctgcc	Amplifies *phiLOV* [for pMC-phiLOV]
N39	ctagatttctcctctttaaaggaattcgc	Amplifies MC-GFP excluding *gfpmut2* [for pMC-phiLOV]
N40	ggatcccatggtacgcgtg	Amplifies MC-GFP excluding *gfpmut2* [for pMC-phiLOV]
pMC-LuxS		
N41	tttaaagaggagaaatctagatgccgttgttagatagc	Amplifies *luxS* [for pMC-LuxS]

N42	gcacgcgtaccatgggatccttacctgcaacttctctttc	Amplifies *luxS* [for pMC-LuxS]
N43	ggatcccatggtacgcgtg	Amplifies MC-GFP excluding *gfpmut2* [for pMC-LuxS]
N44	ctagatttctcctctttaaaggaattcgc	Amplifies MC-GFP excluding *gfpmut2* [for pMC-LuxS]
pS1 and S2		
N47	gaataattttctgatgttttagagctagaaatagc	Replaces 108gRNA with S1gRNA [for pS1]
N48	aggatcttatcgcatactagtattatacctaggac	Replaces 108gRNA with S1 gRNA [for pS1]
N49	gaataattttctgatgttttagagctagaaatagc	Replaces 108gRNA with S2 gRNA [for pS2]
N50	aggatcttatcgcatactagtattatacctaggac	Replaces 108gRNA with S2 gRNA [for pS2]
pNB02		
N53	gaataattttctgatgttttagagctagaaatagc	Replaces 108 spacer with S1 spacer in Sc-S108 [for NB02]
N54	aggatcttatcgcataagcttaaatctgcctcttttc	Replaces 108 spacer with S1 spacer in Sc-S108 [for NB02]
pNB01		
N55	ggagtcgcataagggagagcgaattctaaagatctttgacagctagc	Amplifies S1 gRNA with BBa_J23119 promoter
N56	gaaggctctcaagggcatcgggcccagtctttcgactg	Amplifies S1 gRNA with BBa_J23119 promoter
N57	cgatgcccttgagagccttc	Amplifies pTT01 backbone
N58	cgctctcccttatgcgac	Amplifies pTT01 backbone
N59	gcctgggaagaaagagttcagaaaatttttaaaaaaattaccggaggtggctaagtgtaggctggagctgcttc	Overlaps with *luxS* for NB2031 strain
N60	ctaagccagttcatttgaactggctttttttcaattaattgtgaagatagtttactgacatatgaatatcctccttag	Overlaps with *luxS* for NB2031 strain

5.2.1 List of Sequences and spacers

Spacers:

Spacer Control **(5'-3')**: tgagaccagtctcggaagctcaaaggtctc
Spacer 108 **(5'-3')**: gcgtgttgtggaagatccggcctgcagcca
Spacer NC-1 **(5'-3')**: gcgtgttgtggaagatccggcctgcagcca
Spacer NC-4 **(5'-3')**: gcgtgttgtggaagatccggcctgcagcca
Spacer NC-5 **(5'-3')**: gcgtgttgtggaagatccggcctgcagcca
Spacer S1 **(5'-3')**: atgcgataagatcctgaataattttctgat
Spacer S2 **(5'-3')**: atgcgataagatcctgaataattttctgat

Synthetic Intergenic Region for pIntdCas9-ω and pIntdCas9-ω_{ssRA} (5'-3'):
aagcagaggagcaaaagctcatttctgaagaggacttgttgcggaaacgacgagaacagttgaaacacaaacttgaaca
gctacggaactcttgtgcgtaaggaaaagtaaggaaaacgattccttctaacagaaatgtcctgagcaatcacctatgaact

gtcgactcgagcctctatggattatcaccttggctgcaggccggatcttccacaacacgcacggtgttacattaggcatacc
ggtcttgacagctagctcagtcctagggattgtgctagcgaattccctttaaagaggagaaatctagatg

HDV-S1gRNA-HH (5'-3')
atagcgggctcacccagaaacgctccatggtcccattcgccatgccgaagcatgttgcccagccggcgccagcgagga
ggctgggacctgccggccaaaagcaccgactcggtgccacttttcaagttgataacggactagccttattttaacttgctatt
tctagctctaaaacatcagaaattattcaggatcttatcgcatgacgagcttactcgtttcgtcctcacggactcatcagatgcg
aaagcttaaatctgcct

HDV-108gRNA-HH (5'-3')
Gacagcttatcatcgatattccatggtcccattcgccatgccgaagcatgttgcccagccggcgccagcgaggaggctgg
gaccatgccggccaaaagcaccgactcggtgccacttttcaagttgataacggactagccttattttaacttgctatttctagc
tctaaaactggctgcaggccggatcttccacaacacgcgacgagcttactcgtttcgtcctcacggactcatcaggcgtgta
tagcgggctcacccagaaacgctccatg

HDV-ControlgRNA-HH (5'-3')
atagcgggctcacccagaaacgctccatggtcccattcgccatgccgaagcatgttgcccagccggcgccagcgagga
ggctgggaccatgccggccaaaagcaccgactcggtgccacttttcaagttgataacggactagccttattttaacttgcta
tttctagctctaaaacgagacctttgagcttccgagactggtctcagacgagcttactcgtttcgtcctcacggactcatcagt
gagacaagcttaaatctgcct

5.2.2 Strains

All the strains used in this study are listed in **Table 5-1**. Two new strains NB101 and NB2031 are created for use in Crispr experiments. *E. coli* NB101 (ZK126 Δ*rpoZ)* was generated from *E. coli* ZK126[201] as background strain using primers described here.[194] *E. coli* NB2031 (NB101 Δ*luxS)* was generated using primers N59 and N60 listed in **Table 5-2**. Both strains were prepared using λ red recombinase.[203]

5.2.3 Plasmid Preparation

List of all the plasmids used in this study are listed in **Table 5-1**. List of all the primers used for each plasmid and strain construction are listed separately in **Table 5-2**. List of all spacers and synthesized gene parts are listed in 5.2.1

5.2.3.1 Plasmids created using Site directed Mutagenesis

I prepared p108gRNA and pControlgRNA by swapping spacers in the pgRNA vector (Addgene plasmid # 44251) through site directed mutagenesis and standard protocols (New England Bio labs). I prepared non-cognate gRNA1, 4 and 5 (pMC-gRNA 1, 4 and 5) by site directed mutagenesis as well by swapping spacers with p108gRNA as vector. I prepared plasmid pS1 and pS2 for SoxS repression by swapping the 108-spacer sequence with spacer S1 and S2 in p108gRNA. I prepared pMC-phiLOV $_{ssRA}$ by amplifying phiLOV overlapping primers encoded with ssRA tag. I prepared pNB02 by swapping 108spacer in pSC-S108 with S1 spacer. See 5.2.4 for plasmid maps.

5.2.3.2 Preparation of pdCas9- ω, pdCas9-2ω, and pdCas9-3ω

To study whether the number of ω subunits attached to each dCas9 molecule play a role in efficiency of transcriptional activation, I created pdCas9-ω, pdCas9-2ω and pdCas9-3ω respectively. I used a two-stage process to create these plasmids. Firstly, I PCR amplified ω1, ω2 and ω3 subunits separately and used pTrcHisA (Invitrogen) as a shuttle vector to add all the ω subunits. Firstly, I added ω3 subunit into pTrcHisA through NEB restriction enzymes EcoRI and Hind-III to create pTrc-ω. Then, I added ω2 subunit to pTrc-ω through restriction digestion with enzymes Bgl-II and EcoRI to create pTrc-2ω. Then, I employed another round of restriction digestion with enzymes NheI and Bgl-II to add ω1 subunit to pTrc-2ω to create pTrc-3ω. Then independent gene cassettes 1ω, 2ω and 3ω were removed from pTrc-1ω, pTrc-2ω and

pTrc-3ω plasmids through restriction digestion with Xho-1 and EcoRI and Gibson assembled into pdCas9-Bacteria (Addgene plasmid # 44249) vector amplified with primers N11 and N12 to create pdCas9-ω, pdCas9-2ω, and pdCas9-3ω respectively. All ω subunits and dCas9 had a GGGS linker in between each of them.

5.2.3.3 Preparation of plasmids with Gibson Assembly

pdCas9-ω_{ssRA}: I PCR amplified ω subunit in pTrc-ω using primers encoding the ssRA tag and Gibson assembled into amplicon derived from pdCas9-Bacteria and primers N11 and N12. **pIntdCas9-ω and pIntdCas9-ω_{ssRA}**: A pTet promoter intergenic region containing synthetic promoter for Tet repressor and reduced strength RBS site for dCas9 was reported[204]. The sequence of the synthetic intergenic region is mentioned in list of sequences. I amplified plasmids pdCas9-ω and pdCas9-ω_{ssRA} with primers N 15 and N16 and Gibson assembled into the synthetic intergenic region (gene fragment from IDT) to create pIntdCas9-ω and pIntdCas9-ω_{ssRA}. **pTrc-108gRNA:** I PCR amplified 108gRNA sequence from p108gRNA plasmid and Gibson assembled into pTrcHisA (Invitrogen). **pSoxS-108gRNA**: I PCR amplified 108gRNA sequence from p108gRNA plasmid and Gibson assembled into pTT01[99]. **pSc-S108gRNA**: I replaced Amp^r cassette and pBR322 origin in pSoxS-108gRNA with Kan^r and pSC101* cassette from pWJ89[194] though PCR and Gibson assembly. **pMC-GFP:** I replaced Kan^r and pSC101* cassette in pWJ89 with Amp^r and pBR322 cassette from pgRNA though PCR and Gibson assembly**. pMC-phiLOV:** I replaced *gfpmut2* in pMC-GFP with *phiLOV* from pTT01 though PCR and Gibson assembly. **pMC-LasI:**

I replaced *gfpmut2* in pMC-GFP with *lasI* from pET200-*lasI* (lab stocks). **pNB01:** I PCR amplified S1gRNA and J23119 promoter from pS1 and Gibson assembled into pTT01. **pNB03 and 04**: Firstly, I synthesized gene fragments encoding HH-gRNA-HDV for 108gRNA, ControlgRNA and S1gRNA. Additionally, I prepared a PCR amplicon excluding the 108gRNA from pSC-S108 and used it as vector to insert various HH-gRNA-HDV sequences under SoxS promoter. pNB03 contained HH-S1gRNA-HDV and HH-108gRNA-HDV. pNB04 contained HH-ControlgRNA-HDV and HH-108gRNA-HDV See 5.2.4 for plasmid maps.

5.2.4 Plasmid Maps

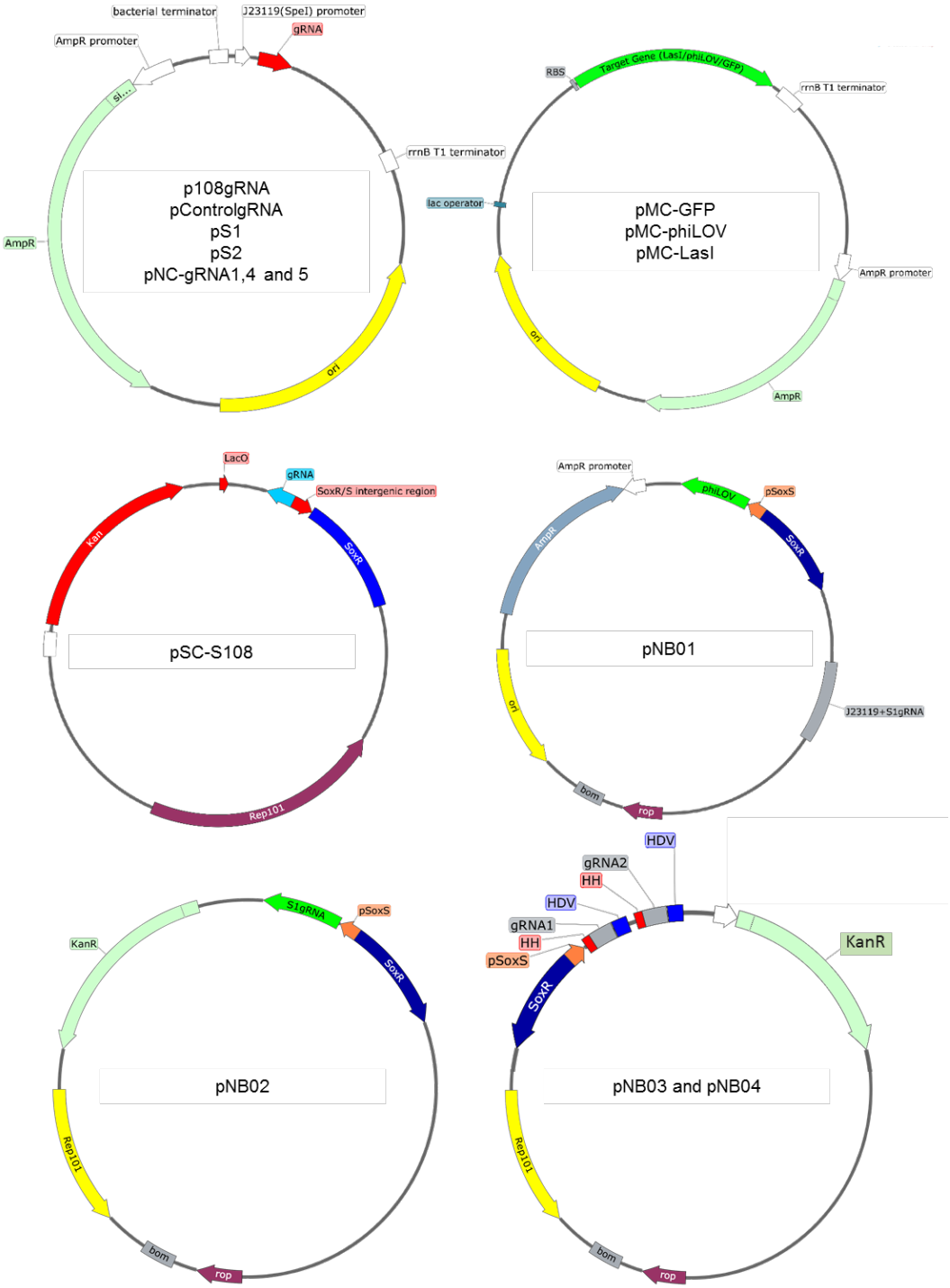

5.2.5 Media and growth conditions

I used lysogeny broth (LB) for all experiments performed in aerobic conditions with 250 r.p.m shaking. I grew overnight cultures in LB media at 37ºC and the following day re-inoculated the cultures in fresh LB media at 1:100 ratio and used as per instructions in each specific experiment. For experiments performed in anaerobic conditions, I first grew overnight cultures in LB media at 37ºC and the following day re-inoculated the cultures in fresh LB media at 1:100 ratio and grew the cells till OD 0.6. Then I washed the cells, re-suspended in minimal-M9 (1 × M9 salts, 0.4% glucose, 0.2% casamino acids, 2 mM $MgSO_4$, 0.1 mM $CaCl_2$ and 100 mM MOPS) and used for further experiments. I created anaerobic conditions in a Coy anaerobic chamber (Grass Lake, MI) as per manufacturer instruction using nitrogen and a gas mixture comprising of 90% nitrogen, 5% carbon dioxide and 5% hydrogen.

5.2.6 Fluorescence measurements using plate reader and flow cytometry

I used plate readers to measure GFP fluorescence measurements with an excitation wavelength of 488nm and emission wavelength of 520nm. In each well, 200µl of cells in LB media were used and LB fluorescence was removed from all measurements. I used flow cytometry to measure phiLOV fluorescence. I used a constant forward and side scatter settings to capture cells and measured mean green fluorescence levels of phiLOV with a 488nm laser and a 530/30 green filter. A

minimum of 50,000 cells were used for fluorescence measurements of each sample and analysis was done in FACSDiva and MS-Excel.

5.2.7 Electrochemical set-up and electrochemical conversion of Fcn (R) to Fcn (O)

Electrochemical experiments were performed inside the Coy anaerobic chamber. Our electrochemical set-up set up consisted of a wound gold wire (0.5 mm diameter, ~50 cm in length) as both working and counter electrodes and an Ag/AgCl electrode (CH Instruments) as reference. A CH Instruments, Inc. (Austin, TX) 600-series potentiostat was used for controlling voltages. Agar salt bridges were prepared as described here[99]. Our sample setup consisted of two glass vials with one vial consisting of 1 ml of cells supplemented with 50 mM Fcn (R) and PYO and the other consisting of 1 ml of 50 mM Fcn(O). Two gold wire electrodes were immersed in both vials and the reference electrode in the vials with cells. Both vials were also connected by two salt bridges. For electrochemical conversion of Fcn (R) to Fcn (O), I applied a voltage of 0.5V to cells via the working electrode and after oxidation, cells were removed from vials, transferred to culture tubes and incubated in a mini 37ºC incubator inside the anaerobic chamber without shaking. For time course experiments in **Figure 5-7**, 100 µls of cells was taken at each time point and fixed with 2% paraformaldehyde for a minimum of 15 mins and used for FACS.

5.2.8 AI-1 reporter assay

I grew AI-1 reporter cells (JLD271 strain containing pAL105[205]) overnight in LB media with kanamycin and tetracycline at 37°C and the next day diluted the reporter cells 2500x in fresh media. Then, I added 10μL of each conditioned media sample with 90 μL of diluted reporter cells in FACS tubes (Becton Dickinson) and incubated for 3 hours in a 30°C shaker. After incubation, I measured luminescence using a GloMAX luminometer (Promega). For each experiment, I built a standard curve comprising of 0, 12, 24, 36, 48, 60nM AI-1 concentrations using the standard AI-1.

5.3 Results

5.3.1 Optimization of a 'tunable and controllable' CRISPRa system in bacteria

In this study, I intended to create a tunable and controllable CRISPR-Cas9 mediated transcriptional activation (CRISPRa) system to target and activate specific genes in bacteria. In this pursuit, I characterized the strain used for transcriptional activation, optimized the expression conditions including promoters and copy numbers of plasmids expressing the two components of CRISPRa system: dCas9 based transcriptional activator and spacers; number of transcriptional activator subunits fused to dCas9 and the mode of delivery of spacers.

First, I optimized the strain used for transcriptional activation experiments. Previously, Bikard et. al., had reported a 23-fold and 7-fold CRISPR mediated transcriptional activation (CRISPRa) of GFP with two different spacers namely 108 and 105. RNA polymerase subunit ω (*rpoZ*) was used as the transcriptional activator and was genetically fused to *S. pyogenes* dCas9 in a Δ*rpoZ* strain of E. coli MG 1655 (JEN202).[194] Since I had previously characterized Quorum Sensing (QS) in W3110 strains and I intended to integrate QS with CRISPRa in this study, I first removed *rpoZ* in ZK126 (W3110 Δ*lacZ*) to create NB101. Then, I repeated the same CRISPRa experiments reported in Bikard et. al., in our lab and observed the transcriptional activation to be ~16-fold and 6-fold using spacers 108 and 105 in the JEN202 strain. I obtained comparable activations in the newly created NB101 strain as well using the

same 108 spacer and the GFP target plasmid **(Figure 5-1)**. In further studies, I used NB101 strain as host strain for all our experiments. Subsequently, I also deleted *luxS* responsible for production of the QS enabling molecule Autoindicer-2 (AI-2) in the NB101 strain to create NB2031 strain. Deletion of *luxS* had no effect on CRISPRa (data not shown).

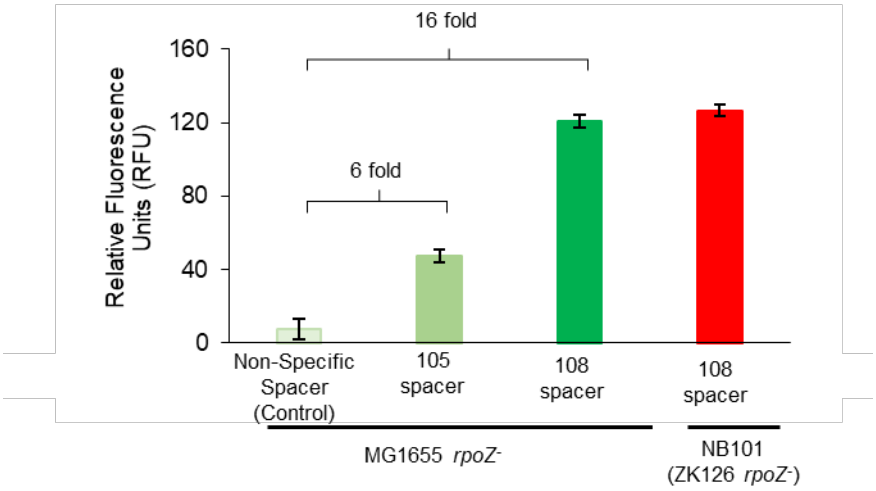

Figure 5-1 Comparison of CRISPR activation obtained from NB101 strain (ZK126 rpoZ$^-$) and MG1655 rpoZ$^-$ strain.

I performed CRISPRa experiment using the spacers (105, 108 and non-specific spacer), target plasmid (pWJ89) and MG1655 *rpoZ*$^-$ strain as detailed in Bikard et. al. I also used the 108-spacer in the newly created NB101 (ZK126 *rpoZ*$^-$) strain and measured CRISPRa using GFP from pWJ89. Data indicates GFP fluorescence measured using the plate reader after 16 hours of re-inoculation, n=3.

Previously, Bikard et. al., had used constitutive *S. pyogenes* promoters to express both dCas9-ω and 108 spacer for transcriptional activation and spacers were expressed in the form of tracrRNA: crRNA hybrids to target and activate GFP plasmid pWJ89.

Here, I studied whether spacer expression can be moved from the tracrRNA: crRNA hybrid system to the short gRNA system for CRISPRa. In our study, I used the same spacer 108 to target GFP in the same plasmid as reported in Bikard et.al., however, I expressed the spacers in the form of short guide RNA(gRNA) placed under a strong constitutive promoter (J23119) in p108gRNA (See 5.2.3.1). In addition, I placed the dCas9-ω under a Tet promoter, pdCas9-ω (See 5.2.3.2) and examined dCas9-ω in absence of the inducer anhydrotetracycline (aTc) using only leaky expression from Tet promoter **(Figure 5-2A)**. I grew NB101 cells harboring plasmids p108gRNA, pdCas9-ω and pWJ89 in LB media at 37°C and measured GFP fluorescence over time using a plate reader (See 5.2.6).

I found that the combination of the use of gRNA instead of tracrRNA: crRNA hybrid, strong constitutive promoters for gRNA expression and leaky expression of dCas9-ω under the Tet promoters resulted in ~5-fold greater GFP activation (**Figure 5-2 B and C**) in comparison to GFP activation with spacers expressed as tracrRNA: crRNA hybrids along with dCas9-ω from native S. *pyogenes* promoters. These results indicated the importance of relative expression levels of dCas9-ω and spacers and the mode of spacer expression for an efficient CRISPRa system in bacteria.

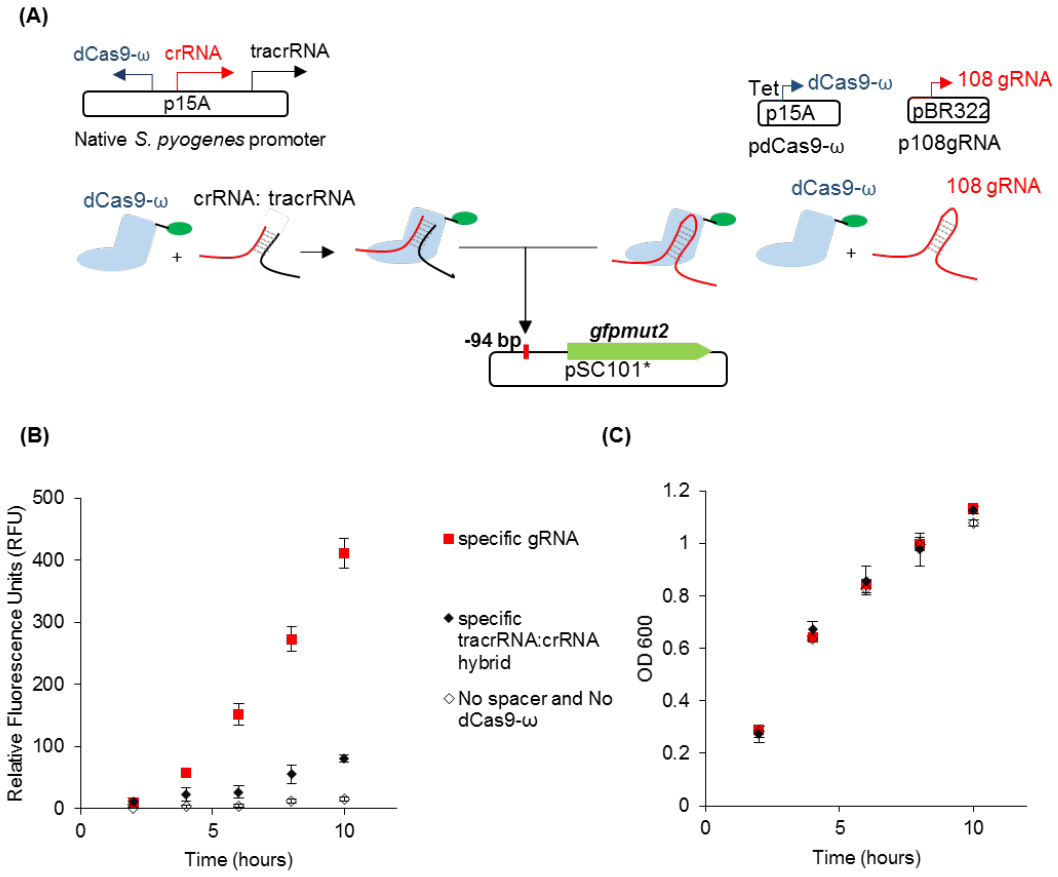

Figure 5-2 Comparison of CRISPR activation from tracrRNA: crRNA and gRNA delivery systems.

(A) Scheme of CRISPR-Cas9 mediated transcriptional activation (CRISPRa) of GFP in target plasmid pWJ89 using tracrRNA: crRNA and gRNA systems for spacer delivery. In tracrRNA: crRNA system, spacers were expressed as tracrRNA:crRNA hybrids in combination with dCas9-ω from S. pyogenes promoters. In gRNA system, spacers were expressed as single short gRNA under constitutive J23119 promoters from p108gRNA and dCas9-ω from the Tet promoter in pdCas9-ω under leaky expression conditions. **(B)** Fluorescence and **(C)** OD measured using plate reader for 10 hours after re-inoculation, n =3

To increase CRISPRa, a common strategy used in eukaryotic CRISPRa systems is to increase transcriptional activator domains per dCas9 molecule. For example,

VP160, a 10mer of eukaryotic transcriptional activator VP16 had greater CRISPRa than VP16.[193] I attempted to study whether the increase in ω subunits fused to dCas9 resulted in increased CRISPRa in bacteria.

To this end, I engineered dCas9 with up to three ω subunits with flexible linker tags (GGGS) in between each ω subunit and dCas9 to create pdCas9-ω, pdCas9-ωω and pdCas9-ωωω (See 5.2.3.2). All dCas9-ω fusions were under a Tet promoter but I studied CRISPRa using leaky expression from the Tet promoter. I targeted these different transcriptional activators to the GFP plasmid (pWJ89) via the same 108-spacer from p108gRNA (**Figure 5-3 A**) and measured GFP fluorescence mediated by CRISPRa. Fluorescence data indicated that unlike the eukaryotic transcriptional activators, dCas9 engineered with a single ω resulted in higher transcriptional activation than dCas9 fused with two or three ω subunits **(Figure 5-3 B)**. Controls including dCas9-ω with nonspecific spacers (pControlgRNA) and dCas9 lacking ω subunits had negligible transcriptional activation.

Considering that the distance between spacers and transcriptional start sites (TSS) of the target gene is important for transcriptional activation[194], I used the same spacer to test all the dCas9-ω fusions. With increasing number of ω subunits as transcriptional activators, it needs to be tested whether re-optimization of spacer sequences in relation to TSS of target gene leads to improvement of CRISPRa in bacteria

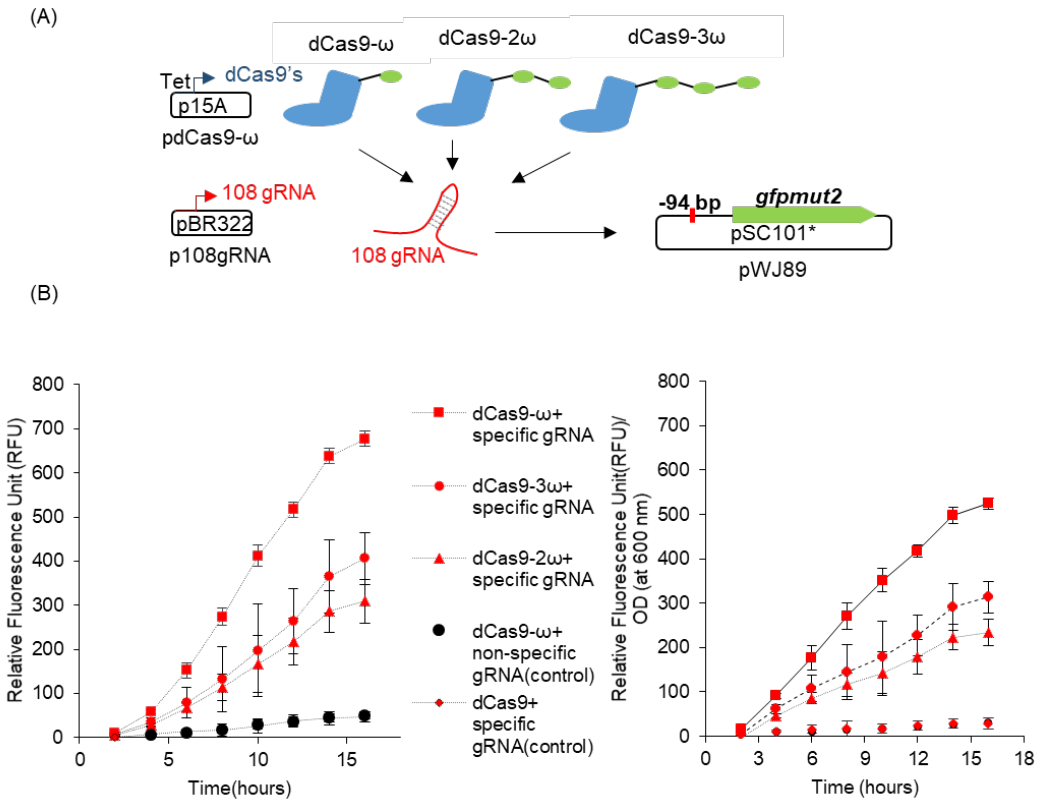

Figure 5-3 Role of the number of ω subunits fused to dCas9 on CRISPRa in bacteria.

(A) Comparison of the effect of the number of ω subunits fused to dCas9 for CRISPRa of GFP. I created different dcas9s (dCas9-ω, dCas9-2ω and dCas9-3ω) placed under the Tet promoter and measured CRISPRa of GFP (pWJ89) using leaky expression of dCas9 fusions from the Tet promoter in NB101 cells. **(B)** GFP Fluorescence and GFP Fluorescence/OD data indicating transcriptional activation from various dCas9-ω fusions across 16 hours post re-inoculation. GFP and OD was measured through plate reader. n=3

To create a tunable and controllable CRISPRa system, I intended to express the CRISPR elements, dCas9-ω as well as gRNA from inducible promoters. I tried to control expression of dCas9-ω from Tet promoters through induction of Tet promoters with aTc **(Supplementary Figure 5- and Supplementary Figure 5-1)**, but I was unable to create a controllable CRISPRa response. So, I used leaky expression of dCas9-ω from the Tet promoters in all further experiments.

Next, I studied whether controlling the levels of gRNA might lead to a tunable CRISPRa. I had performed all our experiments with gRNAs expressed from strong constitutive J23119 promoter in p108gRNA. I intended to study whether controlling gRNA expression by placing gRNA expression under inducible promoters might lead to a tunable CRISPRa.

In this experiment, I moved gRNA expression from constitutive J23119 promoter to the Trc and SoxS promoters (pTrc-108gRNA and pSoxS-108gRNA respectively, See 5.2.3.3) while retaining the same plasmid origin (pBR322) **(Figure 5-4A)**. I induced both the promoters (IPTG for pTrc and PYO for pSoxS promoter) and measured the gRNA levels expressed after 6 hours of induction. I also measured CRISPRa mediated GFP fluorescence at 4 and 8 hours.

qPCR results **(Figure 5-4B)** indicated that there was an increase in gRNA expression from both the pTrc and pSoxS promoters with increasing inducer concentrations. However, fluorescence data indicated that there was no change in CRISPRa with increasing gRNA expression from both pTrc and pSoxS promoters

(**Figure 5-4 C and D**). Leaky expression of gRNAs from both the promoters displayed saturating CRISPRa response.

To reduce leaky expression of gRNAs, I replaced the origin of the plasmid expressing gRNA under SoxS promoter from a high copy pBR322 origin to a low copy pSC101 origin to create pSC-S108 plasmid. Additionally, I also replaced pSC101 origin in target GFP plasmid pWJ89 with pBR322 to create pMC-GFP (**Figure 5-5 A**). With this re-arrangement of copy numbers of target genes as well as promoters that express gRNA, I studied whether controllable gRNA expression from SoxS promoters can result in a controllable CRISPRa response in bacteria.

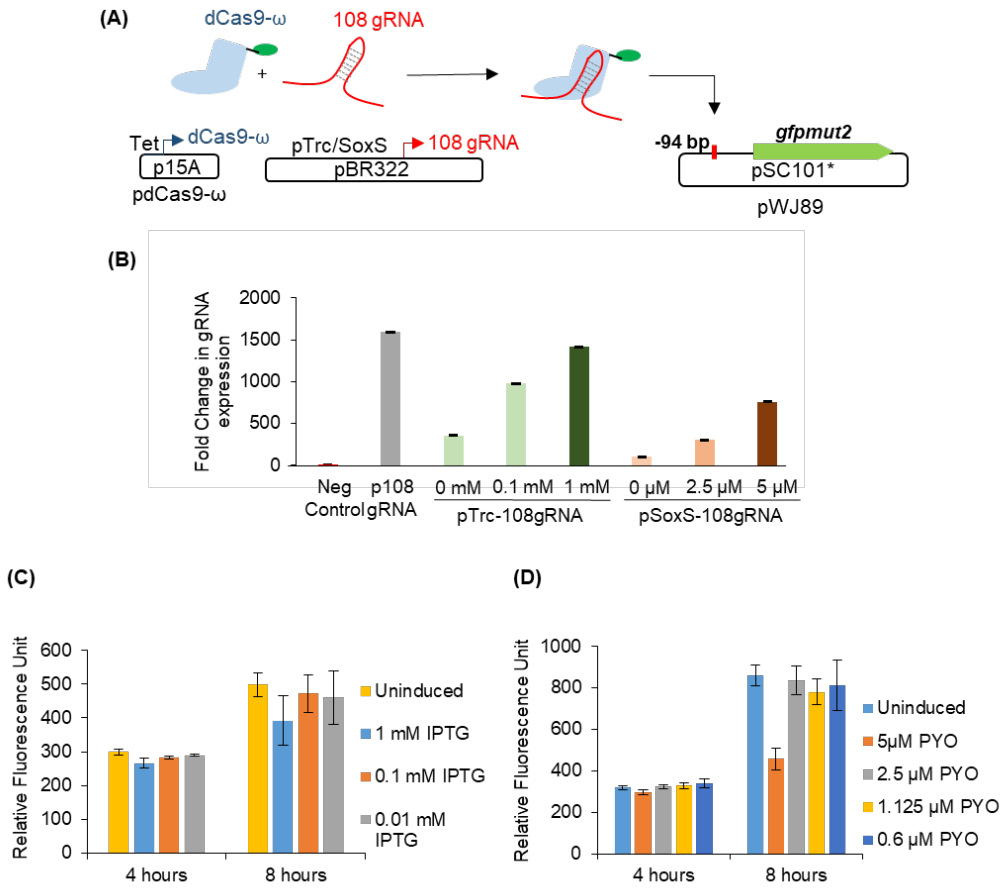

Figure 5-4 Controlling gRNA expression using inducible promoters to control CRISPRa.

Scheme of controlling gRNA expression from the inducible pTrc and pSoxS promoters to mediate a tunable and inducible CRISPRa response. I engineered 108gRNA sequence into plasmids with pTrc (pTrc-108gRNA) and pSoxS (pSoxS-108gRNA) promoters and transformed them along with pWJ89 and pdCas9-ω into NB101 cells. (**B)** I induced pTrc and pSoxS promoters with varying concentrations of inducers (IPTG and Pyocyanin for pTrc and pSoxS respectively) and performed qPCR at 6 hours to measure relative gRNA expression levels. Negative control was mRNA from an *E coli* strain lacking gRNA expression and positive control was gRNAs expressed under J23119 constitutive promoter from p108gRNA in NB101 cells. CRISPRa resulting from the gRNA expression induced from pTrc **(C)** and pSoxS **(D)** promoters was measured by GFP fluorescence at 4 and 8 hours post gRNA induction. n=3

I transformed the newly created high copy number target plasmid pMC-GFP and low copy SoxS promoter expressing gRNA, pSC-S108 plasmid into NB101 cells along with pdCas9-ω. I induced the SoxS promoter with varying concentrations of PYO and measured the relative gene expression levels of gRNA from SoxS promoters (**Figure 5-5 B**) as well as measured the GFP fluorescence mediated by CRISPRa (**Figure 5-5C)**. Results indicated that with increasing concentrations of PYO, there was increase in concentration of gRNA expression from SoxS promoter as well as increase in GFP fluorescence from target plasmids due to CRISPRa.

In sum, I have shown that by moving away from the tracrRNA: crRNA hybrid system from native *S. pyogenes* promoters to a short gRNA system under synthetic promoters, I could generate a ~5-fold higher CRISPRa response **(Figure 5-2)**. In contrast to eukaryotic transcriptional activators, addition of more bacterial transcription activating subunits per dCas9 molecule did not result in increase of CRISPRa in bacteria **(Figure 5-3)**. By varying the stoichiometric ratios of not just gRNA but also the number of targets, I was able to develop a tunable CRISPR based transcriptional activation system (CRISPRa) **(Figure 5-5)** in bacteria.

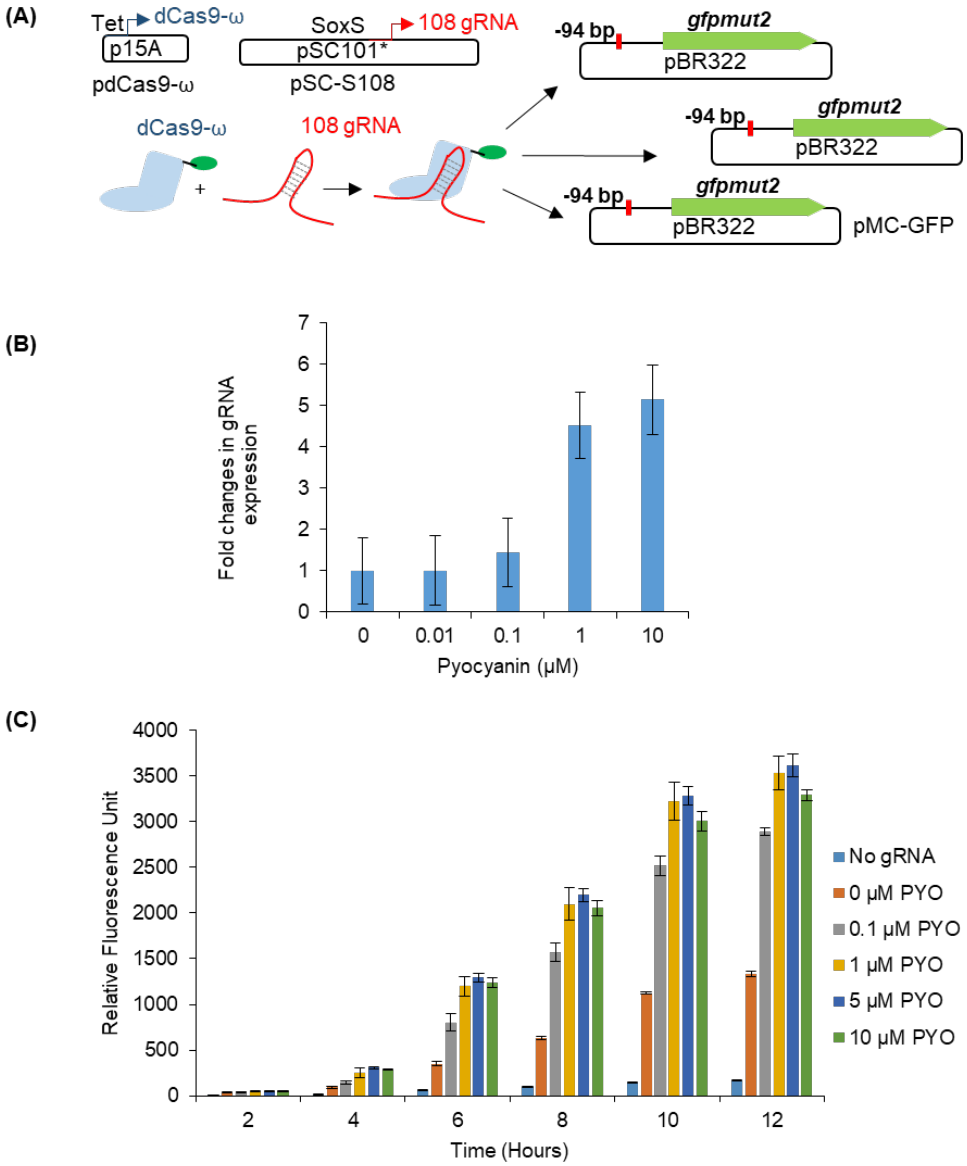

Figure 5-5 Tunable CRISPRa system by controlling gRNA expression.

(A) Scheme of a tunable CRISPRa system. I placed pSoxS promoter expressing the gRNA for transcriptional activation in a pSC101* origin plasmid (pSC-S108) and moved the GFP target to a pBR322 origin plasmid (pMC-GFP). I transformed pSC-S108, pMC-GFP and pdCas9-ω into NB101 cells and induced the pSoxS promoter with varying concentrations of Pyocyanin. **(B)** qPCR data indicating relative gRNA expression levels from SoxS promoter with different Pyocyanin concentrations after 6 hours of induction. **(C)** CRISPRa mediated GFP expression using fluorescence measurements in a plate reader across 12 hours post induction. n=3

5.3.2 Electrical control of CRISPRa

Having shown that I can tune CRISPRa by controlling gRNA expression from a low copy SoxS promoter, I next wanted to display tunable electrical control over gRNA expression resulting in an electrically tunable CRISPRa. Previously, electrically induced SoxS promoters were used for direct expression of specific transgenes in bacteria.[99] In this study, I planned to use the same SoxS promoters to express gRNAs that in turn mediated the CRISPR-Cas9 mediated transcriptional activation (CRISPRa) of target genes. To display this, I first optimized the concentrations of mediators PYO and Fcn that are required for electrical activation of SoxS promoter.

SoxS promoters can be induced by just PYO under aerobic conditions with oxygen acting as electron acceptor for intracellular recycle of PYO. Under anaerobic conditions, the role of electron acceptor can be taken up by redox mediators such as Ferricyanide (Fcn (O)). By electrically controlling the conversion of Fcn (R) to Fcn (O), the redox capacitance of the system can be controlled and as a result SoxS promoter activity can be controlled as well.[99] To perform experiments under anaerobic conditions without oxygen, I replaced the reporter gene from *gfpmut2* in pMC-GFP with *phiLOV* through Gibson assembly to create pMC-phiLOV (See 5.2.3.3) and used it as target for CRISPRa experiments. phiLOV is capable of fluorescing under both aerobic and anaerobic conditions.[206] I transformed NB101 cells with pSC-S108, pdCas9-ω and pMC-phiLOV and grew the cells aerobically in LB media at 37°C. At OD 0.6, I washed the cells and re-suspended them in M9 minimal media with MOPS and performed further experiments (See 5.2.5).

To characterize gRNA expression from SoxS promoters and the resulting CRISPRa, I first directly added Fcn (O). With a constant Fcn (O) concentration of 5mM, I added different PYO concentrations, grew the cells for 6 hours at 37°C in both aerobic and anaerobic conditions and measured phiLOV fluorescence through FACS. I observed the CRISPRa response to increase with increasing concentrations of PYO under both aerobic and anaerobic conditions. However, with time, CRISPRa responses in aerobic and anaerobic conditions were directly opposite of each other with fluorescence increasing in aerobic conditions over time while decreasing in anaerobic conditions (**Figure 5-6 A and B)**. I also varied the concentrations of Fcn (O) and PYO simultaneously and observed CRISPRa responses under anaerobic conditions after 2 hours of induction. phiLOV fluorescence increased with increasing concentrations of Fcn (O) and PYO with the highest PYO and Fcn (O) concentrations (10μM and 50 mM respectively) yielding ~18-fold CRISPRa **(Figure 5-6C)**.

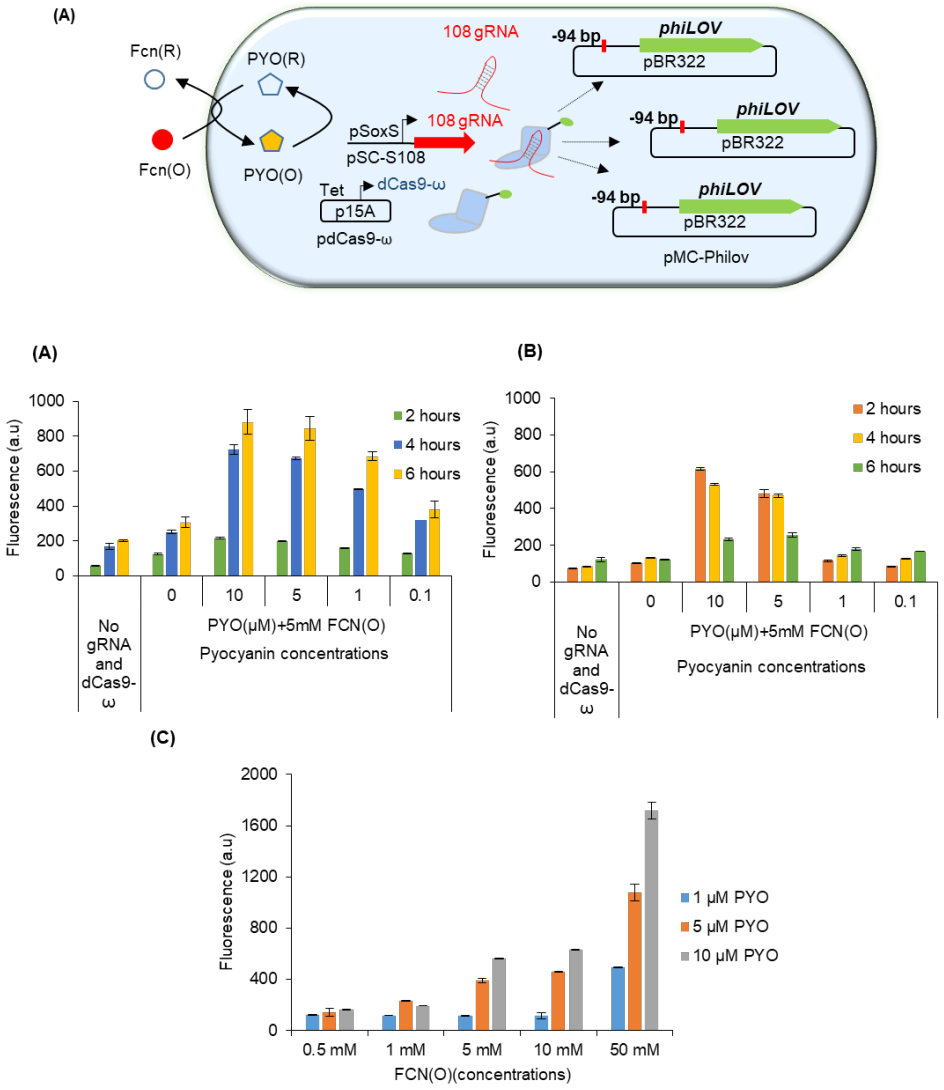

Figure 5-6 Ferricyanide and Pyocyanin mediated control of SoxS promoters for gRNA expression and CRISPRa

I optimized the Pyocyanin and Ferricyanide concentrations required for induction of gRNA expression from SoxS promoters. I transformed pSc-S108, pMC-phiLOV and pdCas9-ω into NB101 cells and measured gRNA mediated CRISPRa of phiLOV from pMC-phiLOV by FACS. With a constant Ferricyanide (Fcn (O)) concentration of 5mM, I varied the concentrations of Pyocyanin and grew the cells under aerobic **(A)** as well as anaerobic conditions **(B)** and measured CRISPRa across time through phiLOV

fluorescence. I also varied both Pyocyanin and Ferricyanide concentrations simultaneously and measured phiLOV fluorescence **(C)** after 2 hours. n=3.

Next, I sought to display electrical control of CRISPRa by electrically oxidizing Fcn (R) to Fcn (O). I prepared NB101 cells with pSC-S108, pdCas9-ω and pMC-phiLOV plasmids as before in **Figure 5-6**. After growing to OD 0.6 in LB under aerobic conditions, I switched to anaerobic conditions and re-suspended the cells in M9 minimal media containing 50mM of Fcn (R) and 5 µM of PYO. To electrically convert Fcn (R) to Fcn (O), I used a three electrode set-up connected to a potentiostat and applied an oxidation potential of +0.5V across the solution at room temperature to oxidize Fcn, as described earlier[99] (**Figure 5-7 A**). After oxidation, I moved the cells to 37°C and grew for 6 hours. I varied the total charge (represented in Coulomb) that is transferred from electrode to the solution for oxidation of Fcn (R) and measured the expression levels of gRNA from the SoxS promoter as well as phiLOV from CRISPRa (**Figure 5-7 B)**. In addition, I also measured phiLOV fluorescence through FACS (**Figure 5-7 C)**. **Figure 5-7 B** indicates the relative gene expression levels of gRNA and phiLOV after 2 hours of electrical induction. With increasing charge there was increasing levels of gRNA expression from the SoxS promoter as well as phiLOV expression due to CRISPRa mediated by gRNA and dCas9-ω. At -0.5C, however, there was a decrease in gRNA and phiLOV expression levels. **Figure 5-7 C** indicates the fluorescence obtained across 6 hours with varying levels of electric charge applied. As expected, with increasing charge of up to -0.4C, there was increasing fluorescence due to CRISPRa with a maximum of ~ 13-fold transcriptional activation.

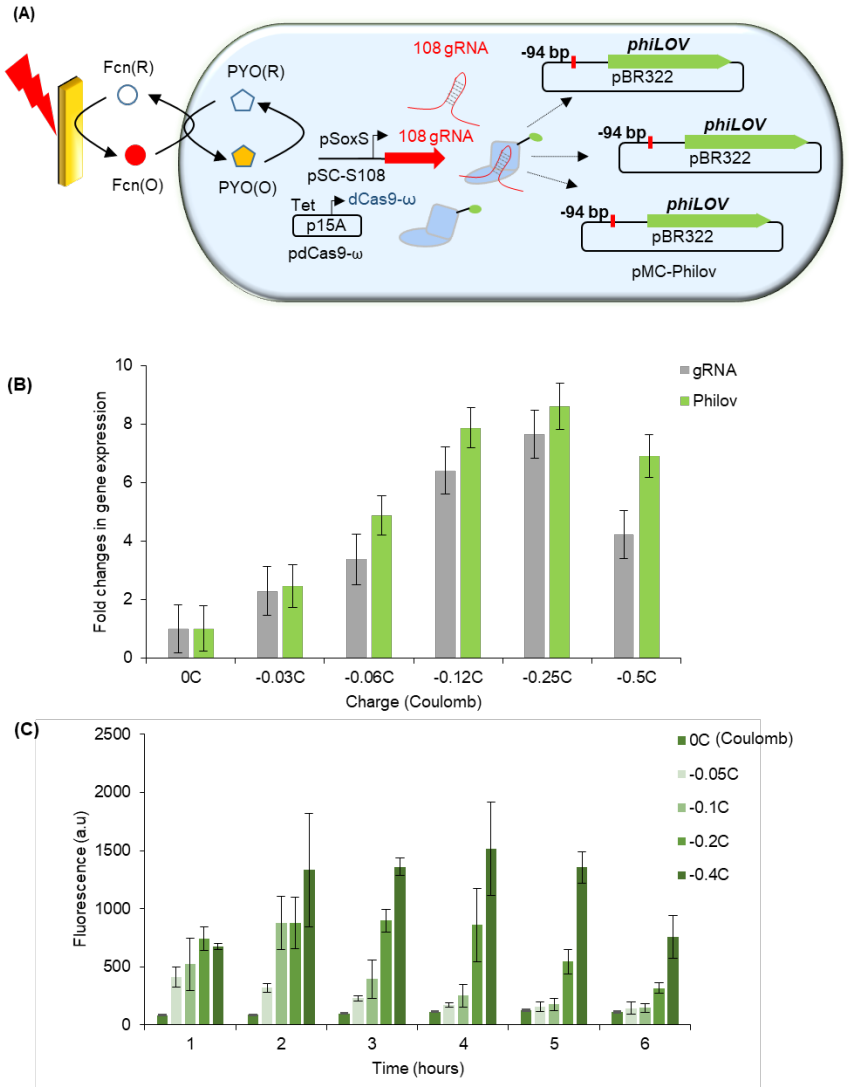

Figure 5-7 Electrical control of SoxS promoters for gRNA expression and CRISPRa

Scheme of electrical induction of SoxS promoters for gRNA expression. I transformed pSc-S108, pMC-phiLOV and pdCas9-ω into NB101 cells and grew them in LB media to OD 0.6. Later, cells were re-suspended in in minimal M9 media with 50mM Ferrocyanide (Fcn(R)) and 5 µM Pyocyanin and grown under anaerobic conditions at 37ºC. I electrically oxidized 50mM Ferrocyanide (Fcn(R)) to Ferricyanide (Fcn (O)) by application of 0.5V through a three-electrode setup attached to a potentiostat. Total

charge provided for oxidation of (Fcn(R)) to (Fcn (O)) is represented in Coulomb. Fcn (O) activated gRNA expression from pSoxS promoter resulting in CRISPRa. **(B)** qPCR data indicating the relative levels of gRNA expressed with different electrical charges after 2 hours of induction. **(C)** Fluorescence data indicating CRISPRa of phiLOV with different electrical charges applied. Fluorescence is measured across 6 hours using FACS.

In sum, I have displayed PYO and Fcn mediated control of gRNA expression from SoxS promoters leading to a tunable CRISPRa response. I optimized concentrations of mediators required for CRISPRa **(Figure 5-6)** and displayed tunable electrical control of CRISPRa **(Figure 5-7)** by controlling the oxidative state of Fcn leading to ~13-fold change in transcriptional activation.

5.3.3 Re-purposing CRISPRa for repression of SoxS in the genome to improve SoxS promoter responses

Bacteria has well developed oxidative stress response mechanisms that are primarily mediated by SoxRS and OxyRS regulons.[207] Since Pyocyanin (PYO), an oxidative stress inducing molecule, is the primary component in electrical activation of SoxS promoters, I next studied whether repression of SoxS mediated oxidative stress responses resulted in increased electrical activation of SoxS promoters. To study this, I intended to repurpose the CRISPRa system for repression of SoxS and SoxS mediated oxidative stress responses in bacteria.

One of the advantages of the CRISPR-Cas9 system is the ability to simultaneously target different sets of genes in the genome and modulate transcription. In cases where both transcriptional activation and repression functions needs to be simultaneously performed, two different orthogonal dCas9s are used to delineate

silencing and activation functions in the same cell.[208] Transcriptional activators can also be repurposed for repression (labelled as CRISPRi) by simply targeting the dCas9 activator fusion to the promoter region or downstream of TSS of target gene.[189, 209]

I intended to re-purpose the bacterial CRISPRa system with transcriptional activator dCas9-ω for repression of the *soxS* in the genome of *E. coli*. The ideal location in a gene to target dCas9 for maximum repression is the -35 to -10 promoter region.[194] However, since I used the same *E. coli soxS* promoter in the pSC-S108 plasmid for electrical activation of gRNAs, I chose to avoid the promoter region and target a region downstream of *soxS* transcriptional start site (TSS). *soxS* had two NGG PAM sites proximal to TSS at +4bp and +5bp in the non-coding strand. I designed gRNAs designated S-1 and S-2 (sequence of spacers in 5.2.1) with spacers targeting +4bp and +5bp sites respectively (**Figure 5-8 A**).

I expressed S1 and S2 gRNAs from plasmids pS1 and pS2 using strong constitutive promoter J23119. As controls, I also used pControlgRNA. I transformed the respective gRNA plasmids and dCas9 plasmids into NB101 cells and grew the cells in LB media at 37^0C. At OD 0.6, I induced the *soxS* in the genome with 5 µM PYO in aerobic conditions and after three hours of induction, I collected RNA samples and performed qPCR experiments. I compared the relative levels of *soxS* repression using gRNAs S1 and 2 in combination with both dCas9 and dCas9-ω (**Figure 5-8B**). With 5 µM PYO and controlgRNAs, there was a ~12 to 17-fold increase in expression of *soxS* in comparison to the PYO nil condition. However, both *soxS* specific gRNAs S1 and S2 prevented upregulation of the *soxS* from the SoxR promoter in the genome. In

addition, both dCas9 and dCas9-ω repressed *soxS* in the genome to basal expression levels using gRNAs S1 and S2 (**Figure 5-8B**). Since *soxS* repression from S1gRNA was marginally better than S2, I used S1 for all further experiments.

With SoxS being a transcription factor, I expected that the repression of *soxS* via CRISPR might lead to prevention of upregulation of various SoxS regulated genes involved in the oxidative stress defense response. To prove this, I measured the gene expression levels of two SoxS regulated genes: *sodA* (Superoxide dismutase A) and *fumC* (Fumarate hydratase) using qPCR. Under aerobic conditions, I induced cells containing pS1 and dCas9-ω plasmids at OD 0.6 with 5μM PYO in LB media for 3 hours and measured relative levels of *sodA* and *fumC.* As expected, in the presence of pS1 and dCas9-ω, both *sodA* and *fumC* were not activated above their basal expression levels. (**Figure 5-8 C**).

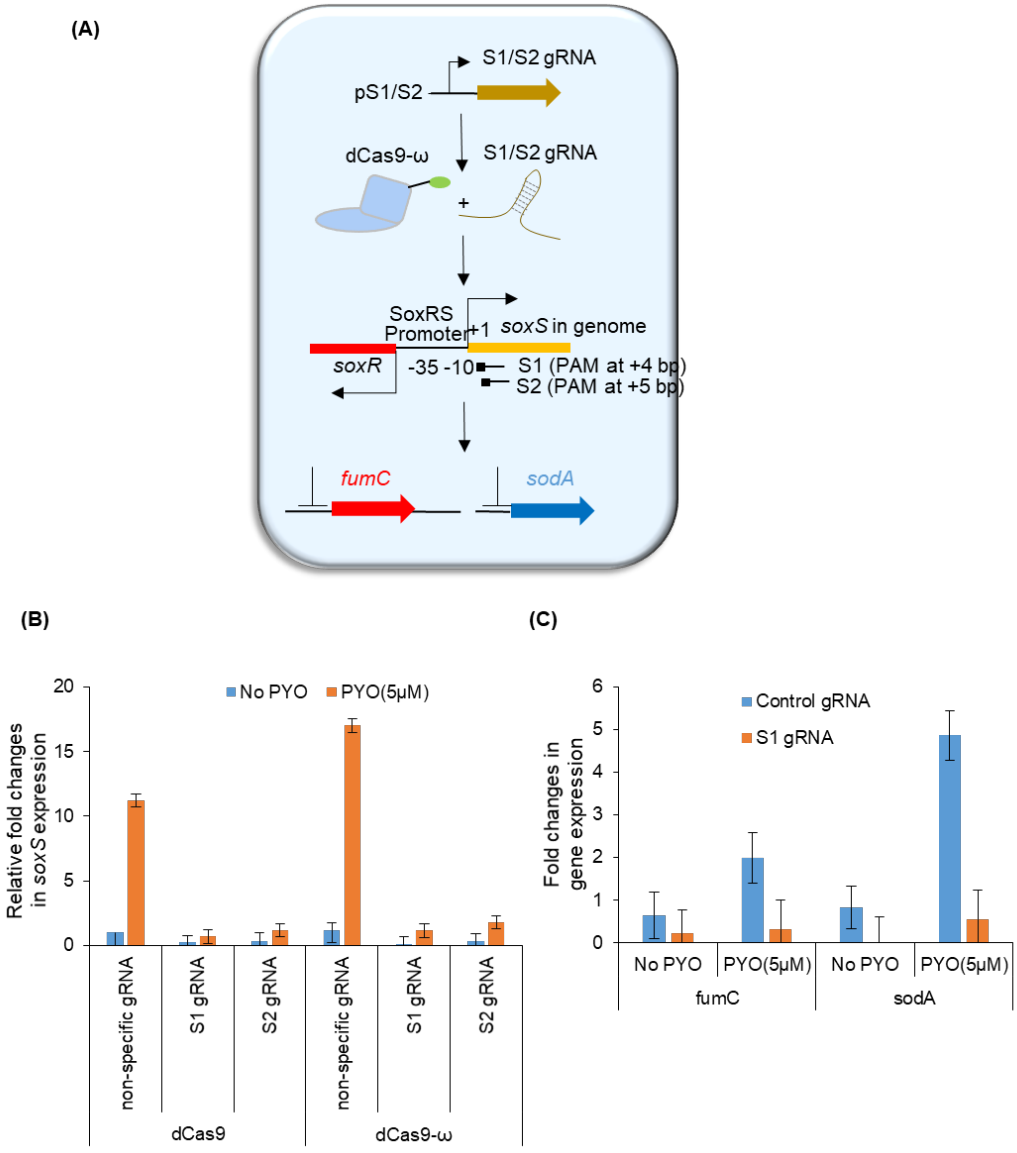

Figure 5-8 Using dCas9-ω for repression of host oxidative defense mechanisms:

Scheme indicating dCas9-ω mediated CRISPRi of *soxS* in the *E coli* genome resulting in repression of *fumC* and *sodA*. I targeted two PAM sites in the *soxS* coding region (+4 and +5 bp in the non-coding strand) with S1 and S2 gRNAs expressed from pS1 and pS2 plasmids under J23119 promoters. Both pS1 and pS2 are transformed with dCas9 as well as dCas9-ω independently for repression of *soxS* in genome in NB101 cells. Cells are induced with 5μM Pyocyanin in aerobic conditions and after 6 hour

incubation, *soxS* repression was measured using qPCR. **(A)** indicates qPCR data comparing repression of *soxS* in *E. coli* using dCas9 and dCas9-ω fusions with S1 and S2 gRNA. **(B)** indicates the indirect repression of *sodA* and *fumC* due to repression of *soxS* in genome mediated by S1 gRNA and dCas9-ω.

To re-confirm these results, I also added 0.5mM Paraquat, a known oxidative stress inducing molecule that targeted SoxRS regulon.[210] I performed similar experiments as in **Figure 5-8** and induced the cells with 0.5 mM Paraquat in aerobic conditions. After three hours of induction, I collected RNA samples and performed qPCR experiments to measure relative levels of *soxS, sodA* and *fumC.* Addition of paraquat led to ~75-fold activation of the *soxS* with the control gRNAs (**Figure 5-9A**). In the presence of *soxS* specific gRNA S1 and dCas9-ω, *soxS* was repressed to pre-Paraquat levels and similarly *sodA* (**Figure 5-9B**) and *fumC* (**Figure 5-9C**) genes were not upregulated due to absence of elevated SoxS.

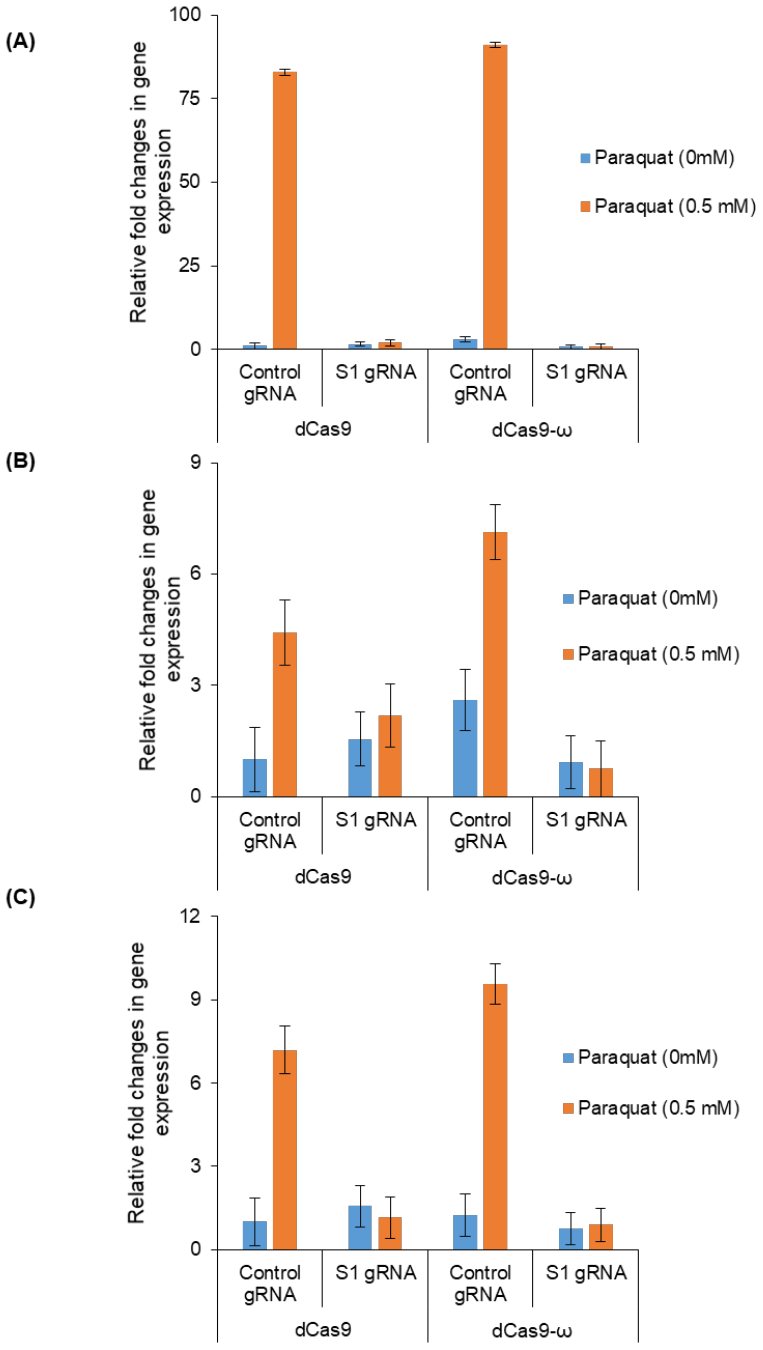

Figure 5-9 CRISPRa based repression of *soxS* with Paraquat as superoxide inducing molecule

(A), (B) and **(C)** indicate repression of s*oxS*, *sodA* and *fumC* respectively with S1gRNA from pS1 and dCas9-ω upon induction of *soxS* in *E coli* genome with 0.5 mM

Paraquat. All qPCR data indicate gene levels 6 hours after induction of SoxS promoter with Paraquat.

Next, I studied if the repression of s*oxS* in the *E coli* genome lead to improved SoxS promoter activity (**Figure 5-10 A**). To study this, I engineered S1gRNA sequence expressed under the J23119 constitutive promoter into a previously described electrogenetic reporter plasmid pTT01 containing *phiLOV* under the SoxS promoter[99] to create pNB01 (See 5.2.4). I inserted this plasmid into NB101 cells along with pdCas9-ω, grew them at 37°C till OD 0.6 and then suspended the cells in M9 minimal media. Then under anaerobic conditions, I induced the cells with 5mM Fcn (O) and 5 µM PYO and measured phiLOV fluorescence levels through FACS. As controls, I also transformed pTT01 into NB101 and DJ901 cells (Δ*soxRS*). phiLOV fluorescence measurements indicated that the addition of the S1gRNA component into the pTT01 reporter plasmid led to a 3 to 4-fold increase in phiLOV expression in NB101 cells (WT for *soxS*) and was comparable to DJ901 (Δ*soxRS)* cells (**Figure 5-10 B)**. I also engineered expression of S1gRNA under a SoxS promoter with a pSC101* origin in a plasmid labelled pNB02 (5.2.4). I transformed pNB02 into NB101 cells containing dCas9-ω and pTT01 phiLOV reporter plasmids. Upon induction with PYO, I observed a similar ~3-fold increase in phiLOV fluorescence as well.

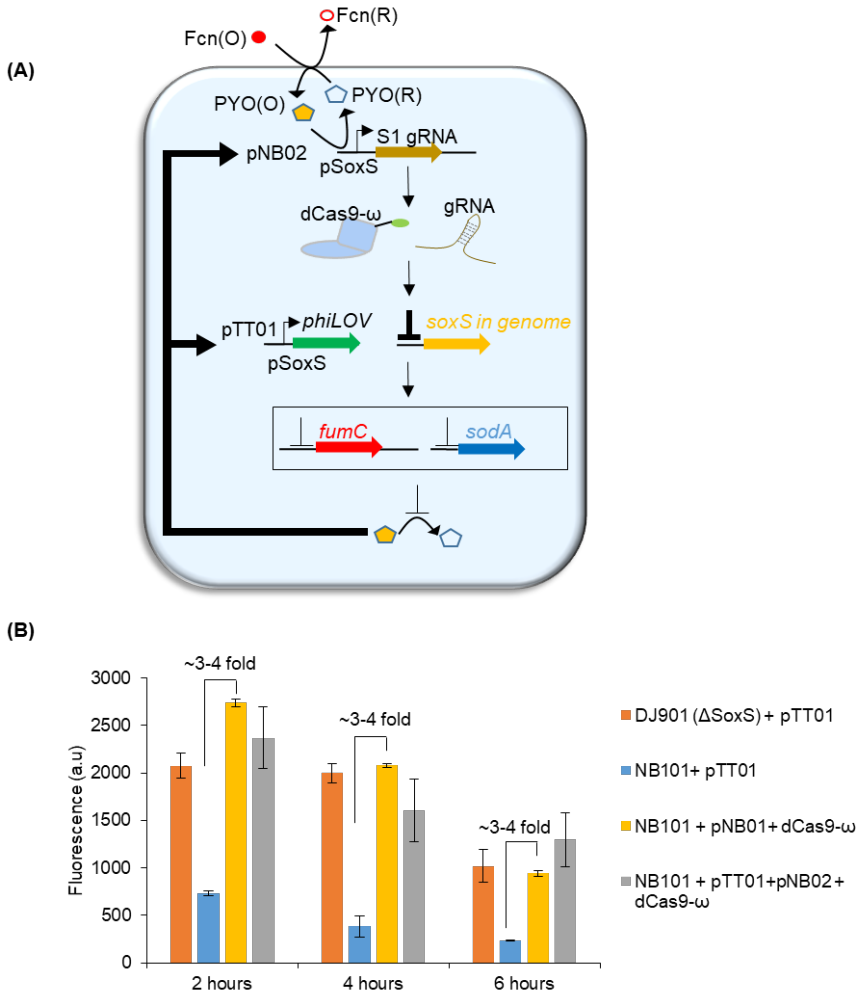

Figure 5-10 Repression of SoxS leads to enhanced SoxS promoter activity.

(A) Scheme of *soxS* repression in *E coli* leading to repression of oxidative stress defense mechanism genes *fumC* and *sodA* and resulting in enhanced SoxS promoter activity. I inserted *soxS* specific S1 gRNA under J23119 promoter into reporter plasmid pTT01 expressing phiLOV from SoxS promoter to create pNB01. I also created pNB02 expressing S1 gRNA from SoxS promoter. **(B)** I transformed pNB01 and pNB02 independently into NB101 cells along with dCas9-ω and induced with 5mM Fcn (O) and 5 µM PYO under anaerobic conditions and measured phiLOV fluorescence through FACS across 6 hours.

In sum, I have displayed that the transcriptional activator dCas9-ω can be repurposed for CRISPRi by targeting the dCas9-ω downstream of the TSS of genes of interest **(Figure 5-8)**. I also showed that by repressing global oxidative stress response mediator *soxS*, I could indirectly repress genes involved in oxidative stress defense response resulting in an overall enhancement of SoxS promoter activity with a ~3-4-fold increase **(Figure 5-10)** in transcription from SoxS promoters.

5.3.4 Simultaneous activation and repression of genes using CRISPRa

Having shown that I could repurpose the dCas9 based transcriptional activator to repress genes, I sought to study whether the transcriptional activator can simultaneously perform CRISPRi and CRISPRa at different sites. With repression of *soxS* in the genome leading to a ~3-4-fold increase in SoxS promoter activity, I explored whether this enhancement from SoxS promoter activity can lead to an increased gRNA expression for CRISPRa.

To display this, I intended to express two gRNAs from the SoxS promoter to mediate CRISPRa of reporter genes as well as CRISPRi of *soxS* in the *E. coli* genome. For this purpose, I engineered both S1gRNA targeting *soxS* in the genome and 108gRNA targeting phiLOV in pMC-phiLOV into a single transcript and expressed it from the SoxS promoter in a plasmid labelled pNB03 (See5.2.3.3). To mediate gRNA processing, I introduced self-cleaving ribozyme hammerhead (HH)[195] at the 5’ end of each gRNA and ribozyme hepatitis delta virus (HDV)[196, 211] at the 3’ end of each

gRNA. I also built a construct (pNB04, See 5.2.3.3) expressing ControlgRNA and 108gRNA for controls (**Figure 5-11 A and B**). As additional controls for ribozyme processing, I also included pSC-S108gRNA plasmid expressing just the 108gRNA for phiLOV activation.

I individually transformed these plasmids along with pdCas9-ω and target plasmid pMC-phiLOV into NB101 cells and grew the cells in LB media at 37^{0}C. At OD 0.6, I suspended the cells in Minimal M9 and induced the cells with various concentrations of Fcn (O) and PYO under anaerobic conditions and measured phiLOV fluorescence after 2 hours.

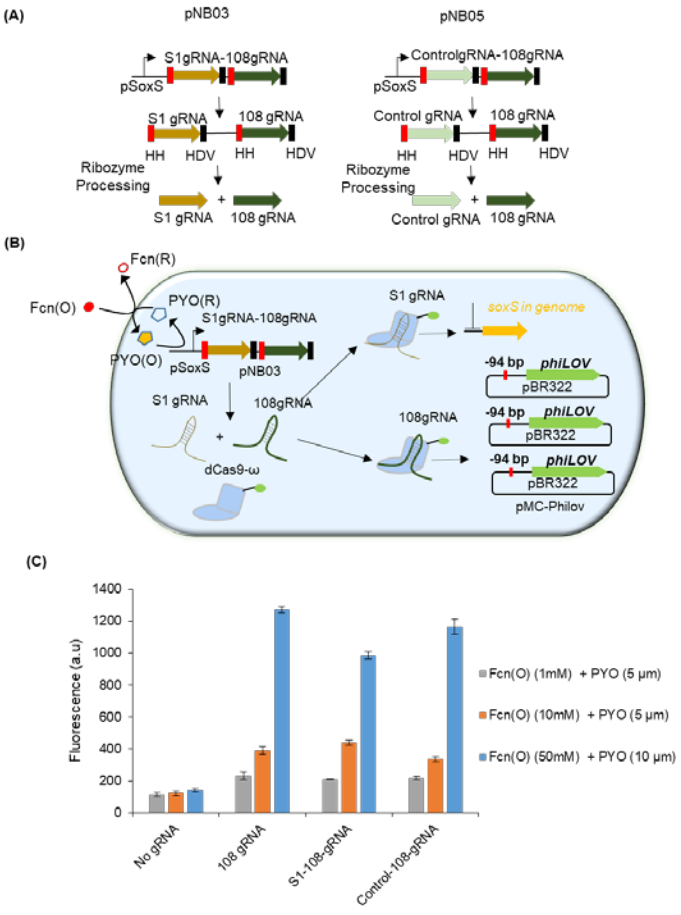

Figure 5-11 Simultaneous activation and repression of multiple genes using dCas9-ω.

(A) Scheme of plasmids pNB03 and pNB04. pNB03 plasmid expresses two gRNAs (*soxS* specific S1gRNA for repression and phiLOV specific 108gRNA for activation) from the pSoxS promoter as a single transcript. Both gRNAs are flanked with ribozymes HH at the 5' end and HDV at the 3' end. Upon transcription, ribozymes self-cleave leading to formation of two separate gRNAs. Similarly, pNB04 expressed a non-specific control gRNA and 108 gRNA for phiLOV activation. **(B)** I transformed pNB03 and pNB04 independently into NB101 cells along with dCas9-ω and pMC-phiLOV, induced with 5mM Fcn (O) and 5 µM PYO under anaerobic conditions and **(C)** measured phiLOV fluorescence through FACS across 6 hours. As controls, I also used pSC-S108 plasmid expressing just 108gRNA for phiLOV activation.

Results indicated that there was phiLOV fluorescence in all gRNA expression conditions indicating that the 108gRNA responsible for activation of phiLOV was fully functional (**Figure 5-11 C**). However, activation of phiLOV with pNB03 (expressing S1gRNA as well as 108gRNA) was not higher than activation of phiLOV with pSC-S108 (expressing 108gRNA only) indicating that there was no improvement in CRISPRa arising from S1gRNA mediated *soxS* repression in the genome.

To analyze whether the S1gRNA is functional post the ribozyme processing of S1-108gRNA hybrids, I tested the effect of S1-108gRNA hybrid on SoxS promoter activity. Results from **Figure 5-10** indicated that the S1gRNA, when expressed independently in pNB01 and pNB02, improved the activity of the SoxS promoter in pTT01 by ~3-4 fold. I expected the same from S1-108gRNA hybrid expressed from pNB03 as well. I transformed pNB03 with pTT01, the SoxS promoter containing reporter plasmid and pdCas9-ω in NB101 cells. As controls, I also used pS1 with constitutive S1gRNA expression in combination with pTT01 and pdCas9-ω. I grew the

cells as before and induced the populations with 5mM Fcn (O) and 5 µM PYO for 2 hours under anaerobic conditions. Results showed that the pNB03 plasmids did enhance the SoxS promoter activity by 1-fold. These results indicated that S1gRNA that is expressed in combination with 108gRNA from pNB03 plasmids were functional post ribozyme processing. However, S1gRNA when expressed in combination with another gRNA gave just 1-fold increase in SoxS promoter activity in comparison to 3-fold increase when expressed independently.

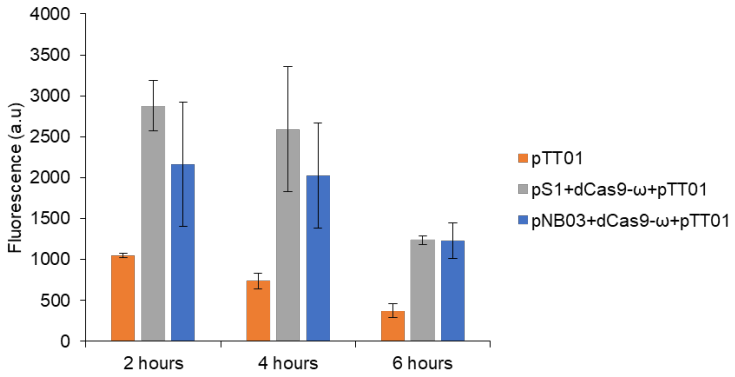

Figure 5-12 Multiplexed gRNAs support feedback on SoxS promoters

I transformed pNB03 (expressing both *soxS* specific S1 gRNA and 108gRNA for phiLOV) along with dCas9-ω and pTT01 reporter plasmid into NB101 cells, induced with 5mM Fcn (O) and 5 µM PYO under anaerobic conditions and measured phiLOV fluorescence through FACS across 6 hours. As controls, I also used pS1 plasmid expressing just *soxS* specific S1gRNA. n=3.

In sum, I have displayed simultaneous CRISPR based repression and activation of two genes using a transcriptional activator dCas9-ω (**Figure 5-11** and **Figure 5-12)**. I have also shown that while CRISPR based repression of *soxS* in genome leads to 4-fold increase in SoxS promoter activity, similar increases in CRISPRa is not achieved

indicating the limitations of connecting feedback loops between CRISPRi and CRISPRa systems.

Future Work:

CRISPR based activation of Quorum Sensing (QS) is discussed in **Appendix** section of this thesis.

5.4 Discussion

In this work, firstly I did basic characterization of the poorly understood bacterial CRISPR-Cas9 mediated transcriptional activation (CRISPRa) system. I optimized the expression conditions including promoters, plasmid copy numbers for expression of gRNA as well as dCas9 based transcriptional activators and copy numbers of the target genes to create a tunable CRISPRa system. Secondly, I successfully integrated the CRISPRa system with the SoxRS based electrogenetic system to create an electrically tunable CRISPRa with a maximum ~13-fold transcriptional activation. Thirdly, I repurposed the dCas9 based transcriptional activator to repress the oxidative stress defense responses in bacteria resulting in a ~3-4-fold increase in electrogenetic promoter activity.

While I created a tunable CRISPRa system by controlling gRNA expression, all our efforts to control dCas9 expression for the development of a tunable and controllable CRISPRa was unsuccessful. While minimal leaky expression of dCas9 from Tet promoters was sufficient for transcriptional activation, any attempt to increase the expression of dCas9 from the leaky expression level was unsuccessful. This problem has been overcome in the recent past in mammalian systems through various post translational approaches. Both dCas9 and transcriptional activators are engineered with dimerizing domains and expressed as two separate proteins. Upon optical[212] or small molecule induction[213], both components dimerize together for transcriptional

activation. This approach of inducible transcriptional activations needs to be adapted in the microbial contexts.

I successfully integrated CRISPRa system into electrogenetic circuits and activated *phiLOV* by up to ~13-fold. However, direct transcription of *phiLOV* from SoxS promoters was reported to be ~40-fold under similar copy number conditions.[99] The apparent differences in transcriptional activation can be attributed to the differences in the way transcription is initiated in these two scenarios. In SoxS promoters, the RNA polymerase is assembled on the promoter and upon SoxR oxidation there is a conformational change in -35 region of the SoxS promoter leading to transcriptional activation[214]. In CRISPR systems, transcriptional activator ω subunit works by recruiting and stabilizing RNA polymerase and the sigma factor at promoter sites, thereby making the process of transcription less efficient. However, incorporation of CRISPR as an intermediate layer between electrogenetic promoters and genes of interest provides the flexibility to electrically target, activate and repress multiple genes at the same time.

In this study, I was able to successfully repurpose the dCas9-ω transcriptional activator for transcriptional repression. Direct repression of *soxS*, the global oxidative stress defense response mediating transcriptional factor in the genome led to prevention of upregulation ~15 genes whose products mediate defense against oxidative stresses. A net effect of all the repression led to ~4-fold increase in SoxS promoter activity indicated by Philov fluorescence. This ~4-fold increase in SoxS promoter activity can be attributed to the lower metabolic burden obtained due to lack of onset of oxidative

stress defense responses or alternatively with the sustained presence of reactive oxygen species (ROS) inside cells in the absence of oxidative stress defense responses that actively work to reduce ROS. Both theories need to be analyzed further to decipher the exact reasons for enhanced SoxS promoter activity.

In conclusion, I propose a new paradigm by which direct connection between electronic signals and central dogma of host organisms can be mediated. Emergence of CRISPR provides the capability to target specific genes in the genome of organisms and integration of CRISPR with electronics provides the capability to electrically turn ON and OFF several genes simultaneously. As a proof of concept, I have demonstrated that I could use this capability to temporally silence host defense responses to electronic signals and drive better transgene activation in response to electrical signals. I believe that the further development of this capability to electronically target select genes across the host genome could be a significant new tool in bioelectronics research where so far the focus has been on targeting specific cells rather than specific genes in cells. This work also has potential applications in the field of synthetic biology where problems pertaining to chassis compatibility are ubiquitous. Simultaneous activation and repression mechanisms are crucial for moderating or supporting host behavior for the successful adaptation of synthetic biology toolsets across a wide range of organisms.

5.5 Supplementary data

5.5.1 Regulating dCas9 expression from Tet promoters for a controllable CRISPRa system

In all the previous experiments, I had been using leaky expression dCas9-ω from the Tet promoter in pdCas9-ω. To create a controllable CRISPRa system, I intended to regulate expression of dCas9-ω under the Tet promoter in pdCas9-ω. To the NB101 cells containing p108gRNA, pdCas9-ω and pWJ89 plasmids, I added varying concentrations of inducer aTc from 100 nM to 10 pM at the time of re-inoculation and grew at 37°C. After 6 hours, I measured the relative gene expression levels of dCas9-ω and GFP through qPCR (dCas9-ω was indicated by *rpoZ* encoding for ω subunit. ω was genetically fused to dCas9). In addition to the relative gene expression levels of dCas9-ω and GFP **(Supplementary Figure 5- A)**, I measured GFP fluorescence **(Supplementary Figure 5- B)** and cell growth (OD) **(Supplementary Figure 5- C)** as well at 4 and 8 hours.

qPCR data indicated that only the 100nM aTc concentration significantly increased dCas9-ω expression levels (indicated by *rpoZ* levels) over leaky expression from Tet promoter. However, the *gfpmut2* expression data at 6 hours showed a markedly different gene expression pattern with 100 pM condition displaying the highest *gfpmut2* expression. aTc concentrations higher than 100 pM had lower *gfpmut2* levels. GFP fluorescence **(Supplementary Figure 5- B)** showed a consistent trend of decrease in fluorescence with increasing concentrations of aTc at both 4 and 8 hours

post inoculation. OD **(Supplementary Figure 5-C)** followed a trend similar to GFP fluorescence as well.

While there was no significant increase in dCas9-ω expression with increase in aTc concentrations from 0 M to 10 nM, there was still a consistent decrease in GFP fluorescence and OD indicating toxicity due to dCas9 induction.

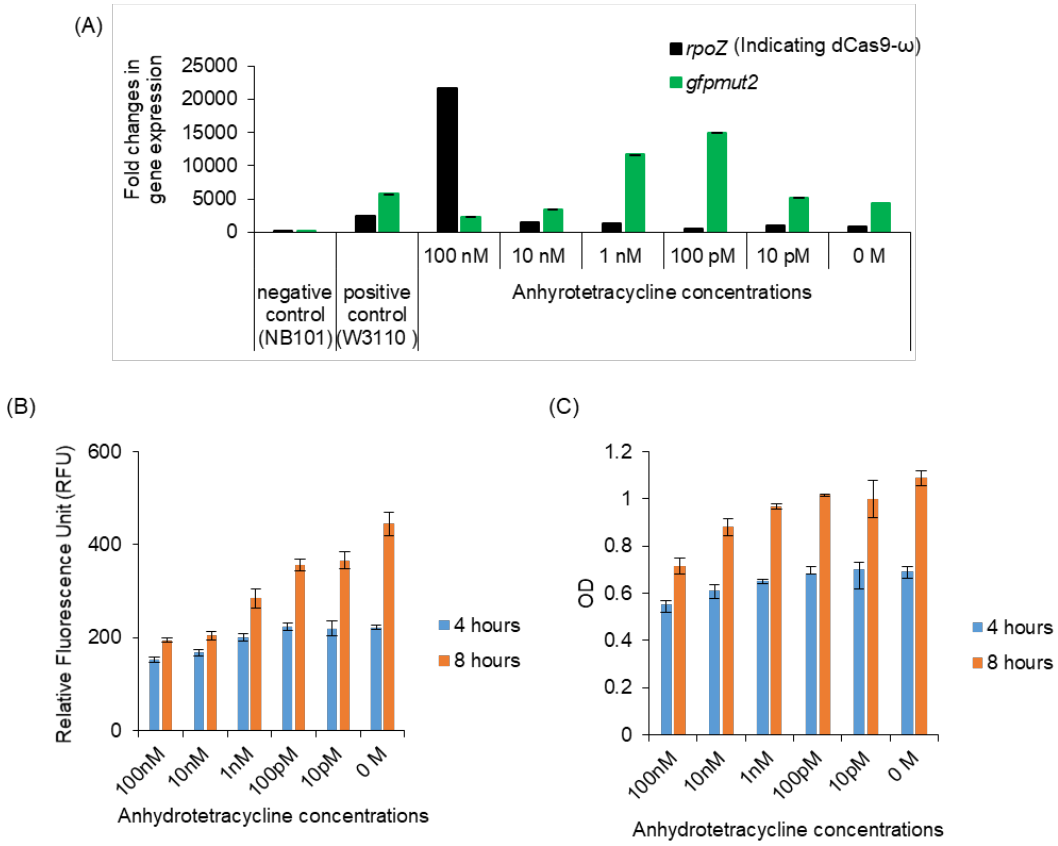

Supplementary Figure 5-Regulating dCas9 expression from Tet promoters for a controllable CRISPRa system.

I transformed pdCas9-ω, p108gRNA and pWJ89 into NB101 cells and induced the Tet promoter in pdCas9-ω for dCas9 expression with different aTc concentrations. **(A)** qPCR data for *rpoZ* and *gfp* measured 6 hours after addition of anhydrotetracycline (aTc). *rpoZ* codes for that ω subunit and indicates relative levels of dCas9-ω fusions.

(B) and **(C)** indicates GFP fluorescence and OD obtained 4 and 8 hours after addition of various concentrations of aTc to induce dCas9-ω expression from the Tet promoter. GFP and OD were measured through plate reader. n=3

To make dCas9-ω based CRISPRa system a controllable system where CRISPRa of target genes occurs only after induction of dCas9-ω, I attempted to regulate expression of dCas9-ω by engineering both at the level of transcription as well as translation.

To remove leaky expression of dCas9-ω from Tet promoters, I added a protein degradative ssRA tag to the C termini of the dCas9-ω fusion (pdCas9-ω_{ssRA}, Error! Reference source not found. **B**). In addition, I removed the natural promoters for Tet Repressor and replaced with a stronger synthetic promoter for Tet repressor to increase expression of Tet repressor and in turn increase repression of the Tet promoter. In addition to that, I also reduced ribosome binding site (RBS) strength by 10 folds for dCas9-ω from the Tet promoter. These measures were reported to have reduced leaky expression of Cas9 resulting in increased genome editing efficiencies.[204] Promoter and RBS changes were introduced into both pdCas9-ω and pdCas9-ω_{ssRA} to create pIntdCas9-ω (**Supplementary Figure 5-1 C**) and pIntdCas9-ω_{ssRA} (**Supplementary Figure 5-1D**). I expected these changes to remove leaky expression of dCas9-ω and make dCas9-ω and in turn dCas9-ω mediated CRISPRa of GFP more inducible.

I transformed all these different dCas9 expression plasmids with p108gRNA and pWJ89 plasmids in NB101 cells and induced varying concentrations of the inducer aTc at the time of re-inoculation and measured GFP fluorescence at 6 hours. Under the

uninduced conditions with no aTc, CRISPRa of GFP due to leaky expression of dCas9-ω decreased with increasing constraints on transcription and translation of dCas9-ω. CRISPRa from pdCas9-ω was the highest followed by the activation from pdCas9-$\omega_{ssRA.}$ CRISPRa from pIntdCas9-ω and pIntdCas9-ω_{ssRA} were even lower (**Supplementary Figure 5-1 E**). These results indicated that the changes introduced both at translation level (addition of ssRA tags to dCas9-ω and reduced RBS strength for dCas9-ω) as well as transcriptional level (increased promote strength for Tet Repressor) reduced the leaky expression of dCas9-ω. At the same time, our effort to make Tet promoter controllable where upon addition of aTc there should be an increase in CRISPRa of GFP, was unsuccessful. There was no increase in transcriptional activation of GFP with addition of aTc in any of the conditions except in the case of pdCas9-ω_{ssRA} where 1nM aTc resulted in a minor increase. These results indicate that while efforts to contain leaky expression of dCas9-ω was successful, our efforts were unsuccessful for a controllable dCas9-ω mediated activation of GFP. In all further experiments, I continued to use the leaky Tet promoter in pdCas9-ω for all experiments.

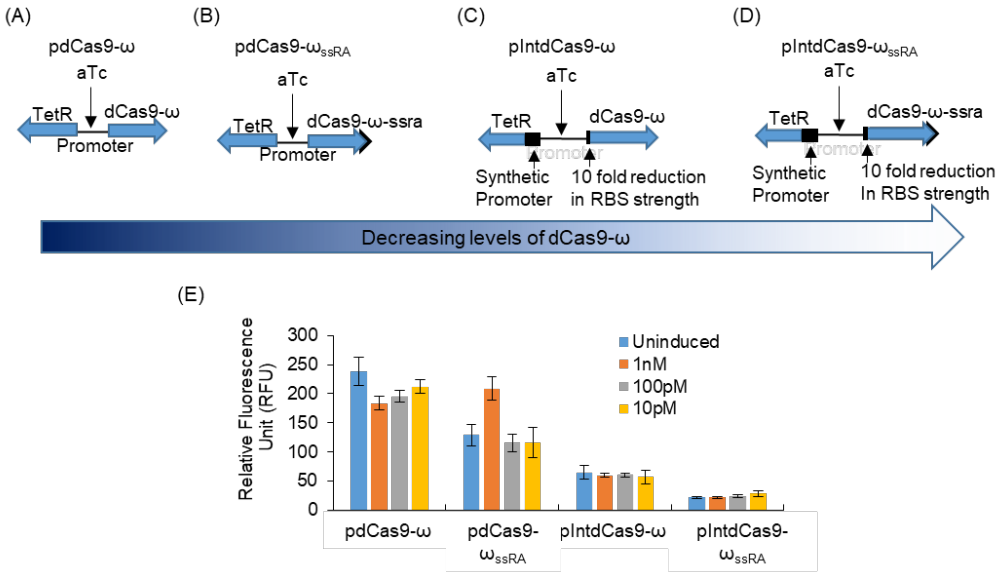

Supplementary Figure 5-1 Engineering dCas9-ω transcription and translation processes to create an inducible CRISPRa system.

(A) Tet promoter with dCas9-ω (pdCas9-ω). **(B)** Same as (A) with dCas9-ω engineered with a ssRA tag at the C termini of dCas9-ω fusion (pdCas9-ω_{ssRA}). **(C)** Engineering of a synthetic promoter for TetR to upregulate expression of Tet repressor and engineering of 10-fold reduction in RBS site strength to decrease translation of dCas9-ω (pIntdCas9-ω). **(D)** Same as C with a ssRA tag at the C termini (pIntdCas9-ω_{ssRA}). **(E)** GFP fluorescence measured through plate reader after 6 hours of addition of different anhydrotetracycline (aTc) concentrations under different dCas9-ω expression conditions (pdCas9-ω, pdCas9-ω_{ssRA}, pIntdCas9-ω and pIntdCas9-ω_{ssRA}). n=3.

5.5.2 Controlling gRNA for a tunable CRISPRa system

While our efforts to regulate dCas9-ω expression were unsuccessful, I next focused our attention towards gRNAs, the second element of the CRISPR-Cas9 transcriptional regulatory system in addition to dCas9 protein. gRNA based tuning of CRISPRi is well documented in bacteria with major criterions for tuning being relative levels of gRNA, spacer sequence similarity with target[215] and position of spacer in relation to TSS of the gene of interest[194]. I sought to analyze whether these criterions

influence CRISPRa as well. Since the distance of spacer from TSS for RNA polymerase recruitment in CRISPRa was optimized earlier and I was already working with the best spacer reported for CRISPRa[194], I examined other factors that may influence CRISPRa.

I first analyzed whether sequence similarity between spacer and target sequence is a determining factor for a tunable CRISPRa. It is known that single point mutations in the seed region of a spacer sequence (the first four bp in the spacer near the PAM site) can significantly reduce the efficiency of CRISPRi[215]. To test if this factor plays a significant role in CRISPRa, I introduced single point mutations by replacing purines with pyrimidines or vice versa in the seed region to create non-cognate gRNAs (expressed in pNC-gRNA 1, 3 and 5). I transformed the non-cognate gRNA plasmids along with pdCas9-ω and pWJ89 plasmids into NB101 strains and grew them in 37°C. I expressed the non-cognate gRNAs from the same constitutive promoter (J23119) as the cognate gRNA (p108gRNA) and measured the effect of non-cognate gRNA on GFP activation. I measured GFP fluorescence levels using plate reader at 4, 8 and 24 hours after re-inoculation. Results indicated that the non-cognate gRNAs had no significant effect on CRISPRa of GFP across 4 and 8 hours (**Supplementary Figure 5-2)** indicating that the introduced single point mutations at seed regions had no effect on CRISPRa.

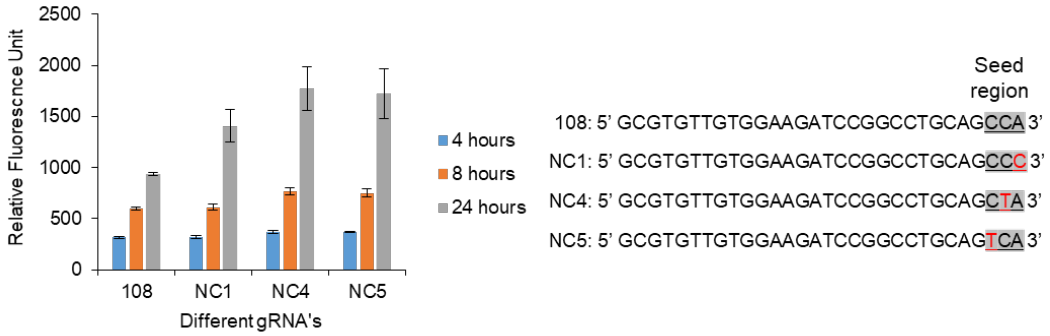

Supplementary Figure 5-2 Engineering the sequence of spacers to modulate CRISPRa in bacteria.

3 non-cognate gRNAs (denoted as NC1, NC4 and NC5) with single point mutations in the seed region of the cognate 108-spacer sequence are expressed under J23119 promoters in pNC1, 3 and 5 plasmids to target GFP (pWJ89) for CRISPRa in NB101 cells. I used dCas9-ω under leaky expression conditions from the Tet promoter in pdCas9-ω and measured GFP fluorescence through plate reader at 4, 8 and 24 hours. n=3.

Chapter 6 Conclusion

In this thesis, I have worked on two different fronts across the bioelectronic interface. On one end, I designed biofabrication frameworks for construction of enzyme cascades that enabled conversion of biological signals to electric signals. On the other end, I integrated the CRISPR-Cas9 based transcriptional regulation frameworks with electrogenetic promoter systems to mediate communication between electrical signals and specific genes in the genomes of bacterial systems.

To enable construction of enzyme cascades for conversion of biologic and electronic signals, I first demonstrated a facile method for the assembly of multi-subunit enzyme complexes on solid supports. I covalently conjugated individual components using engineered Lys and Gln tags and coupled the components using mTG. Using this method, I built a two-enzyme metabolon involving bacterial QS enzymes and displayed control of metabolic flux across these enzymes. Through this method, I was also able to build multi-functional enzyme-Protein G complex that was eluted from assembly beads and used for specific targeted applications.

Next, I implemented the mTG based approach to build enzyme cascades on microchips. I first functionalized the chitosan coated gold chip with a Lys-Tyr-Lys tripeptide using Michael type addition. Then, I conjugated the Gln's engineered enzymes to the Lys's in the tripeptide layer using mTG. This approach of using tripeptides to coat chitosan for conjugation decreased the non-specific binding of proteins to chitosan and the use of rapid mTG based conjugation chemistry quickened

the assembly process. To further simplify the fabrication process, I developed a self-assembling 3D scaffold made up of TMV-VLP's that displays desired functional groups (Gln's) for biocomponent functionalization on the electronic surface. In association with 3D scaffolds, I also adapted the mTG mediated approach to build a three-enzyme cascade on the gold surface to convert methyl cycle intermediates SAH and SAM into homocysteine, an electrochemically readable molecule.

Finally, to electrically control transcriptional regulation in biological systems, I integrated the CRISPR-Cas9 based synthetic transcription factors into electrogenetic promoters in *E coli*. Firstly, I did preliminary characterization CRISPR-Cas9 mediated transcriptional activation (CRISPRa) system in *E coli* and integrated the CRISPRa system with the SoxRS based electrogenetic system to create an electrically tunable CRISPRa. I also repurposed the dCas9 based transcriptional activator to repress the oxidative stress defense responses in bacteria resulting in an overall increase in electrogenetic promoter activity.

Appendix

CRISPR based activation of Quorum Sensing communication

Having shown that I could tune transcriptional activation by controlling the gRNA levels, I sought to develop a CRISPR based QS communication system where electrogenetic CRISPR cells can translate electric signals into QS molecules and QS molecules can mediate transcriptional change in other populations in a microbial consortium.

To display this QS communication concept, I used the CRISPRa system to activate transcription of LasI, a *Pseudomonas aeruginosa* Autoinducer-1 synthase. I replaced the *gfpmut2* in pMC-GFP with the *lasI* (pMC-LasI) and transformed it along with pSC-S108 and pdCas9-ω into NB101 for transcriptional activation. I referred these populations as AI-1 producer cells. I added different concentration of PYO to the producer cells at the time of re-inoculation under aerobic conditions and activated gRNA expression resulting in CRISPRa of LasI. After 4 hours, I collected the condition media from the cells and incubated with AI-1 reporter cells (JLD271 strain with pAL105) that luminesce in response to AI-1. Relative AI-1 activities are measured via an AI-1 reporter assay (See 5.2.8) after 4 hours **(Figure 1)**. Results indicated that AI-1 activity increased with increasing concentrations of PYO and saturated at 5 μM.

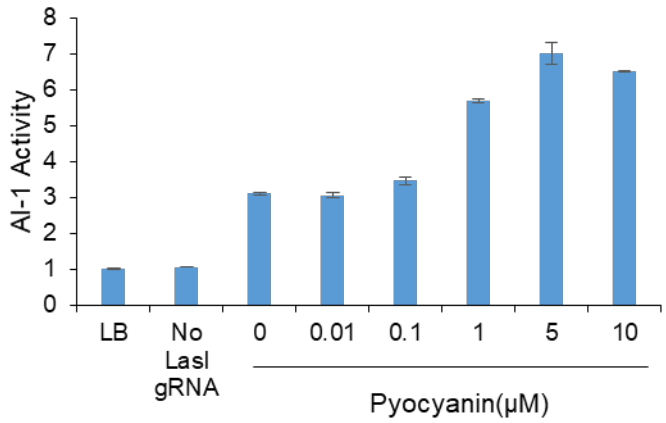

Figure 1 Activation of LasI QS synthase using CRISPRa under aerobic conditions.

I transformed pMC-LasI, pSC-S108 and pdCas9-ω into NB101 cells and induced with different concentrations of Pyocyanin under aerobic conditions for 4 hours in LB media. Conditioned media is collected and relative AI-1 activity is measured through luminescence from JLD271 strain containing pAL105 (See 5.2.8 for AI-1 assay). n=3.

To spatially delineate electrically responsive AI-1 producer populations and responder populations and mediate communication between the two microbial populations, I intended to encapsulate these two populations in two different alginate-chitosan capsules. I adapted a previously described alginate microfluidic encapsulation system[105] to generate AI-1 producer cell capsules. Cells were first re-inoculated from overnight cultures into fresh LB at a dilution of 1:100 and grown to an OD_{600} of ~0.5. I then pelleted the cells and re-suspended the pellet in an equal volume of 2% alginate. This solution was then extruded through a microfluidic device[1] which allowed the alginate solution to proceed at a fixed flow rate. Beads formed at the tip of the capillary were uniformly sheared by air pulses developed at the tip of the capillary tube

and I collected the beads in a solution containing 1% w/v Chitosan and 1% w/v $CaCl_2$. After 30 minutes of incubation, I collected the beads by carefully decanting excess chitosan and $CaCl_2$ and gently washed the capsules three times with MOPS-M9 media prepared without $CaCl_2$. I varied the frequency of the air pulses and collected the capsules. **Figure 2 A** shows the microscope images of the capsules collected with different frequencies and the differences in diameter of the capsules collected at different frequencies (**Figure 2 B**). With increasing frequency, the diameter of the capsules decreased as expected.

To prove that the capsules containing AI-1producer cells can respond to PYO, I collected capsules with a 5Hz pulse. I varied the time of the 5Hz pulse from 20 to 160 seconds and collected the capsules. Post treatments with calcium and chitosan, capsules containing AI-1 producing cells were incubated with 5 μM PYO in M9 minimal media under aerobic conditions for 2 hours at 37˚C. After incubation, I collected conditioned media and performed the AI-1 activity assay. As controls, I also had capsules incubated without PYO. Results indicated that capsules incubated with PYO produced more AI-1 than controls and with increase in time of the frequency pulse, there was a corresponding increase in AI-1 activity **(Figure 2 C)**.

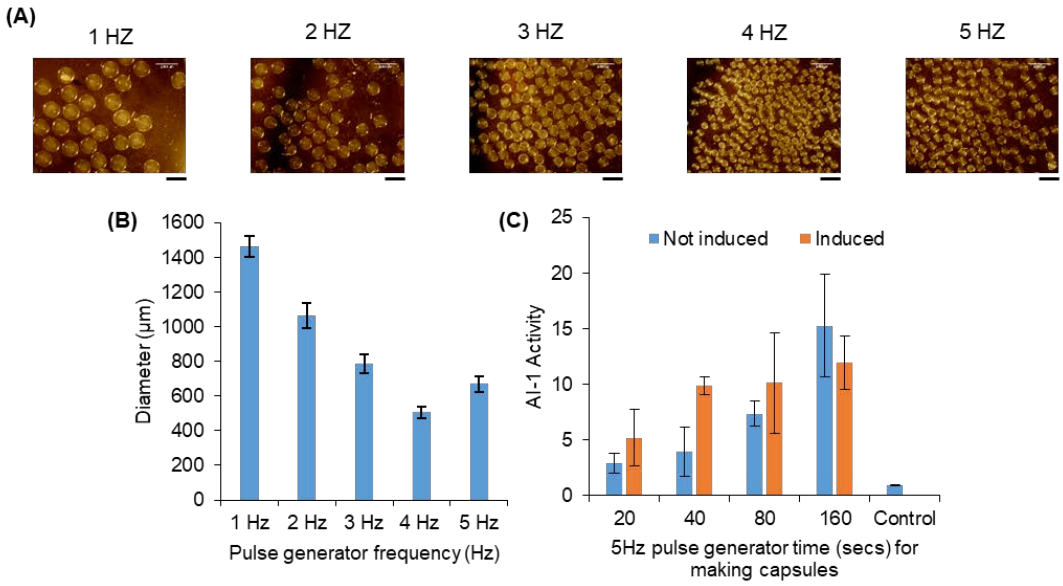

Figure 2 Activation of LasI QS synthase using CRISPRa from AI-1 producer capsules

Role of the frequency of pulse generator used to shear the capsules from the tip of the encapsulation system on capsule size, capsule number and AI-1 activity. (A) indicates microscopic images of capsules obtained using different pulse generator frequencies, scale bar: 2mm. (B) indicates the average size of the capsules obtained using different pulse generator frequencies. n=50. I also made AI-1 producer capsules and collected capsules with different exposure times (20-160 seconds) to a 5Hz pulse. I induced these capsules in minimal M9 media with 5µM Pyocyanin under aerobic conditions for 2 hours at 37ºC and measured AI-1 activity. Control capsule had no AI-1 producer cells.

Next to verify whether AI-1 can enter the capsules and activate reporter cells, I prepared reporter cell capsules as before. In this experiment, I used Top10 cells expressing EGFP in response to AI-1 as reporter cells. To the capsules, I added varying concentrations of AI-1, incubated at 37˚C for 3 hours in LB media under aerobic conditions. After incubation, the capsules were washed and analyzed using confocal microscopy. Results indicated that the reporter cells in capsules displayed a linear

range of fluorescence from 0 to 1µM AI-1 concentration, beyond which there was saturation of fluorescence intensity **(Figure 3)**.

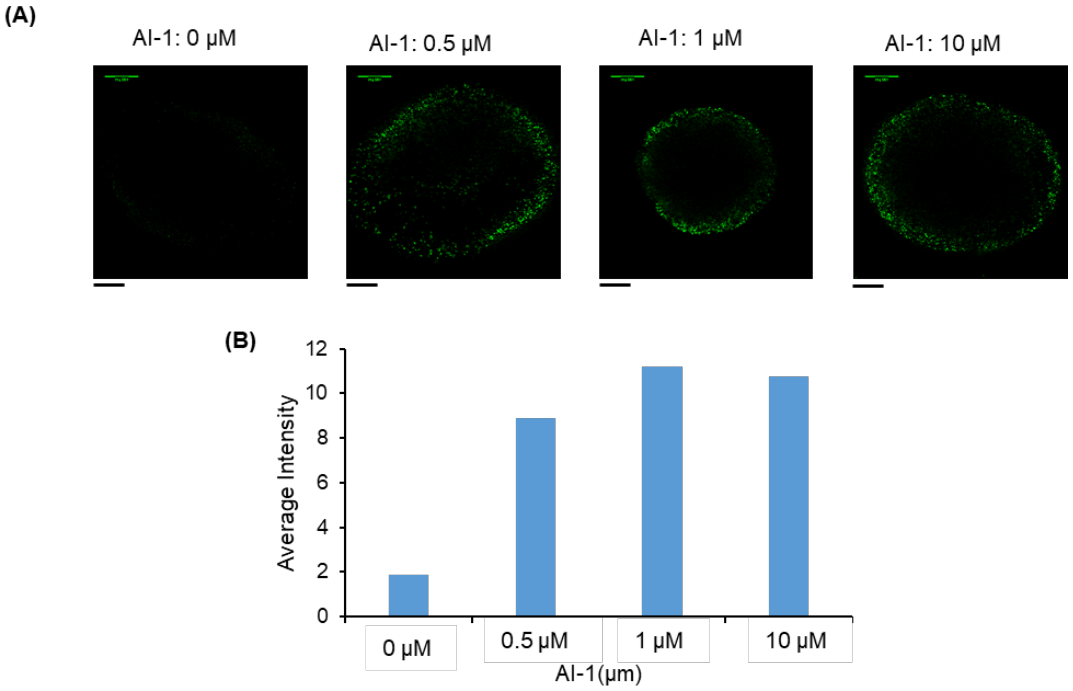

Figure 3 Confocal microscopy images of AI-1 reporter capsules

Alginate-Chitosan capsules containing AI-1 reporter cells are incubated with AI-1 for 3 hours at 37ºC and fluorescence is measured through confocal microscopy. Reporter cells were encapsulated at an OD of 0.5 are incubated with different AI-1 concentrations (left to right: 0 µM, 0.5 µM, 1 µM and 10 µM). Scale: 100 µm. (B) Plot of the average fluorescence intensity versus the AI-1 concentration. n=1.

A fully working system with both AI-1 producing capsules and AI-1 responding capsules in the same environment with one capsule translating electrical signals into biological signals (AI-1) and the other capsule responding to the AI-1 needs to be demonstrated.

Bibliography

1. Gubala, V., et al., *Point of Care Diagnostics: Status and Future.* Analytical Chemistry, 2012. **84**(2): p. 487-515.
2. Preechaburana, P., A. Suska, and D. Filippini, *Biosensing with cell phones.* Trends in Biotechnology. **32**(7): p. 351-355.
3. Bhavnani, S.P., J. Narula, and P.P. Sengupta, *Mobile technology and the digitization of healthcare.* European Heart Journal, 2016. **37**(18): p. 1428-1438.
4. Topol, E.J., *Transforming Medicine via Digital Innovation.* Science translational medicine, 2010. **2**(16): p. 16cm4-16cm4.
5. Sun, F.T. and M.J. Morrell, *Closed-loop Neurostimulation: The Clinical Experience.* Neurotherapeutics, 2014. **11**(3): p. 553-563.
6. Grosman, B., et al., *Hybrid Closed-Loop Insulin Delivery in Type 1 Diabetes During Supervised Outpatient Conditions.* Journal of Diabetes Science and Technology, 2016. **10**(3): p. 708-713.
7. Kovatchev, B.P., et al., *Safety of Outpatient Closed-Loop Control: First Randomized Crossover Trials of a Wearable Artificial Pancreas.* Diabetes Care, 2014. **37**(7): p. 1789-1796.
8. Yu, J., et al., *Microneedle-array patches loaded with hypoxia-sensitive vesicles provide fast glucose-responsive insulin delivery.* Proceedings of the National Academy of Sciences, 2015. **112**(27): p. 8260-8265.
9. Shao, J., et al., *Smartphone-controlled optogenetically engineered cells enable semiautomatic glucose homeostasis in diabetic mice.* Science Translational Medicine, 2017. **9**(387).
10. Farra, R., et al., *First-in-Human Testing of a Wirelessly Controlled Drug Delivery Microchip.* Science Translational Medicine, 2012.
11. Williams, B., et al., *Novel Description of the 24-Hour Circadian Rhythms of Brachial Versus Central Aortic Blood Pressure and the Impact of Blood Pressure Treatment in a Randomized Controlled Clinical Trial.* Hypertension, 2013. **61**(6): p. 1168.
12. Abraham, W.T., et al., *Wireless pulmonary artery haemodynamic monitoring in chronic heart failure: a randomised controlled trial.* The Lancet. **377**(9766): p. 658-666.
13. Adamson, P.B., et al., *Wireless Pulmonary Artery Pressure Monitoring Guides Management to Reduce Decompensation in Heart Failure With Preserved Ejection Fraction.* Circulation: Heart Failure, 2014. **7**(6): p. 935.
14. Hafezi, H., et al., *An Ingestible Sensor for Measuring Medication Adherence.* IEEE Transactions on Biomedical Engineering, 2015. **62**(1): p. 99-109.
15. Clark, L.C. and C. Lyons, *ELECTRODE SYSTEMS FOR CONTINUOUS MONITORING IN CARDIOVASCULAR SURGERY.* Annals of the New York Academy of Sciences, 1962. **102**(1): p. 29-&.

16. Luppa, P.B., et al., *Point-of-care testing (POCT): Current techniques and future perspectives.* Trac-Trends in Analytical Chemistry, 2011. **30**(6): p. 887-898.
17. Lauks, I.R., et al., *Cartridge for a blood monitoring analyzer*. 1993, Google Patents.
18. Toner, M. and D. Irimia, *Blood-on-a-chip.* Annual Review of Biomedical Engineering, 2005. **7**: p. 77-103.
19. Chin, C.D., V. Linder, and S.K. Sia, *Lab-on-a-chip devices for global health: Past studies and future opportunities.* Lab on a Chip, 2007. **7**(1): p. 41-57.
20. Clerc, O. and G. Greub, *Routine use of point-of-care tests: usefulness and application in clinical microbiology.* Clinical Microbiology and Infection, 2010. **16**(8): p. 1054-1061.
21. Catlin, D.H., K.D. Fitch, and A. Ljungqvist, *Medicine and science in the fight against doping in sport.* Journal of Internal Medicine, 2008. **264**(2): p. 99-114.
22. Arruda, D.L., et al., *Microelectrical sensors as emerging platforms for protein biomarker detection in point-of-care diagnostics.* Expert Review of Molecular Diagnostics, 2009. **9**(7): p. 749-755.
23. Daniels, J.S. and N. Pourmand, *Label-free impedance biosensors: Opportunities and challenges.* Electroanalysis, 2007. **19**(12): p. 1239-1257.
24. Gervais, L., N. de Rooij, and E. Delamarche, *Microfluidic Chips for Point-of-Care Immunodiagnostics.* Advanced Materials, 2011. **23**(24): p. H151-H176.
25. Zhang, C.-y. and J. Hu, *Single Quantum Dot-Based Nanosensor for Multiple DNA Detection.* Analytical Chemistry, 2010. **82**(5): p. 1921-1927.
26. Yang, M., et al., *Carbon Nanotubes with Enhanced Chemiluminescence Immunoassay for CCD-Based Detection of Staphylococcal Enterotoxin B in Food.* Analytical Chemistry, 2008. **80**(22): p. 8532-8537.
27. Sassolas, A., L.J. Blum, and B.D. Leca-Bouvier, *Immobilization strategies to develop enzymatic biosensors.* Biotechnology Advances, 2012. **30**(3): p. 489-511.
28. Umana, M. and J. Waller, *PROTEIN-MODIFIED ELECTRODES - THE GLUCOSE-OXIDASE POLYPYRROLE SYSTEM.* Analytical Chemistry, 1986. **58**(14): p. 2979-2983.
29. Sohail, M. and S.B. Adeloju, *Electroimmobilization of nitrate reductase and nicotinamide adenine dinucleotide into polypyrrole films for potentiometric detection of nitrate.* Sensors and Actuators B-Chemical, 2008. **133**(1): p. 333-339.
30. Asuncion Alonso-Lomillo, M., et al., *Electrochemical determination of levetiracetam by screen-printed based biosensors.* Bioelectrochemistry, 2009. **74**(2): p. 306-309.
31. Hu, S.S., et al., *Biosensor for detection of hypoxanthine based on xanthine oxidase immobilized on chemically modified carbon paste electrode.* Analytica Chimica Acta, 2000. **412**(1-2): p. 55-61.

32. Xue, H.G. and Z.Q. Shen, *A highly stable biosensor for phenols prepared by immobilizing polyphenol oxidase into polyaniline-polyacrylonitrile composite matrix.* Talanta, 2002. **57**(2): p. 289-295.
33. Bruns, N. and J.C. Tiller, *Amphiphilic network as nanoreactor for enzymes in organic solvents.* Nano Letters, 2005. **5**(1): p. 45-48.
34. Ichimura, K., *A CONVENIENT PHOTOCHEMICAL METHOD TO IMMOBILIZE ENZYMES.* Journal of Polymer Science Part a-Polymer Chemistry, 1984. **22**(11): p. 2817-2828.
35. Leca, B. and J.L. Marty, *Reagentless ethanol sensor based on a NAD-dependent dehydrogenase.* Biosensors & Bioelectronics, 1997. **12**(11): p. 1083-1088.
36. Cosnier, S., et al., *Entrapment of enzyme within organic and inorganic materials for biosensor applications: Comparative study.* Materials Science & Engineering C-Biomimetic and Supramolecular Systems, 2006. **26**(2-3): p. 442-447.
37. Haider, T. and Q. Husain, *Calcium alginate entrapped preparations of Aspergillus oryzae beta galactosidase: Its stability and applications in the hydrolysis of lactose.* International Journal of Biological Macromolecules, 2007. **41**(1): p. 72-80.
38. Wang, Q., et al., *Natural supramolecular building blocks: Cysteine-added mutants of cowpea mosaic virus.* Chemistry & Biology, 2002. **9**(7): p. 813-819.
39. Azmi, N.E., et al., *Biosensor based on glutamate dehydrogenase immobilized in chitosan for the determination of ammonium in water samples.* Analytical Biochemistry, 2009. **388**(1): p. 28-32.
40. Cui, X., et al., *Highly sensitive lactate biosensor by engineering chitosan/PVI-Os/CNT/LOD network nanocomposite.* Biosensors & Bioelectronics, 2007. **22**(12): p. 3288-3292.
41. Tsai, Y.-C., S.-Y. Chen, and H.-W. Liaw, *Immobilization of lactate dehydrogenase within multiwalled carbon nanotube-chitos anhanocompo site for application to lactate biosensors.* Sensors and Actuators B-Chemical, 2007. **125**(2): p. 474-481.
42. Lee, C.-A. and Y.-C. Tsai, *Preparation of multiwalled carbon nanotube-chitosan-alcohol dehydrogenase nanobiocomposite for amperometric detection of ethanol.* Sensors and Actuators B-Chemical, 2009. **138**(2): p. 518-523.
43. Tsai, Y.-C., S.-Y. Chen, and C.-A. Lee, *Amperometric cholesterol biosensors based on carbon nanotube-chitosan-platinum-cholesterol oxidase nanobiocomposite.* Sensors and Actuators B-Chemical, 2008. **135**(1): p. 96-101.
44. Tembe, S., et al., *Electrochemical biosensor for catechol using agarose-guar gum entrapped tyrosinase.* Journal of Biotechnology, 2007. **128**(1): p. 80-85.
45. Sassolas, A., L.J. Blum, and B.D. Leca-Bouvier, *New electrochemiluminescent biosensors combining polyluminol and an enzymatic matrix.* Analytical and Bioanalytical Chemistry, 2009. **394**(4): p. 971-980.

46. Chaubey, A., et al., *Co-immobilization of lactate oxidase and lactate dehydrogenase on conducting polyaniline films.* Analytica Chimica Acta, 2000. **407**(1-2): p. 97-103.
47. Luo, P., et al., *Determination of serum alcohol using a disposable biosensor.* Forensic Science International, 2008. **179**(2-3): p. 192-198.
48. Kong, T., et al., *An amperometric glucose biosensor based on the immobilization of glucose oxidase on the ZnO nanotubes.* Sensors and Actuators B-Chemical, 2009. **138**(1): p. 344-350.
49. Shen, J. and C.-C. Liu, *Development of a screen-printed cholesterol biosensor: Comparing the performance of gold and platinum as the working electrode material and fabrication using a self-assembly approach.* Sensors and Actuators B-Chemical, 2007. **120**(2): p. 417-425.
50. Rahman, M.A., et al., *Functionalized conducting polymer as an enzyme-immobilizing substrate: An amperometric glutamate microbiosensor for in vivo measurements.* Analytical Chemistry, 2005. **77**(15): p. 4854-4860.
51. Gwenin, C.D., et al., *The orientationally controlled assembly of genetically modified enzymes in an amperometric biosensor.* Biosensors & Bioelectronics, 2007. **22**(12): p. 2869-2875.
52. Yao, D., A.G. Vlessidis, and N.P. Evmiridis, *Development of an interference-free chemiluminescence method for monitoring acetylcholine and choline based on immobilized enzymes.* Analytica Chimica Acta, 2002. **462**(2): p. 199-208.
53. Choi, K.-m., et al., *Chimeric Capsid Protein as a Nanocarrier for siRNA Delivery: Stability and Cellular Uptake of Encapsulated siRNA.* Acs Nano, 2011. **5**(11): p. 8690-8699.
54. Cruz, S.S., et al., *Assembly and movement of a plant virus carrying a green fluorescent protein overcoat.* Proceedings of the National Academy of Sciences of the United States of America, 1996. **93**(13): p. 6286-6290.
55. Brown, A.D., et al., *Carboxylate-Directed In Vivo Assembly of Virus-like Nanorods and Tubes for the Display of Functional Peptides and Residues.* Biomacromolecules, 2013. **14**(9): p. 3123-3129.
56. Hess, G.T., et al., *Orthogonal Labeling of M13 Minor Capsid Proteins with DNA to Self-Assemble End-to-End Multiphage Structures.* Acs Synthetic Biology, 2013. **2**(9): p. 490-496.
57. Geiger, F.C., et al., *TMV nanorods with programmed longitudinal domains of differently addressable coat proteins.* Nanoscale, 2013. **5**(9): p. 3808-3816.
58. Klem, M.T., et al., *2-D array formation of genetically engineered viral cages on Au surfaces and imaging by atomic force microscopy.* Journal of the American Chemical Society, 2003. **125**(36): p. 10806-10807.
59. Miller, R.A., A.D. Presley, and M.B. Francis, *Self-assembling light-harvesting systems from synthetically modified tobacco mosaic virus coat proteins.* Journal of the American Chemical Society, 2007. **129**(11): p. 3104-3109.

60. Wen, A.M. and N.F. Steinmetz, *Design of virus-based nanomaterials for medicine, biotechnology, and energy.* Chemical Society Reviews, 2016. **45**(15): p. 4074-4126.
61. Capehart, S.L., et al., *Controlled Integration of Gold Nanoparticles and Organic Fluorophores Using Synthetically Modified M52 Viral Capsids.* Journal of the American Chemical Society, 2013. **135**(8): p. 3011-3016.
62. Hovlid, M.L., et al., *Encapsidated Atom-Transfer Radical Polymerization in Q beta Virus-like Nanoparticles.* Acs Nano, 2014. **8**(8): p. 8003-8014.
63. Wu, F.C., et al., *Expanding the genetic code for site-specific labelling of tobacco mosaic virus coat protein and building biotin-functionalized virus-like particles.* Chemical Communications, 2014. **50**(30): p. 4007-4009.
64. Lu, Y., et al., *Escherichia coli-based cell free production of flagellin and ordered flagellin display on virus-like particles.* Biotechnology and Bioengineering, 2013. **110**(8): p. 2073-2085.
65. Patterson, D.P., P.E. Prevelige, and T. Douglas, *Nanoreactors by Programmed Enzyme Encapsulation Inside the Capsid of the Bacteriophage P22.* Acs Nano, 2012. **6**(6): p. 5000-5009.
66. Rurup, W.F., et al., *Predicting the Loading of Virus-Like Particles with Fluorescent Proteins.* Biomacromolecules, 2014. **15**(2): p. 558-563.
67. Carette, N., et al., *A virus-based biocatalyst.* Nature Nanotechnology, 2007. **2**(4): p. 226-229.
68. Minten, I.J., et al., *Catalytic capsids: the art of confinement.* Chemical Science, 2011. **2**(2): p. 358-362.
69. Jordan, P.C., et al., *Self-assembling biomolecular catalysts for hydrogen production.* Nature Chemistry, 2016. **8**(2): p. 179-185.
70. Patterson, D.P., et al., *Encapsulation of an Enzyme Cascade within the Bacteriophage P22 Virus-Like Particle.* Acs Chemical Biology, 2014. **9**(2): p. 359-365.
71. Nam, Y.S., et al., *Virus-templated iridium oxide-gold hybrid nanowires for electrochromic application.* Nanoscale, 2012. **4**(11): p. 3405-3409.
72. French, R.H., et al., *Long range interactions in nanoscale science.* Reviews of Modern Physics, 2010. **82**(2): p. 1887-1944.
73. Shenton, W., et al., *Inorganic-organic nanotube composites from template mineralization of tobacco mosaic virus.* Advanced Materials, 1999. **11**(3): p. 253-+.
74. Dogic, Z. and S. Fraden, *Ordered phases of filamentous viruses.* Current Opinion in Colloid & Interface Science, 2006. **11**(1): p. 47-55.
75. Onsager, L., *MOTION OF IONS - PRINCIPLES AND CONCEPTS.* Science, 1969. **166**(3911): p. 1359-&.
76. Liu, Y., et al., *Tin-Coated Viral Nanoforests as Sodium-Ion Battery Anodes.* Acs Nano, 2013. **7**(4): p. 3627-3634.

77. Nam, K.T., et al., *Stamped microbattery electrodes based on self-assembled M13 viruses.* Proceedings of the National Academy of Sciences of the United States of America, 2008. **105**(45): p. 17227-17231.
78. Oh, D., et al., *Biologically enhanced cathode design for improved capacity and cycle life for lithium-oxygen batteries.* Nature Communications, 2013. **4**.
79. Lee, Y.J., et al., *Biologically Activated Noble Metal Alloys at the Nanoscale: For Lithium Ion Battery Anodes.* Nano Letters, 2010. **10**(7): p. 2433-2440.
80. Oh, D., et al., *M13 Virus-Directed Synthesis of Nanostructured Metal Oxides for Lithium-Oxygen Batteries.* Nano Letters, 2014. **14**(8): p. 4837-4845.
81. Yang, L.M.C., et al., *Virus electrodes for universal biodetection.* Analytical Chemistry, 2006. **78**(10): p. 3265-3270.
82. Bruckman, M.A., et al., *Tobacco mosaic virus based thin film sensor for detection of volatile organic compounds.* Journal of Materials Chemistry, 2010. **20**(27): p. 5715-5719.
83. Zang, F., et al., *An electrochemical sensor for selective TNT sensing based on Tobacco mosaic virus-like particle binding agents.* Chemical Communications, 2014. **50**(85): p. 12977-12980.
84. Aljabali, A.A.A., et al., *Controlled immobilisation of active enzymes on the cowpea mosaic virus capsid.* Nanoscale, 2012. **4**(18): p. 5640-5645.
85. Koch, C., et al., *Modified TMV Particles as Beneficial Scaffolds to Present Sensor Enzymes.* Frontiers in Plant Science, 2015. **6**.
86. Hamid, S. and R. Hayek, *Role of electrical stimulation for rehabilitation and regeneration after spinal cord injury: an overview.* European Spine Journal, 2008. **17**(9): p. 1256-1269.
87. Gorman, P.H., *An Update on Functional Electrical Stimulation after Spinal Cord Injury.* Neurorehabilitation and Neural Repair, 2000. **14**(4): p. 251-263.
88. Lovley, D.R., *The microbe electric: conversion of organic matter to electricity.* Current Opinion in Biotechnology, 2008. **19**(6): p. 564-571.
89. Lovley, D.R., *Bug juice: harvesting electricity with microorganisms.* Nature Reviews Microbiology, 2006. **4**(7): p. 497-508.
90. Clauwaert, P., et al., *Biological denitrification in microbial fuel cells.* Environmental Science & Technology, 2007. **41**(9): p. 3354-3360.
91. Holmes, D.E., et al., *Microarray and genetic analysis of electron transfer to electrodes in Geobacter sulfurreducens.* Environmental Microbiology, 2006. **8**(10): p. 1805-1815.
92. Bretschger, O., et al., *Current production and metal oxide reduction by Shewanella oneidensis MR-1 wild type and mutants.* Applied and Environmental Microbiology, 2007. **73**(21): p. 7003-7012.
93. Kim, B.-C., et al., *Insights into genes involved in electricity generation in Geobacter sulfurreducens via whole genome microarray analysis of the OmcF-deficient mutant.* Bioelectrochemistry, 2008. **73**(1): p. 70-75.

94. El-Naggar, M.Y., et al., *Electrical transport along bacterial nanowires from Shewanella oneidensis MR-1*. Proceedings of the National Academy of Sciences of the United States of America, 2010. **107**(42): p. 18127-18131.
95. Agapakis, C.M. and P.A. Silver, *Modular electron transfer circuits for synthetic biology: insulation of an engineered biohydrogen pathway.* Bioengineered bugs, 2010. **1**(6): p. 413-8.
96. Fischbach, M. and C.A. Voigt, *Prokaryotic gene clusters: A rich toolbox for synthetic biology.* Biotechnology Journal, 2010. **5**(12): p. 1277-1296.
97. Simpson, M.L., et al., *Whole-cell biocomputing.* Trends in Biotechnology, 2001. **19**(8): p. 317-323.
98. Vilanova, C., et al., *Aequorin-expressing yeast emits light under electric control.* Journal of Biotechnology, 2011. **152**(3): p. 93-95.
99. Tschirhart, T., et al., *Electronic control of gene expression and cell behaviour in Escherichia coli through redox signalling.* 2017. **8**: p. 14030.
100. Weber, W., et al., *A synthetic mammalian electro-genetic transcription circuit.* Nucleic Acids Research, 2009. **37**(4): p. e33-e33.
101. Nissim, L., et al., *Multiplexed and programmable regulation of gene networks with an integrated RNA and CRISPR/Cas toolkit in human cells.* Molecular cell, 2014. **54**(4): p. 698-710.
102. Jusiak, B., et al., *Engineering Synthetic Gene Circuits in Living Cells with CRISPR Technology.* Trends in Biotechnology. **34**(7): p. 535-547.
103. Bhokisham, N., et al., *Modular construction of multi-subunit protein complexes using engineered tags and microbial transglutaminase.* Metabolic Engineering, 2016. **38**: p. 1-9.
104. Bhokisham, N., et al., *Data on biochemical fluxes generated from biofabricated enzyme complexes assembled through engineered tags and microbial transglutaminase.* Data in Brief.
105. Bhokisham, N., et al., *A Facile Two-Step Enzymatic Approach for Conjugating Proteins to Polysaccharide Chitosan at an Electrode Interface.* Cellular and Molecular Bioengineering, 2017. **10**(1): p. 134-142.
106. Bhokisham, N., et al., *Data on biochemical fluxes generated from biofabricated enzyme complexes assembled through engineered tags and microbial transglutaminase.* Data in brief, 2016. **8**: p. 1031-5.
107. Shao, Y., et al., *Graphene Based Electrochemical Sensors and Biosensors: A Review.* Electroanalysis, 2010. **22**(10): p. 1027-1036.
108. Wang, J., *Carbon-Nanotube Based Electrochemical Biosensors: A Review.* Electroanalysis, 2005. **17**(1): p. 7-14.
109. Wang, J., *Electrochemical glucose biosensors.* Chemical reviews, 2008. **108**(2): p. 814-825.
110. Dittrich, P.S. and A. Manz, *Lab-on-a-chip: microfluidics in drug discovery.* Nature Reviews Drug Discovery, 2006. **5**(3): p. 210-218.
111. Haeberle, S. and R. Zengerle, *Microfluidic platforms for lab-on-a-chip applications.* Lab on a Chip, 2007. **7**(9): p. 1094-1110.

112. Fernandes, R., et al., *Engineered biological nanofactories trigger quorum sensing response in targeted bacteria.* Nat Nano, 2010. **5**(3): p. 213-217.
113. Koeller, K.M. and C.-H. Wong, *Enzymes for chemical synthesis.* Nature, 2001. **409**(6817): p. 232-240.
114. Matosevic, S., N. Szita, and F. Baganz, *Fundamentals and applications of immobilized microfluidic enzymatic reactors.* Journal of Chemical Technology & Biotechnology, 2011. **86**(3): p. 325-334.
115. Lopez-Gallego, F. and C. Schmidt-Dannert, *Multi-enzymatic synthesis.* Current Opinion in Chemical Biology, 2010. **14**(2): p. 174-183.
116. Hanefeld, U., L. Gardossi, and E. Magner, *Understanding enzyme immobilisation.* Chemical Society Reviews, 2009. **38**(2): p. 453-468.
117. Brady, D. and J. Jordaan, *Advances in enzyme immobilisation.* Biotechnology Letters, 2009. **31**(11): p. 1639-1650.
118. Zargar, A., G.F. Payne, and W.E. Bentley, *A 'bioproduction breadboard': programming, assembling, and actuating cellular networks.* Current Opinion in Biotechnology, 2015. **36**: p. 154-160.
119. You, C. and Y.H.P. Zhang, *Self-Assembly of Synthetic Metabolons through Synthetic Protein Scaffolds: One-Step Purification, Co-immobilization, and Substrate Channeling.* ACS Synthetic Biology, 2012. **2**(2): p. 102-110.
120. Dueber, J.E., et al., *Synthetic protein scaffolds provide modular control over metabolic flux.* Nat Biotech, 2009. **27**(8): p. 753-759.
121. Hirakawa, H., et al., *Intramolecular electron transfer in a cytochrome P450cam system with a site-specific branched structure.* Protein Engineering Design and Selection, 2007. **20**(9): p. 453-459.
122. Kitaoka, M., et al., *Transglutaminase-Mediated Synthesis of a DNA–(Enzyme)n Probe for Highly Sensitive DNA Detection.* Chemistry – A European Journal, 2011. **17**(19): p. 5387-5392.
123. Lin, C.-W. and A.Y. Ting, *Transglutaminase-Catalyzed Site-Specific Conjugation of Small-Molecule Probes to Proteins in Vitro and on the Surface of Living Cells.* Journal of the American Chemical Society, 2006. **128**(14): p. 4542-4543.
124. Liu, Y., et al., *Biofabricating Multifunctional Soft Matter with Enzymes and Stimuli-Responsive Materials.* Advanced Functional Materials, 2012. **22**(14): p. 3004-3012.
125. Plagmann, I., et al., *Transglutaminase-catalyzed covalent multimerization of camelidae anti-human TNF single domain antibodies improves neutralizing activity.* Journal of Biotechnology, 2009. **142**(2): p. 170-178.
126. Strop, P., *Versatility of Microbial Transglutaminase.* Bioconjugate Chemistry, 2014. **25**(5): p. 855-862.
127. Tanaka, T., N. Kamiya, and T. Nagamune, *Peptidyl Linkers for Protein Heterodimerization Catalyzed by Microbial Transglutaminase.* Bioconjugate Chemistry, 2004. **15**(3): p. 491-497.

128. Yung, C.W., et al., *Transglutaminase crosslinked gelatin as a tissue engineering scaffold.* Journal of Biomedical Materials Research Part A, 2007. **83A**(4): p. 1039-1046.
129. Zhu, J., et al., *S-Ribosylhomocysteinase (LuxS) is a mononuclear iron protein.* Biochemistry, 2003. **42**(16): p. 4717-26.
130. Cornell, K.A. and M.K. Riscoe, *Cloning and expression of Escherichia coli 5'-methylthioadenosine/S-adenosylhomocysteine nucleosidase: identification of the pfs gene product.* Biochim Biophys Acta, 1998. **1396**(1): p. 8-14.
131. Sambrook, J., *Molecular cloning : a laboratory manual / Joseph Sambrook, David W. Russell*, ed. D.W. Russell and L. Cold Spring Harbor. 2001, Cold Spring Harbor, N.Y: Cold Spring Harbor Laboratory.
132. Wu, H.C., et al., *Autonomous bacterial localization and gene expression based on nearby cell receptor density*. Vol. 9. 2013.
133. Gordonov, T., et al., *Electronic modulation of biochemical signal generation.* Nat Nano, 2014. **9**(8): p. 605-610.
134. Hilgers, M.T. and M.L. Ludwig, *Crystal structure of the quorum-sensing protein LuxS reveals a catalytic metal site.* Proceedings of the National Academy of Sciences, 2001. **98**(20): p. 11169-11174.
135. Lee, J.E., et al., *Structure of E. coli 5'-methylthioadenosine/S-adenosylhomocysteine Nucleosidase Reveals Similarity to the Purine Nucleoside Phosphorylases.* Structure, 2001. **9**(10): p. 941-953.
136. Vendeville, A., et al., *Making 'sense' of metabolism: autoinducer-2, LUXS and pathogenic bacteria.* Nat Rev Micro, 2005. **3**(5): p. 383-396.
137. Björck, L. and G. Kronvall, *Purification and some properties of streptococcal protein G, a novel IgG-binding reagent.* The Journal of Immunology, 1984. **133**(2): p. 969-74.
138. Spolaore, B., et al., *Local Unfolding Is Required for the Site-Specific Protein Modification by Transglutaminase.* Biochemistry, 2012. **51**(43): p. 8679-8689.
139. Lewis, H.A., et al., *A Structural Genomics Approach to the Study of Quorum Sensing: Crystal Structures of Three LuxS Orthologs.* Structure, 2001. **9**(6): p. 527-537.
140. Wu, L.Q. and G.F. Payne, *Biofabrication: using biological materials and biocatalysts to construct nanostructured assemblies.* Trends in Biotechnology, 2004. **22**(11): p. 593-599.
141. Mironov, V., et al., *Biofabrication: a 21st century manufacturing paradigm.* Biofabrication, 2009. **1**(2).
142. Yi, L., et al., *Biofabrication to build the biology–device interface.* Biofabrication, 2010. **2**(2): p. 022002.
143. Nakamura, M., et al., *Biomatrices and biomaterials for future developments of bioprinting and biofabrication.* Biofabrication, 2010. **2**(1).
144. Kim, E., et al., *Chitosan to Connect Biology to Electronics: Fabricating the Bio-Device Interface and Communicating Across This Interface.* Polymers, 2015. **7**(1): p. 1-46.

145. Charles, P.T., et al., *Reduction of Non-Specific Protein Adsorption Using Poly(ethylene) Glycol (PEG) Modified Polyacrylate Hydrogels In Immunoassays for Staphylococcal Enterotoxin B Detection.* Sensors, 2009. **9**(1): p. 645-655.
146. Chaki, N.K. and K. Vijayamohanan, *Self-assembled monolayers as a tunable platform for biosensor applications.* Biosensors & Bioelectronics, 2002. **17**(1-2): p. 1-12.
147. Zhou, Y., et al., *Chitosan-N-poly (ethylene oxide) brush polymers for reduced nonspecific protein adsorption.* Journal of Colloid and Interface Science, 2007. **305**(1): p. 62-71.
148. Luo, X., et al., *Biofabrication of stratified biofilm mimics for observation and control of bacterial signaling.* Biomaterials, 2012. **33**(20): p. 5136-5143.
149. Lewandowski, A.T., et al., *Protein assembly onto patterned microfabricated devices through enzymatic activation of fusion pro-tag.* Biotechnology and Bioengineering, 2008. **99**(3): p. 499-507.
150. Kim, E., et al., *Amplified and in Situ Detection of Redox-Active Metabolite Using a Biobased Redox Capacitor.* Analytical Chemistry, 2013. **85**(4): p. 2102-2108.
151. Chen, T.H., et al., *In vitro protein-polysaccharide conjugation: Tyrosinase-catalyzed conjugation of gelatin and chitosan.* Biopolymers, 2002. **64**(6): p. 292-302.
152. Duckworth, H.W. and J.E. Coleman, *PHYSICOCHEMICAL AND KINETIC PROPERTIES OF MUSHROOM TYROSINASE.* Journal of Biological Chemistry, 1970. **245**(7): p. 1613-+.
153. Molloy, S., et al., *Engineering of a bacterial tyrosinase for improved catalytic efficiency towards D-tyrosine using random and site directed mutagenesis approaches.* Biotechnology and Bioengineering, 2013. **110**(7): p. 1849-1857.
154. Chen, H., et al., *Anti-HER2 antibody and ScFvEGFR-conjugated antifouling magnetic iron oxide nanoparticles for targeting and magnetic resonance imaging of breast cancer.* International Journal of Nanomedicine, 2013. **8**: p. 3781-3794.
155. Yang, X., et al., *Orthogonal Enzymatic Reactions for the Assembly of Proteins at Electrode Addresses.* Langmuir, 2009. **25**(1): p. 338-344.
156. Lewis, K.B., et al., *Crosslinking kinetics of the human transglutaminase, factor XIII A(2) , acting on fibrin gels and gamma-chain peptides.* Biochemistry, 1997. **36**(5): p. 995-1002.
157. Fernandes, R., et al., *Electrochemically induced deposition of a polysaccharide hydrogel onto a patterned surface.* Langmuir, 2003. **19**(10): p. 4058-4062.
158. Lewandowski, A.T., et al., *Tyrosine-based "activatable pro-tag": Enzyme-catalyzed protein capture and release.* Biotechnology and Bioengineering, 2006. **93**(6): p. 1207-1215.

159. Fernandes, R., et al., *Biological nanofactories facilitate spatially selective capture and manipulation of quorum sensing bacteria in a bioMEMS device.* Lab on a Chip, 2010. **10**(9): p. 1128-1134.
160. Fernandes, R. and W.E. Bentley, *AI-2 Biosynthesis Module in a Magnetic Nanofactory Alters Bacterial Response Via Localized Synthesis and Delivery.* Biotechnology and Bioengineering, 2009. **102**(2): p. 390-399.
161. Wu, H.-C., et al., *Biofabrication of Antibodies and Antigens Via IgG-Binding Domain Engineered With Activatable Pentatyrosine pro-tag.* Biotechnology and Bioengineering, 2009. **103**(2): p. 231-240.
162. Lewandowski, A.T., et al., *Towards Area-Based In Vitro Metabolic Engineering: Assembly of Pfs Enzyme onto Patterned Microfabricated Chips.* Biotechnology Progress, 2008. **24**(5): p. 1042-1051.
163. Huang, N.P., et al., *Poly(L-lysine)-g-poly(ethylene glycol) layers on metal oxide surfaces: Surface-analytical characterization and resistance to serum and fibrinogen adsorption.* Langmuir, 2001. **17**(2): p. 489-498.
164. Gray, J.J., *The interaction of proteins with solid surfaces.* Current Opinion in Structural Biology, 2004. **14**(1): p. 110-115.
165. Maune, H.T., et al., *Self-assembly of carbon nanotubes into two-dimensional geometries using DNA origami templates.* Nature Nanotechnology, 2010. **5**(1): p. 61-66.
166. Sacca, B. and C.M. Niemeyer, *DNA Origami: The Art of Folding DNA.* Angewandte Chemie-International Edition, 2012. **51**(1): p. 58-66.
167. Lai, Y.-T., et al., *Structure and Flexibility of Nanoscale Protein Cages Designed by Symmetric Self-Assembly.* Journal of the American Chemical Society, 2013. **135**(20): p. 7738-7743.
168. Zhou, Y. and T. Shimizu, *Lipid nanotubes: A unique template to create diverse one-dimensional nanostructures.* Chemistry of Materials, 2008. **20**(3): p. 625-633.
169. Namiki, Y., et al., *Nanomedicine for Cancer: Lipid-Based Nanostructures for Drug Delivery and Monitoring.* Accounts of Chemical Research, 2011. **44**(10): p. 1080-1093.
170. Culver, J.N., et al., *Plant virus directed fabrication of nanoscale materials and devices.* Virology, 2015. **479**(Supplement C): p. 200-212.
171. Izard, T., et al., *Principles of quasi-equivalence and Euclidean geometry govern the assembly of cubic and dodecahedral cores of pyruvate dehydrogenase complexes.* Proceedings of the National Academy of Sciences of the United States of America, 1999. **96**(4): p. 1240-1245.
172. Brown, S., *Metal-recognition by repeating polypeptides.* Nat Biotech, 1997. **15**(3): p. 269-272.
173. Whaley, S.R., et al., *Selection of peptides with semiconductor binding specificity for directed nanocrystal assembly.* Nature, 2000. **405**(6787): p. 665-668.

174. Kowalewski, T. and D.M. Holtzman, *In situ atomic force microscopy study of Alzheimer's β-amyloid peptide on different substrates: New insights into mechanism of β-sheet formation.* Proceedings of the National Academy of Sciences, 1999. **96**(7): p. 3688-3693.
175. Hayamizu, Y., et al., *Bioelectronic interfaces by spontaneously organized peptides on 2D atomic single layer materials.* 2016. **6**: p. 33778.
176. Balci, S., et al., *Printing and Aligning Mesoscale Patterns of Tobacco mosaic virus on Surfaces.* Advanced Materials, 2008. **20**(11): p. 2195-2200.
177. Stephanopoulos, N. and M.B. Francis, *Choosing an effective protein bioconjugation strategy.* 2011. **7**: p. 876.
178. Bäcker, M., et al., *A New Class of Biosensors Based on Tobacco Mosaic Virus and Coat Proteins as Enzyme Nanocarrier.* Procedia Engineering, 2016. **168**(Supplement C): p. 618-621.
179. Royston, E., et al., *Self-Assembly of Virus-Structured High Surface Area Nanomaterials and Their Application as Battery Electrodes.* Langmuir, 2008. **24**(3): p. 906-912.
180. Wu, H.-C., et al., *Conferring biological activity to native spider silk: A biofunctionalized protein-based microfiber.* Biotechnology and Bioengineering, 2017. **114**(1): p. 83-95.
181. Sauerbrey, G., *Verwendung von Schwingquarzen zur Wägung dünner Schichten und zur Mikrowägung.* Zeitschrift für Physik, 1959. **155**(2): p. 206-222.
182. Cai, H. and S. Clarke, *A Novel Methyltransferase Catalyzes the Methyl Esterification of trans-Aconitate in Escherichia coli.* Journal of Biological Chemistry, 1999. **274**(19): p. 13470-13479.
183. Price, C.I. and A.D. Pandyan, *Electrical stimulation for preventing and treating post-stroke shoulder pain: a systematic Cochrane review.* Clinical Rehabilitation, 2001. **15**(1): p. 5-19.
184. Kroon, J.R.d., et al., *Therapeutic electrical stimulation to improve motor control and functional abilities of the upper extremity after stroke: a systematic review.* Clinical Rehabilitation, 2002. **16**(4): p. 350-360.
185. Rijkhoff, N.J., et al., *Urinary bladder control by electrical stimulation: review of electrical stimulation techniques in spinal cord injury.* Neurourol Urodyn, 1997. **16**(1): p. 39-53.
186. Kloth, L.C., *Electrical Stimulation for Wound Healing: A Review of Evidence From In Vitro Studies, Animal Experiments, and Clinical Trials.* The International Journal of Lower Extremity Wounds, 2005. **4**(1): p. 23-44.
187. Cameron, D.E., C.J. Bashor, and J.J. Collins, *A brief history of synthetic biology.* Nat Rev Micro, 2014. **12**(5): p. 381-390.
188. Demple, B., *Redox signaling and gene control in the Escherichia coli soxRS oxidative stress regulon — a review.* Gene, 1996. **179**(1): p. 53-57.
189. Farzadfard, F., S.D. Perli, and T.K. Lu, *Tunable and Multifunctional Eukaryotic Transcription Factors Based on CRISPR/Cas.* ACS Synthetic Biology, 2013. **2**(10): p. 604-613.

190. Deltcheva, E., et al., *CRISPR RNA maturation by trans-encoded small RNA and host factor RNase III.* Nature, 2011. **471**(7340): p. 602-607.
191. Gilbert, L.A., et al., *Genome-Scale CRISPR-Mediated Control of Gene Repression and Activation.* Cell, 2014. **159**(3): p. 647-661.
192. Dominguez, A.A., W.A. Lim, and L.S. Qi, *Beyond editing: repurposing CRISPR-Cas9 for precision genome regulation and interrogation.* Nat Rev Mol Cell Biol, 2016. **17**(1): p. 5-15.
193. Chavez, A., et al., *Highly efficient Cas9-mediated transcriptional programming.* Nat Meth, 2015. **12**(4): p. 326-328.
194. Bikard, D., et al., *Programmable repression and activation of bacterial gene expression using an engineered CRISPR-Cas system.* Nucleic Acids Research, 2013. **41**(15): p. 7429-7437.
195. Scott, W.G., et al., *Capturing the Structure of a Catalytic RNA Intermediate: The Hammerhead Ribozyme.* Science, 1996. **274**(5295): p. 2065-2069.
196. Nakano, S.-i., D.M. Chadalavada, and P.C. Bevilacqua, *General Acid-Base Catalysis in the Mechanism of a Hepatitis Delta Virus Ribozyme.* Science, 2000. **287**(5457): p. 1493-1497.
197. Hilton, I.B., et al., *Epigenome editing by a CRISPR-Cas9-based acetyltransferase activates genes from promoters and enhancers.* Nat Biotech, 2015. **33**(5): p. 510-517.
198. Mathew, R. and D. Chatterji, *The evolving story of the omega subunit of bacterial RNA polymerase.* Trends in Microbiology, 2006. **14**(10): p. 450-455.
199. Gunnelius, L., et al., *The omega subunit of the RNA polymerase core directs transcription efficiency in cyanobacteria.* Nucleic Acids Research, 2014. **42**(7): p. 4606-4614.
200. Adams, B.L., *The Next Generation of Synthetic Biology Chassis: Moving Synthetic Biology from the Laboratory to the Field.* ACS Synthetic Biology, 2016. **5**(12): p. 1328-1330.
201. Connell, N., et al., *An E. coli promoter induced by the cessation of growth.* Molecular Microbiology, 1987. **1**(2): p. 195-201.
202. Greenberg, J.T., et al., *Positive Control of a Global Antioxidant Defense Regulon Activated by Superoxide-Generating Agents in Escherichia coli.* Proceedings of the National Academy of Sciences of the United States of America, 1990. **87**(16): p. 6181-6185.
203. Datsenko, K.A. and B.L. Wanner, *One-step inactivation of chromosomal genes in Escherichia coli K-12 using PCR products.* Proceedings of the National Academy of Sciences of the United States of America, 2000. **97**(12): p. 6640-6645.
204. Reisch, C.R. and K.L.J. Prather, *The no-SCAR (Scarless Cas9 Assisted Recombineering) system for genome editing in Escherichia coli.* 2015. **5**: p. 15096.

205. Lindsay, A. and B.M.M. Ahmer, *Effect of sdiA on Biosensors of N-Acylhomoserine Lactones.* Journal of Bacteriology, 2005. **187**(14): p. 5054-5058.
206. Buckley, A.M., et al., *LOV-based reporters for fluorescence imaging.* Current Opinion in Chemical Biology, 2015. **27**(Supplement C): p. 39-45.
207. Farr, S.B. and T. Kogoma, *Oxidative stress responses in Escherichia coli and Salmonella typhimurium.* Microbiological Reviews, 1991. **55**(4): p. 561-585.
208. Gao, Y., et al., *Complex transcriptional modulation with orthogonal and inducible dCas9 regulators.* Nat Meth, 2016. **13**(12): p. 1043-1049.
209. Deaner, M., J. Mejia, and H.S. Alper, *Enabling Graded and Large-Scale Multiplex of Desired Genes Using a Dual-Mode dCas9 Activator in Saccharomyces cerevisiae.* ACS Synthetic Biology, 2017.
210. Wu, J. and B. Weiss, *Two-stage induction of the soxRS (superoxide response) regulon of Escherichia coli.* Journal of Bacteriology, 1992. **174**(12): p. 3915-3920.
211. Tang, X., et al., *A CRISPR–Cpf1 system for efficient genome editing and transcriptional repression in plants*. Vol. 3. 2017. 17018.
212. Nihongaki, Y., et al., *Photoactivatable CRISPR-Cas9 for optogenetic genome editing.* Nat Biotech, 2015. **33**(7): p. 755-760.
213. Zetche, B., S.E. Volz, and F. Zhang, *A Split Cas9 Architecture for Inducible Genome Editing and Transcription Modulation.* Nature biotechnology, 2015. **33**(2): p. 139-142.
214. Brown, N.L., et al., *The MerR family of transcriptional regulators.* FEMS Microbiology Reviews, 2003. **27**(2-3): p. 145-163.
215. Cress, B.F., et al., *Rapid generation of CRISPR/dCas9-regulated, orthogonally repressible hybrid T7-lac promoters for modular, tuneable control of metabolic pathway fluxes in Escherichia coli.* Nucleic Acids Research, 2016. **44**(9): p. 4472-4485.